UNIVERSITA' POLITECNICA DELLE MARCHE

Facoltà di Medicina e Chirurgia

Dipartimento di Eccellenza di Scienze Biomediche e Sanità Pubblica

Scuola di dottorato in Scienze Biomediche

XXXIV ciclo

Area 06

Tesi di dottorato:

Profiling of in vitro metabolism of New Psychoactive Substances

Candidata:

Dott.ssa Annagiulia Di Trana

Relatore:

Chiar.mo Prof. Francesco Paolo Busardò

Anno Accademico 2021-2022

"Homo sum, humani nihil a me alienum puto"

Terenzio (Heautontimorumenos I, 1, 25)

Summary

1 Introduction

A New Psychoactive Substance (NPS) is defined by the United Nation Office of Drugs and Drug Addiction (UNODC) as a "substance of abuse, either in a pure form or a preparation, that is not controlled by the 1961 Single Convention on Narcotic Drugs or the 1971 Convention on Psychotropic Substances, but which may pose a public health threat" (UNODC Early Warning Advisory on New Psychoactive Substances, n.d.). The term "new" may be confounding since it does not always refer to newly synthesized substances. Indeed, this wide class of substances comprises also molecules synthesized and patented in the 1970s or even earlier, but only recently distributed in the black market (Pantano et al., 2019).
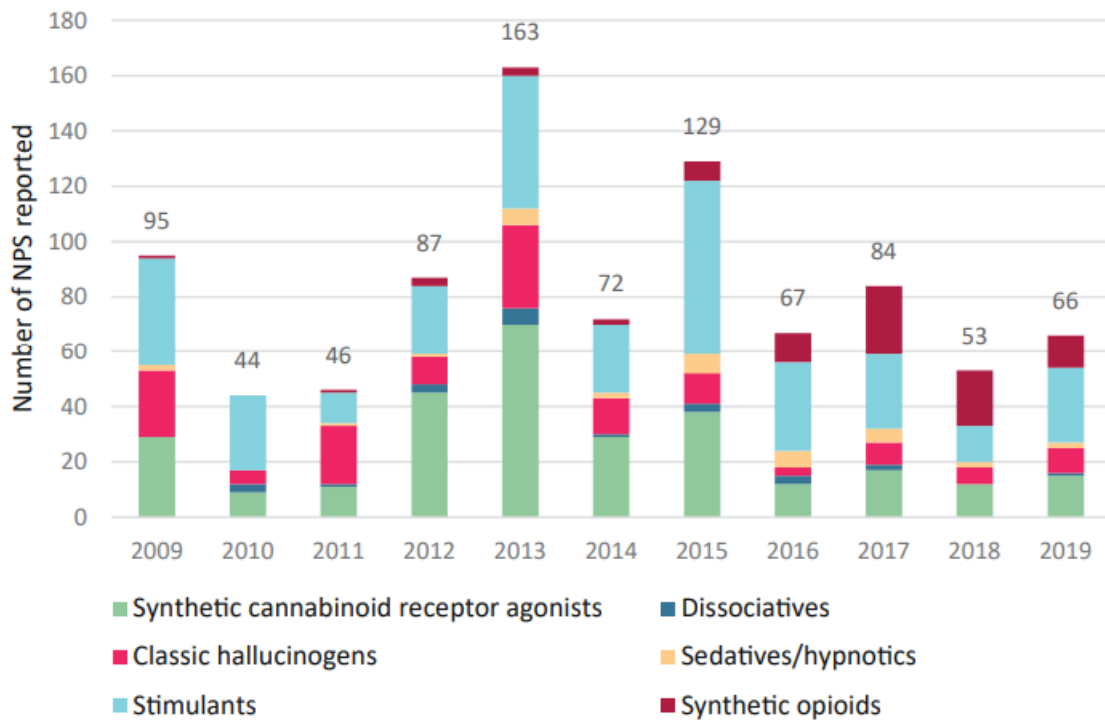
The origin of NPS marketing is lost in time. Anyway, ketamine is recognized as one of the oldest trafficked NPS, which became popular in the United States in the 1980s and then moved to Europe in the 1990s (UNODC, 2013). Since that time, the NPS phenomenon has incredibly spread, affecting more than 120 countries and regions in the World and more than 1,000 different substances have been reported by laboratories, Governments and organizations (United Nations Office On Drugs & Crime(UNODC), 2021).

The NPS may be categorized according to their pharmacological effects into different classes: synthetic cannabinoid receptor agonists (SCRAs), stimulants, dissociatives, classic hallucinogens, sedative/hypnotics, and new synthetic opioids. Furthermore, each class is composed of several structural classes that may count more than 100 analogs, such as synthetic cathinones and phenethylamines (European Monitoring Centre for Drugs and Drug Addiction, 2021). Besides the more popular synthetic molecules, several NPS of natural origin are also marketed, such as kratom, kath, psylocibin, salvinorin A and others (Lo Faro et al., 2019).

According to recent data, 400 different molecules are on the market each year, while the number of new substances reported for the first time has been fluctuating between 163 (in 2013) and 44 (in 2010) since the international monitoring was organized in 2009 (UNODC, 2013). These data suggest the mutating nature of the NPS market that changes its offer every year in response

to different factors such as new legislative efforts, availability of raw materials, abusers' demand.

Remarkably, the newly emerged NPS most prevalent class worldwide changes every year, being the new synthetic cathinones (SCs) and the SCRAs in 2020 (European Monitoring Centre for Drugs and Drug Addiction, 2021; United Nations Office On Drugs & Crime(UNODC), 2021).

Figura 1 NPS reported for the first time at global level (2009-2019)

Among the other factors, the restriction related to COVID-19 pandemic has played an important role in the mutation of the NPS scenario affecting the supply chain at different levels (Annagiulia Di Trana et al., 2020). The limited international mobility, temporary closure of non-essential businesses and intermittent social distancing resulted in an increment in the online drug market, especially via dark web. Moreover, the quick reorganization of public health systems in different countries affected the provision of other medical services, such as toxicological examinations. As a result, the NPS monitoring might not have been effective and the related public health issue might have been again underestimated (A. Di Trana & La Maida, 2021).

Although the number of intoxications and fatalities related to NPS is much lower than that of classic drugs of abuse, such as heroin, it is important to consider that this official esteem may not reflect the reality. Recently, the class of fentanyl analogues has raised concerns for the public health. Fentanyl analogues are synthetic derivatives of fentanyl, a potent μ-opioid receptor agonist with strong anesthetic and analgesic properties. Their potency is substantially higher than that of common opioids (25- to 10,000-fold higher than that of morphine) (A. Di Trana & Del Rio, 2020), and overdose fatalities can be caused by respiratory depression, cardiac arrest, or severe anaphylactic reaction(Brunetti et al., 2020; Pichini et al., 2018). New synthetic opioids, and more specifically fentanyl and analogues, have recently caused a significant spike in intoxications in the United States (Prekupec et al., 2017). Fentanyl and analogues have caused thousands of fatalities, impacting the demographics of opioid-related overdoses (Scholl et al., 2018). New synthetic opioids have also raised concerns in Europe. According to the EMCDDA, 930 seizures of new synthetic opioids were reported in 13 European countries, including seizures of synthetic fentanyl precursors such as N-Phenyl-1-(2-phenylethyl)-4-piperidinamine (4-ANPP), and many cases of acute intoxications were also notified (Brunetti et al., 2020; EMCDDA, 2020). Recently, new synthesis routes for illicit fentanyl manufacture were seemingly adopted by drug traffickers as unusual impurities were detected in seized material, such as phenethyl-4-ANPP (Vandeputte et al., 2021).

Particular attention is raised by the SCs, counting more than 100 analogues detected by international authorities. Synthetic cathinones (SC) are designer analogues of the psychotropic alkaloids of Catha edulis Forsk, S-(-)-cathinone. This natural active principle was consumed for recreational and traditional purposes for centuries before it was listed in Schedule I of the United Nations 1971 Convention on Psychotropic Substances (Lo Faro et al., 2019). Methylone was the first reported synthetic cathinone to the European Monitoring Centre for Drugs and Drug Addiction (EMCDDA) by The Netherlands and Sweden in 2005. Methylone's amphetamine- and cocaine-like effects established SC as a legal alternative to illegal stimulants like 3,4-methylenedioxymethamphetamine (MDMA) (Pieprzyca et al., 2020). In general,

cathinones act as central nervous system stimulants with a mechanism of action similar to, but less potent, than phenethylamines. However, the introduction of different substituents on the amino group (e.g. methyl, ethyl, pyrrolidinyl), the phenyl ring (e.g. methyl, Cl, Br, Fl, methylenedioxy) and the α-carbon produce molecules with varying potencies at the target receptors in the brain. Sympathomimetic effects similar to those occurring following amphetamine (AMP) or cocaine overdose with hallucinations and over-stimulation are observed in SC intoxicated patients (Maurer & Brandt, 2017). The most frequent SC side effects observed are tachycardia, nausea, hyperthermia, rhabdomyolysis, psychomotor tremors, and liver, kidney and lung failure. Death occurred after cardiac arrest or multiorgan failures in most of reported cases. Furthermore, SC induce psychiatric manifestations with fatal consequences such as hallucinations, aggression, anxiety, confusion, paranoia, depression and suicidal thought (La Maida et al., 2021).

The common aspect of all the NPS is that poor pharmacological and toxicological data are available at their first appearance on the black market. This is the most challenging issue for the toxicologist and legal medicine doctor since they are constantly fighting an unknown enemy, with weapons that may be not enough effective. Often, the only report of side effects are reported in dark web fora making the recognition of intoxication difficult at the emergency department. Furthermore, the unavailability of analytical standards affects the prompt detection of NPS in examined biological specimens and seized materials.

In this scenario, my experimental studies find their rational.

1.1 Aim and scope

The aim of the experiments conducted during the Ph.D. project aimed to investigate the in vitro metabolism of two fentanyl analogues, phenylfentanyl and β'-phenylfentanyl, and one synthetic cathinone, 3fluoro-a-pyrrolidinovalerophenone (3F-α-PVP), to elucidate the preliminary pharmacokinetic data on these uninvestigated substances and propose suitable biomarkers of consumption.

To this concern a first incubation batch was set up to study the fentanyl analogues in vitro metabolic fate at the same condition, also to evaluate possible

differences due to the little structural differences. First, the metabolism was predicted in silico. Then, an analytical method in liquid chromatography tandem high resolution mass spectrometry (LC-MS/HRMS) was developed for each molecule of interest, to obtain a chromatographic separation and detect all the eventual metabolites. Finally, the raw data were screened and analysed via a data-mining software with a targeted/untargeted workflow designed for the purpose.

In a second moment, the 3F-α-PVP incubation in human hepatocytes followed by LC-MS/HRMS analysis and targeted/untargeted data mining was performed. In this second experiment, the *in silico* prediction was performed using three softwares, to increase the number of predicted metabolites and therefore their identification.

2 *In vitro* metabolism of phenylfentanyl and β'-phenylfentanyl

2.1 Material and methods

2.1.1 Chemicals and reagents

Phenylfentanyl, β'-phenylfentanyl, 4-ANPP (Cayman chemical; Ann Harbor, MI, USA), and diclofenac (Sigma Aldrich; Milan, Italy) standards were dissolved in LC-MS grade methanol (Carlo Erba; Cornaredo, Italy) to 1-mg/mL stock solutions. The solutions were stored at –20°C until analysis.

Ten-donor-pooled cryopreserved human hepatocytes, thawing medium (TM), and 0.4% trypan blue were purchased from Lonza (Basel, Switzerland). l-Glutamine, HEPES (2-[4-(2-hydroxyethyl)-1-piperazinyl]ethanesulfonic acid), and Williams' Medium E were purchased from Sigma Aldrich. l-Glutamine and HEPES were dissolved in Williams' Medium E to 2 and 20 mmol/L, respectively, prior to analysis. The supplemented Williams' Medium E (sWME) was stored at 4°C until incubation.

LC-MS grade acetonitrile, water, and formic acid were purchased from Carlo Erba.

2.1.2 Hepatocyte incubation

Incubations were conducted as previously described, with minor modifications (Carlier, Diao, Scheidweiler, et al., 2017; Carlier, Diao, Wohlfarth, et al., 2017).

Hepatocytes were thawed at 37°C and gently mixed in 50 mL TM at 37°C in a 50-mL polypropylene conical tube. The tube was centrifuged at 100 g for 5 min and the pellet was washed with 50 mL sWME at 37°C. After centrifugation at 100 g for 5 min, the cells were resuspended in 2 mL sWME. Hepatocyte viability was assessed with the trypan blue exclusion test, and sWME volume was adjusted to 2 x 10^6 viable cells/mL.

Incubations were prepared in sterile 24-well culture plates with 250 µL hepatocyte suspension at 2×10^6 viable cells/mL in sWME at 37°C and 250 µL phenylfentanyl at 20 µmol/L in sWME at 37°C. The samples were placed in an incubator previously set at 37°C (Argo Lab; Carpi, Italy) and metabolic reactions were stopped with 500 µL ice-cold acetonitrile after 0 h or 3 h. The samples were transferred into microtubes, centrifuged for 10 min, 15,000 g, at room temperature, and prepared for analysis (see subsection "2.3. Sample preparation").

Diclofenac was incubated under the same conditions, and 4'-hydroxydiclofenac and diclofenac acyl-β-D-glucuronide were monitored to ensure proper metabolic activity. In addition, negative controls – i.e. hepatocytes in sWME without phenylfentanyl and phenylfentanyl in sWME without hepatocytes – were prepared to assess spontaneous reactions.

2.1.3   Sample preparation

After sample centrifugation, 100 µL of supernatant was vortex mixed with 100 µL acetonitrile and centrifuged for 10 min, 15,000 g, at room temperature. The supernatants were dried under nitrogen at 37°C and the residues were reconstituted with 150 µL of mobile phase A (MPA):mobile phase B (MPB) (8:2 v/v) (see subsection "2.4. Instrumental conditions"). After centrifugation for 10 min, 15,000 g, at room temperature, supernatants were transferred into LC autosampler vials with glass inserts.

2.1.4   Instrumental conditions

LC-HRMS/MS analyses were performed on a DIONEX UltiMate 3000 liquid chromatographer coupled with a Q-Exactive quadrupole-Orbitrap hybrid high-resolution mass spectrometer equipped with a heated electrospray ionization (HESI) source (Thermo Scientific, Waltham, MA, USA).

2.1.5   Liquid chromatography conditions

Sample injection volume was 10 µL. The chromatographic separation was performed through a Kinetex Biphenyl column (150 x 2.1 mm, 2 µm) from

Phenomenex, with a mobile phase gradient composed of 0.1% formic acid in water (MPA) and 0.1% formic acid in acetonitrile (MPB) at a 0.4-mL/min flow rate. Autosampler and column oven temperatures were 10 ± 1 and 37 ± 1 °C, respectively. The phenylfentanyl metabolites separation was achieved through the following chromatographic gradient: the gradient started with 5% MPB held for 2 min, was increased to 40% MPB within 18 min, was increased to 95% MPB within 2 min, and was held for 5 min, before returning to initial conditions within 0.1 min, followed by a 2.9-min equilibration; total run time was 30 min. Whereas, the β'phenylfentanyl chromatographic gradient started with 5% B held for 2 min, increased to 40% B within 18 min, ramped to 95% B within 2 min and held for 2 min before returning to initial conditions within 0.1 min, followed by 2.9 min of re-equilibration.

2.1.6 Mass spectrometry conditions

Samples were injected twice, in positive and negative-ion modes, using the same ionization source and MS settings for both the analytes of interest.

2.1.6.1 Phenylfentanyl incubates

HESI source parameters were: sheath gas flow rate, 50 a.u.; auxiliary gas flow rate, 10 a.u.; spray voltage, 3 kV; capillary temperature, 300°C; auxiliary gas heater temperature, 300°C; S-lens radio frequency level, 50 a.u.; sweep gas was not utilized.

The orbitrap was calibrated prior to analysis and a lock mass list was used for better accuracy (*m/z* 100.07570, 149.0233, and 391.2843 in positive-ion mode, *m/z* 96.9601 and 112.9856 in negative-ion mode (Keller et al., 2008). The mass spectrometer acquired data from 1 to 25 min of the LC gradient in full-scan HRMS (FullMS)/data dependent MS/MS (ddMS^2) mode. The FullMS acquisition range was *m/z* 80–750 with a resolution of 70,000 at full width at half maximum (FWHM) at *m/z* 200; automatic gain control (AGC) target was 2×10^5 and maximum injection time (IT) was 200ms. Up to 5 ddMS^2 scans were triggered for each FullMS scan depending on a priority inclusion list of putative metabolites based on *in silico* predictions and the metabolic fate of phenylfentanyl analogues (Labroo et al., 1997; Marchei et al., 2018a; Solimini et al., 2018; Wilde et al.,

2019b) (Table 1); other ions that were not compiled in the inclusion list might also trigger ddMS[2] scans; intensity threshold for ddMS[2] triggering was 10[4], with a dynamic exclusion of 2.0 s. Additionally, background *m/z* values with a high intensity were assessed during the injection of a blank control (MPA:MPB, 8:2 v/v) in the same analytical conditions and compiled in an exclusion list in positive and negative-ion modes. ddMS[2] isolation window was *m/z* 1.2 with a resolution of 17,500; normalized collision energy (NCE) was 30, 35, and 50 a.u.; AGC target was 2 x 10^{5} and maximum IT was 64ms.

Table 1 *Inclusion list for the MS/MS data-dependent acquisition*

Transformation	Molecular formula	[M+H]$^{+}$ (*m/z*)	[M-H]$^{-}$ (*m/z*)
Parent (phenylfentanyl)	$C_{26}H_{28}N_2O$	385.2274	383.2129
-8C -8H	$C_{18}H_{20}N_2O$	281.1648	279.1503
-7C -4H -O	$C_{19}H_{24}N_2$	281.2012	279.1867
+O	$C_{26}H_{28}N_2O_2$	401.2224	399.2078
-8C -8H +O	$C_{18}H_{20}N_2O_2$	297.1598	295.1452
-7C -4H	$C_{19}H_{24}N_2O$	297.1961	295.1816
+2O	$C_{26}H_{28}N_2O_3$	417.2173	415.2027
+6C +8H +7O	$C_{32}H_{36}N_2O_8$	577.2544	575.2399
+C +2H +O	$C_{27}H_{30}N_2O_2$	415.2380	413.2235
+4O +S	$C_{26}H_{28}N_2O_5S$	481.1792	479.1646
-2H +O	$C_{26}H_{26}N_2O_2$	399.2067	397.1922
+2H +2O	$C_{26}H_{30}N_2O_3$	419.2329	417.2184
+6C +8H +8O	$C_{32}H_{36}N_2O_9$	593.2494	591.2348
+C +2H +2O	$C_{27}H_{30}N_2O_3$	431.2329	429.2184
+5O +S	$C_{26}H_{28}N_2O_6S$	497.1741	495.1595
+7C +10H +8O	$C_{33}H_{38}N_2O_9$	607.2650	605.2505
-8C -8H +2O	$C_{18}H_{20}N_2O_3$	313.1547	311.1401
-2C +7O	$C_{24}H_{28}N_2O_8$	473.1918	471.1773
-7C -6H +O	$C_{19}H_{22}N_2O_2$	311.1754	309.1609
-8C -6H +2O	$C_{18}H_{22}N_2O_3$	315.1703	313.1558
-8C -8H +4O +S	$C_{18}H_{20}N_2O_5S$	377.1166	375.1020
-7C -4H +O	$C_{19}H_{24}N_2O_2$	313.1911	311.1765

-C +4H +6O	$C_{25}H_{32}N_2O_7$	473.2282	471.2137
-6C -2H	$C_{20}H_{26}N_2O$	311.2118	309.1972
-7C -2H +O	$C_{19}H_{26}N_2O_2$	315.2067	313.1922
-7C -4H +3O +S	$C_{19}H_{24}N_2O_4S$	377.1530	375.1384
-13C -17H -N	$C_{13}H_{11}NO$	198.0913	196.0768
-13C -17H -N +O	$C_{13}H_{11}NO_2$	214.0863	212.0717
-13C -17H -N +2O	$C_{13}H_{11}NO_3$	230.0812	228.0666
-7C -9H -N +7O	$C_{19}H_{19}NO_8$	390.1183	388.1038
-12C -15H -N +O	$C_{14}H_{13}NO_2$	228.1019	226.0874
-13C -15H -N +2O	$C_{13}H_{13}NO_3$	232.0968	230.0823
-13C -17H -N +4O +S	$C_{13}H_{11}NO_5S$	294.0431	292.0285
+10C +17H +3N +7O +S	$C_{36}H_{45}N_5O_8S$	708.3062	706.2916
-2H	$C_{26}H_{26}N_2O$	383.2118	381.1972
-18C -18H -2N	$C_8H_{10}O$	123.0804	121.0659
-19C -22H -2N +O	$C_7H_6O_2$	123.0441	121.0295
-13C -9H -N	$C_{13}H_{19}NO$	206.1539	204.1394
-19C -21H -N	C_7H_7NO	122.0600	120.0455

2.1.6.2 β'phenylfentanyl incubates

HESI source parameters were: sheath gas flow rate, 40 a.u.; auxiliary gas flow rate, 5 a.u.; spray voltage, 3 kV; capillary temperature, 300 °C; auxiliary gas heater temperature, 300 °C; S-lens radio frequency level, 50 a.u.; sweep gas flow rate, 2 a.u.

The mass spectrometer acquired data from 1 to 25 min of the LC gradient in full-scan HRMS (FullMS)/data dependent MS/MS (ddMS2) mode. The FullMS acquisition range was m/z 80–750 with a resolution of 70,000 at full width at half maximum at m/z 200; automatic gain control (AGC) target was 2 × 105 and maximum injection time (IT) was 200 ms. Up to 5 ddMS2 scans were triggered for each FullMS scan depending on a priority inclusion list of putative metabolites based on in silico predictions and the metabolic fate of β'-phenylfentanyl analogues (Marchei et al., 2018b; Wilde et al., 2019a)(Table 4); ddMS2 isolation window was m/z 1.2 with a resolution of 17,500; normalized collision energy

(NCE) was 30, 35, and 50 a.u.; AGC target was 2 × 105 and maximum IT was 64 ms.

Table 2 *inclusion list for the β'-phenylfentanyl MS/MS data depending acquisition*

Transformation	Molecular formula	[M + H]+ (m/z)	[M – H]- (m/z)
β'-phenylfentanyl	$C_{28}H_{32}N_2O$	413.2587	411.2442
-20C-22H-2N	$C_8H_{10}O$	123.0804	121.0659
-19C-21H-N	$C_9H_{11}NO$	150.0913	148.0768
-19C-22H-2N+O	$C_9H_{10}O_2$	151.0754	149.0608
-15C-13H-N	$C_{13}H_{19}NO$	206.1539	204.1394
-13C-17H-N	$C_{15}H_{15}NO$	226.1226	224.1081
-13C-17H-N+O	$C_{15}H_{15}NO_2$	242.1176	240.1030
-12C-15H-N+O	$C_{16}H_{17}NO_2$	256.1332	254.1187
-13C-17H-N+2O	$C_{15}H_{15}NO_3$	258.1125	256.0979
-13C-15H-N+2O	$C_{15}H_{17}NO_3$	260.1281	258.1136
-9C-8H-O	$C_{19}H_{24}N_2$	281.2012	279.1867
-9C-8H	$C_{19}H_{24}N_2O$	297.1961	295.1816
-8C-8H	$C_{20}H_{24}N_2O$	309.1961	307.1816
-8C-6H	$C_{20}H_{26}N_2O$	311.2118	309.1972
-9C-8H+O	$C_{19}H_{24}N_2O_2$	313.1911	311.1765
-9C-6H+O	$C_{19}H_{26}N_2O_2$	315.2067	313.1922
-13C-17H-N+4O+S	$C_{15}H_{15}NO_5S$	322.0744	320.0598
-8C-8H+O	$C_{20}H_{24}N_2O_2$	325.1911	323.1765
-7C-6H+O	$C_{21}H_{26}N_2O_2$	339.2067	337.1922
-8C-8H+2O	$C_{20}H_{24}N_2O_3$	341.1860	339.1714
-8C-6H+2O	$C_{20}H_{26}N_2O_3$	343.2016	341.1871
-9C-8H+3O+S	$C_{19}H_{24}N_2O_4S$	377.1530	375.1384
-8C-8H+4O+S	$C_{20}H_{24}N_2O_5S$	405.1479	403.1333
-2H	$C_{28}H_{30}N_2O$	411.2431	409.2285
-7C-9H-N+7O	$C_{21}H_{23}NO_8$	418.1496	416.1351
-2H+O	$C_{28}H_{30}N_2O_2$	427.2380	425.2235
+O	$C_{28}H_{32}N_2O_2$	429.2537	427.2391
+C+2H+O	$C_{29}H_{34}N_2O_2$	443.2693	441.2548
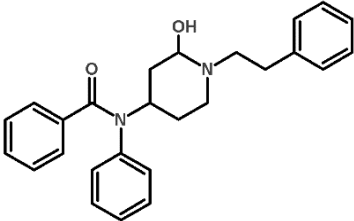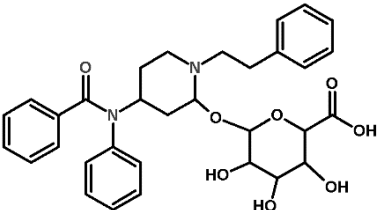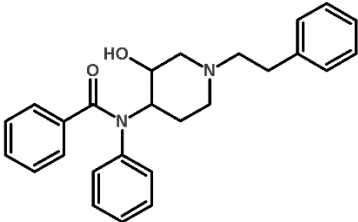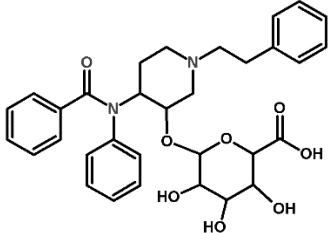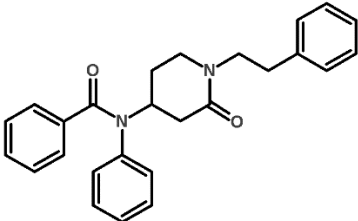
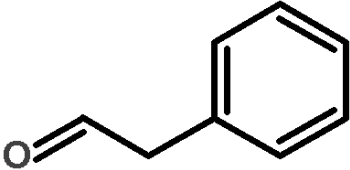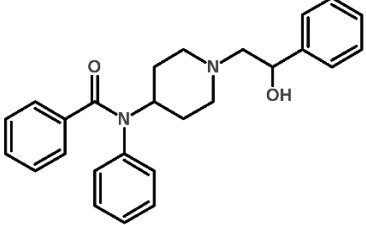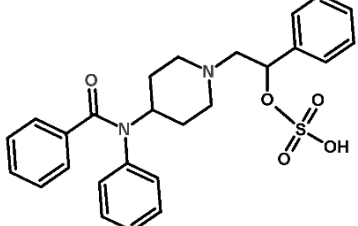|			
+2O	$C_{28}H_{32}N_2O_3$	445.2486	443.2340
+2H+2O	$C_{28}H_{34}N_2O_3$	447.2642	445.2497
+C+2H+2O	$C_{29}H_{34}N_2O_3$	459.2642	457.2497
-3C+6O	$C_{25}H_{32}N_2O_7$	473.2282	471.2137
-2C+7O	$C_{26}H_{32}N_2O_8$	501.2231	499.2086
4O+S	$C_{28}H_{32}N_2O_5S$	509.2105	507.1959
+5O+S	$C_{28}H_{32}N_2O_6S$	525.2054	523.1908
+6C+8H+7O	$C_{34}H_{40}N_2O_8$	605.2857	603.2712
+6C+8H+8O	$C_{34}H_{40}N_2O_9$	621.2807	619.2661
+7C+10H+8O	$C_{35}H_{42}N_2O_9$	635.2963	633.2818
10C+17H+3N+7O+S	$C_{38}H_{49}N_5O_8S$	736.3375	734.3229
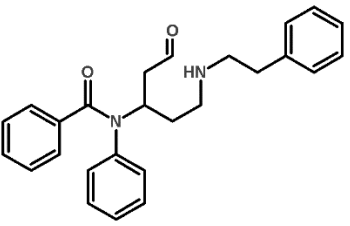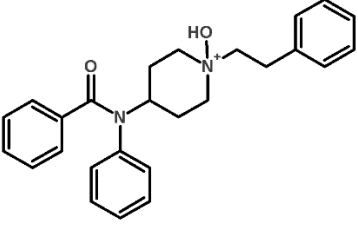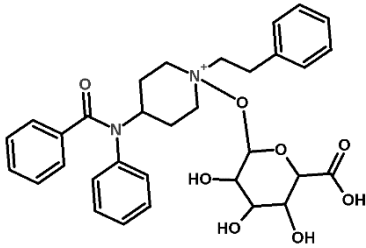
2.1.7   In silico metabolites prediction
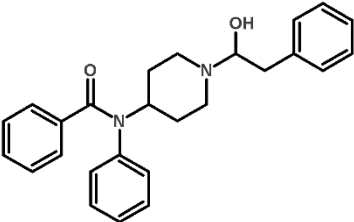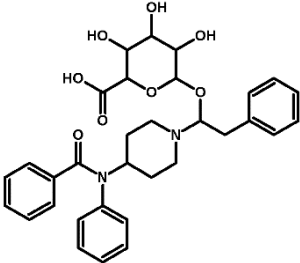
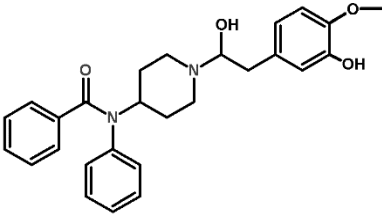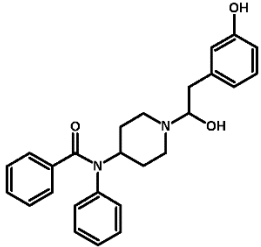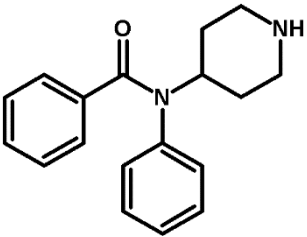Phenylfentanyl and β'phenylfentanyl putative metabolites were predicted using online GLORYx freeware (de Bruyn Kops et al., 2021), available at the New E-Resource for Drug Discovery (NERDD) web portal (Stork et al., 2019). Briefly, GLORYx allows the prediction and ranking of phase I and phase II metabolites through the integration of a machine learning-based sites of reaction prediction to set reaction rules (de Bruyn Kops et al., 2021).

The metabolite list was generated using the phenylfentanyl SMILES string and the "phase I and phase II metabolism" option. Phenylfentanyl and β'phenylfentanyl metabolites with a score higher than 0.30 and 0.25, respectively, were selected and reprocessed to simulate a second-step metabolism reaction; the second-generation metabolite score was multiplied to the first-generation metabolite score and resulting scores higher than 0.18 were considered.

Table 3 Molecular strucure, elemnental composition, metabolic reaction, and predictive score of in silico predicted phentlfentanyl metabolites

Predicted Metabolite	Structure	Elemental composition / Metabolic reaction / Score (combined score)
PM1		$C_{26}H_{28}N_2O_2$ Hydroxylation S: 0.43
PM1.1		$C_{32}H_{36}N_2O_8$ O-Glucuronidation S: 0.47 (0.20)
PM2		$C_{26}H_{28}N_2O_2$ Hydroxylation S: 0.43
PM2.1		$C_{32}H_{36}N_2O_8$ O-Glucuronidation S: 0.79 (0.34)
PM3		$C_{26}H_{26}N_2O_2$ Oxidation S: 0.43

PM4		$C_{26}H_{28}N_2O_2$ Oxidation + piperidine opening S: 0.43
PM5		$C_{26}H_{29}N_2O_2$ N-Oxidation S: 0.43
PM5.1		$C_{32}H_{37}N_2O_8$ O-Glucuronidation S: 0.61 (0.26)
PM6		C_8H_8O N-Dealkylation S: 0.42
PM7		$C_{26}H_{28}N_2O_2$ Hydroxylation S: 0.42
PM7.1		$C_{26}H_{28}N_2O_5S$ O-Sulfation S: 0.64 (0.28)

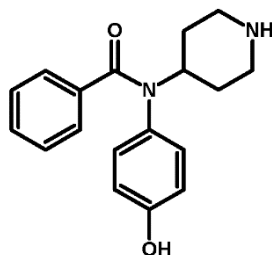|		
PM8		$C_{26}H_{28}N_2O_2$ Hydroxylation S: 0.42
	PM8.1	$C_{32}H_{36}N_2O_8$ O-Glucuronidation S: 0.56 (0.24)
	PM8.2	$C_{26}H_{28}N_2O_3$ Hydroxylation S: 0.42 (0.18)
	PM8.3	$C_{27}H_{30}N_2O_4$ Hydroxylation + O-Methylation S: 0.42 (0.18)
	PM8.4	$C_{26}H_{28}N_2O_3$ Hydroxylation S: 0.42 (0.18)
PM9		$C_{18}H_{20}N_2O$ N-Dealkylation S: 0.42
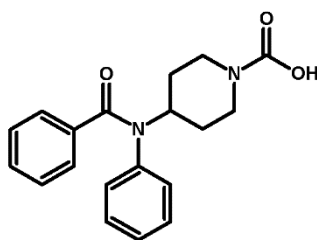
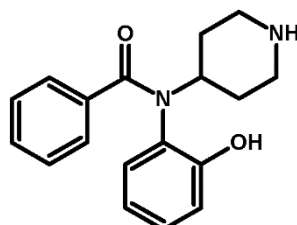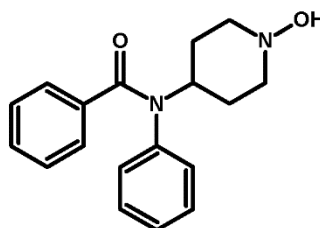|		
PM9.1		$C_{19}H_{20}N_2O_3$ Carboxylation S: 0.94 (0.39)
PM9.2		$C_{18}H_{20}N_2O_2$ Hydroxylation S: 0.44 (0.18)
PM9.3		$C_{18}H_{20}N_2O_2$ Hydroxylation S: 0.44 (0.18)
PM9.4		$C_{18}H_{20}N_2O_2$ Hydroxylation S: 0.44 (0.18)
PM9.5		$C_{18}H_{18}N_2O_2$ Oxidation S: 0.44 (0.18)
PM9.6		$C_{18}H_{20}N_2O_2$ Oxidation + piperidine opening S: 0.44 (0.18)
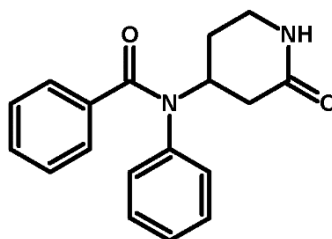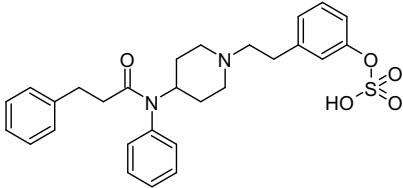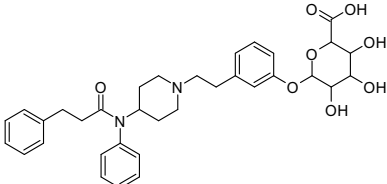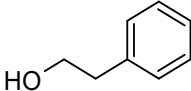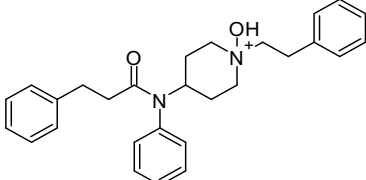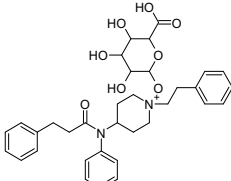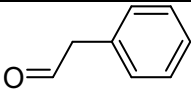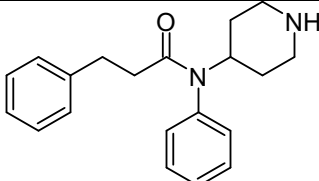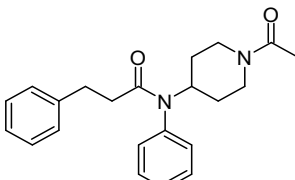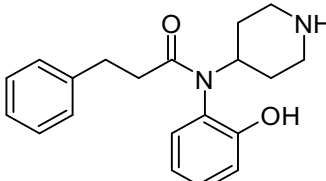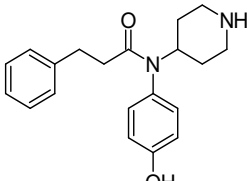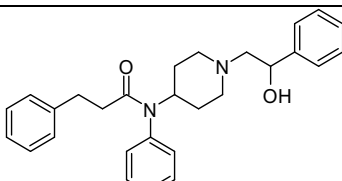
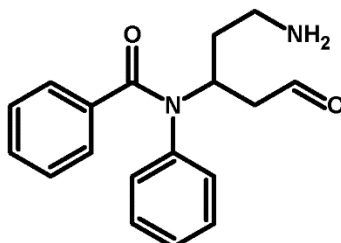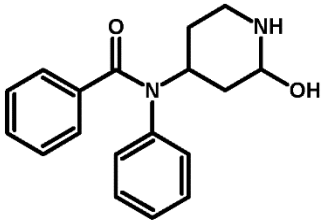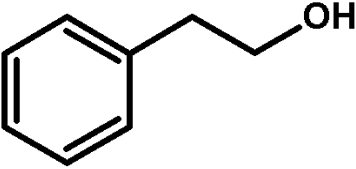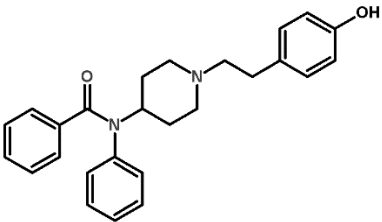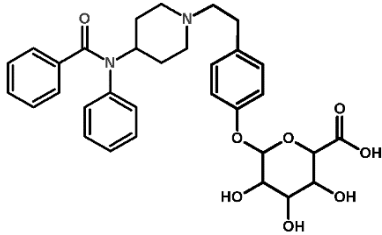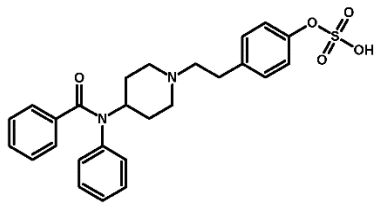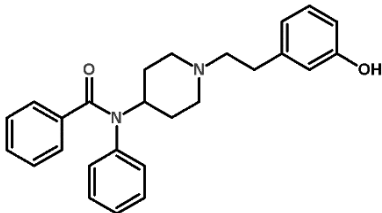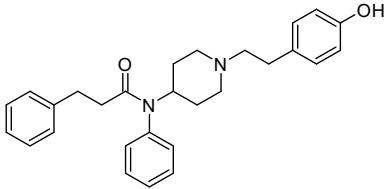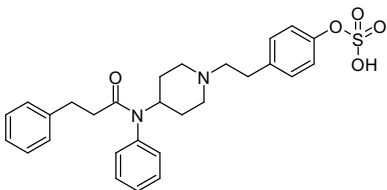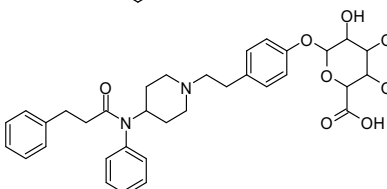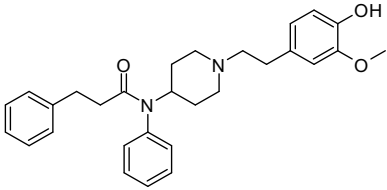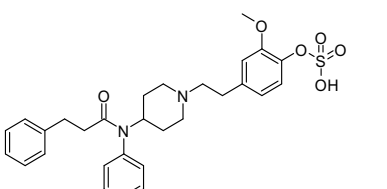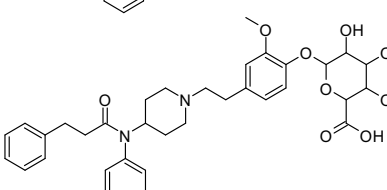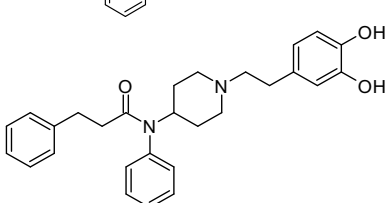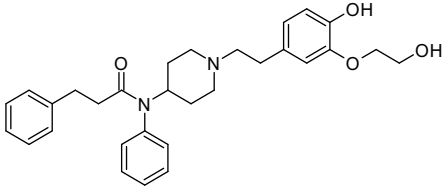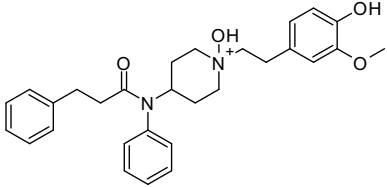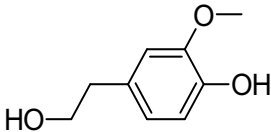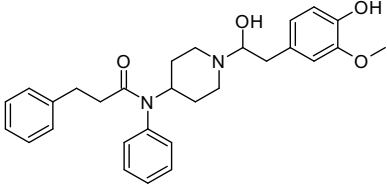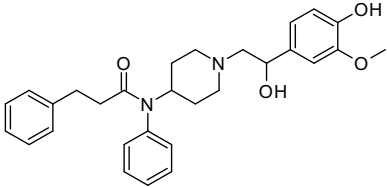|		
PM9.7		$C_{18}H_{20}N_2O_2$ Hydroxylation S: 0.44 (0.18)
PM10		$C_8H_{10}O$ N-Dealkylation S: 0.42
PM11		$C_{26}H_{28}N_2O_2$ Hydroxylation S: 0.30
PM11.1		$C_{32}H_{36}N_2O_8$ O-Glucuronidation S: 0.96 (0.29)
PM11.2		$C_{26}H_{28}N_2O_5S$ O-Sulfation S: 0.96 (0.29)
PM12		$C_{26}H_{28}N_2O_2$ Hydroxylation S: 0.30
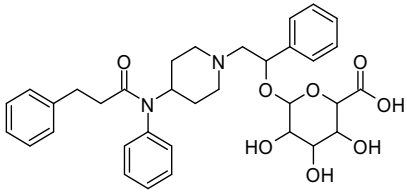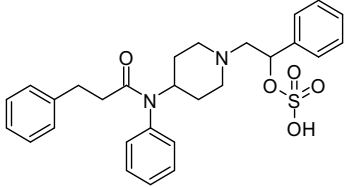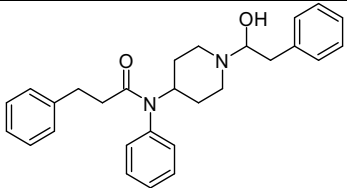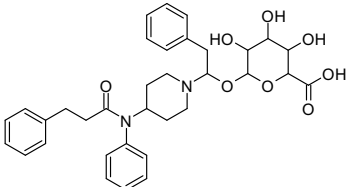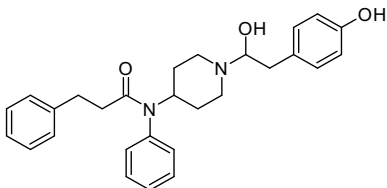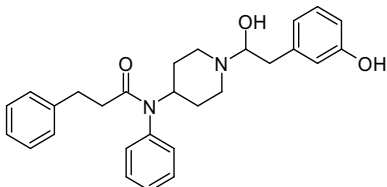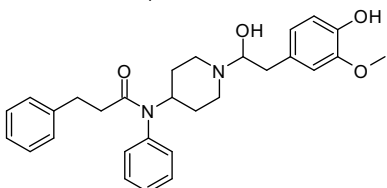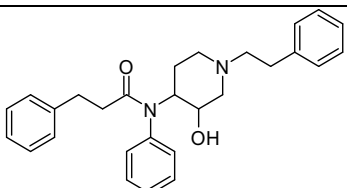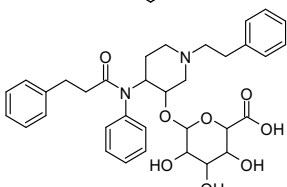
PM12.1		$C_{26}H_{28}N_2O_5S$ O-Sulfation S: 0.97 (0.29)
PM12.2		$C_{32}H_{36}N_2O_8$ O-Glucuronidation S: 0.94 (0.28)
PM13		$C_{27}H_{30}N_2O_3$ Dihydroxylation +O-Methylation S: 0.30
PM13.1		$C_{27}H_{30}N_2O_6S$ O-Sulfation S: 0.96 (0.29)
PM13.2		$C_{33}H_{38}N_2O_9$ O-Glucuronidation S: 0.90 (0.27)
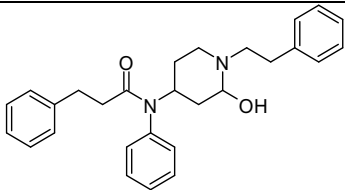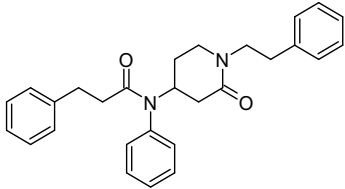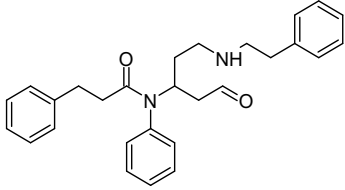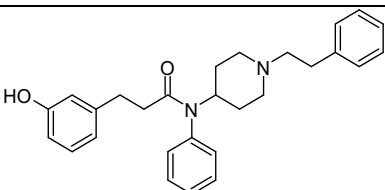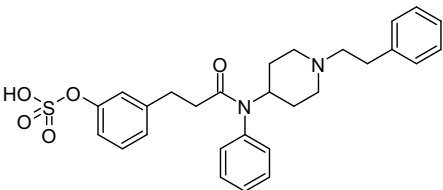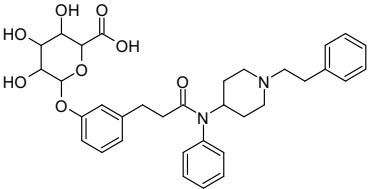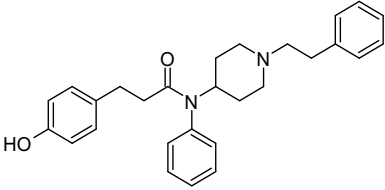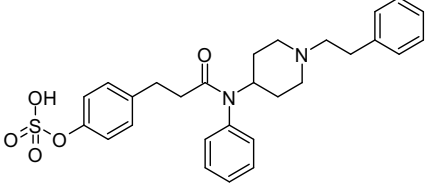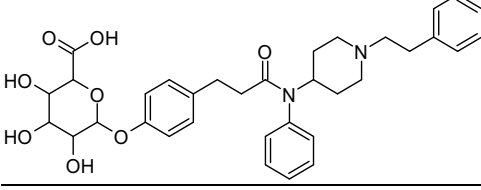
Table 4 β'-phenylfentanyl putative metabolites predicted with online GLORYx freeware and their prediction score (adjusted score for second-generation metabolites).
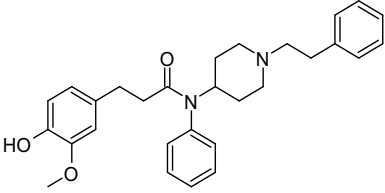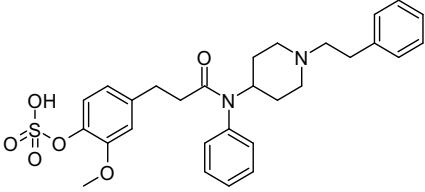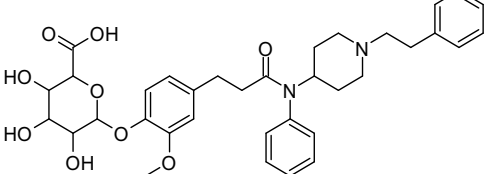
Predicted metabolite (PM')	Structure	Formula; reaction; score (combined score)
PM'1		$C_{28}H_{32}N_2O_2$ Hydroxylation 0.44
PM'1.1		$C_{28}H_{32}N_2O_5S$ O-Sulfation 0.96 (0.42)
PM'1.2		$C_{34}H_{40}N_2O_8$ O-Glucuronidation 0.85 (0.37)
PM'2		$C_{29}H_{34}N_2O_3$ Hydroxylation + O-Methylation 0.44
PM'2.1		$C_{29}H_{34}N_2O_6S$ O-Sulfation 0.96 (0.42)
PM'2.2		$C_{35}H_{42}N_2O_9$ O-Glucuronidation 0.64 (0.28)
PM'2.3		$C_{28}H_{32}N_2O_3$ O-Demethylation 0.45 (0.20)

PM'2.4		$C_{30}H_{36}N_2O_4$ O-Ethylation + Hydroxylation 0.45 (0.20)
PM'2.5		$C_{29}H_{35}N_2O_4$ N-Oxidation 0.42 (0.18)
PM'2.6		$C_9H_{12}O_3$ N-Dealkylation 0.42 (0.18)
PM'2.7		$C_{29}H_{34}N_2O_4$ Hydroxylation 0.42 (0.18)
PM'2.8		$C_{29}H_{34}N_2O_4$ Hydroxylation 0.42 (0.18)
PM'2.9		$C_9H_{10}O_3$ N-Dealkylation 0.42 (0.18)
PM'3		$C_{28}H_{32}N_2O_2$ Hydroxylation 0.44
PM'3.1		$C_{28}H_{32}N_2O_5S$ O-Sulfation 0.97 (0.43)
PM'3.2		$C_{34}H_{40}N_2O_8$ O-Glucuronidation 0.86 (0.38)

PM'4		$C_8H_{10}O$ N-Dealkylation 0.34
PM'5		$C_{29}H_{35}N_2O_4$ N-Oxidation 0.34
PM'5.1		$C_{34}H_{41}N_2O_8$ O-Glucuronidation 0.59 (0.20)
PM'6		C_8H_8O N-Dealkylation 0.34
PM'7		$C_{20}H_{24}N_2O$ N-Dealkylation 0.34
PM'7.1		$C_{22}H_{26}N_2O_2$ N-Acylation 0.93 (0.32)
PM'7.2		$C_{20}H_{24}N_2O_2$ Hydroxylation 0.53 (0.18)
PM'7.3		$C_{20}H_{24}N_2O_2$ Hydroxylation 0.53 (0.18)
PM'8		$C_{28}H_{32}N_2O_2$ Hydroxylation 0.34

PM'8.1		C$_{34}$H$_{40}$N$_2$O$_8$ O-Glucuronidation 0.86 (0.29)
PM'8.2		C$_{28}$H$_{32}$N$_2$O$_5$S O-Sulfation 0.66 (0.22)
PM'9		C$_{28}$H$_{32}$N$_2$O$_2$ Hydroxylation 0.34
PM'9.1		C$_{34}$H$_{40}$N$_2$O$_8$ O-Glucuronidation 0.56 (0.19)
PM'9.2		C$_{28}$H$_{32}$N$_2$O$_3$ Hydroxylation 0.55 (0.19)
PM'9.3		C$_{28}$H$_{32}$N$_2$O$_3$ Hydroxylation 0.55 (0.19)
PM'9.4		C$_{29}$H$_{34}$N$_2$O$_4$ Hydroxylation + O-Methylation 0.55 (0.19)
PM'10		C$_{28}$H$_{32}$N$_2$O$_2$ Hydroxylation 0.31
PM'10.1		C$_{34}$H$_{40}$N$_2$O$_8$ O-Glucuronidation 0.79 (0.24)

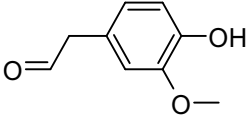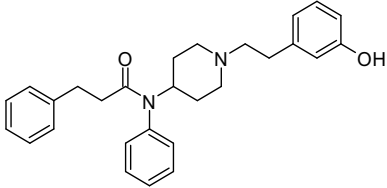|		
PM'11		$C_{28}H_{32}N_2O_2$ Hydroxylation 0.31
PM'12		$C_{28}H_{30}N_2O_2$ Oxidation 0.31
PM'13		$C_{28}H_{30}N_2O_2$ Oxidation + Piperidine opening 0.31
PM'14		$C_{28}H_{32}N_2O_2$ Hydroxylation 0.30
PM'14.1		$C_{28}H_{32}N_2O_5S$ O-Sulfation 0.97 (0.29)
PM'14.2		$C_{34}H_{40}N_2O_8$ O-Glucuronidation 0.86 (0.26)
PM'15		$C_{28}H_{32}N_2O_2$ Hydroxylation 0.30
PM'15.1		$C_{28}H_{32}N_2O_5S$ O-Sulfation 0.96 (0.29)
PM'15.2		$C_{34}H_{40}N_2O_8$ O-Glucuronidation 0.85 (0.26)

PM'16		$C_{29}H_{34}N_2O_3$ Hydroxylation + O-Methylation 0.44
PM'16.1		$C_{29}H_{34}N_2O_6S$ O-Sulfation 0.96 (0.29)
PM'16.2		$C_{35}H_{42}N_2O_9$ O-Glucuronidation 0.64 (0.19)

2.1.8 Data mining

An innovative dual untargeted/targeted approach was adopted to process the data using Compound Discoverer software from Thermo Scientific, version 3.2.0.421 (Annagiulia Di Trana et al., 2021). The development of this specific workflow allowed the automatic extraction of relevant mass spectra and their comparison to a list of expected compounds and online databases (Fig. 2). The same workflow was applied for the data mining of both the

2.1.9 Data pre-processing

The raw data from samples and controls were processed simultaneously. All spectra were selected, and the retention times of the relative chromatographic peaks were aligned between the files to facilitate comparison, following an adaptive curve model, with a maximum shift of 0.1 min and a mass tolerance of 5 ppm. A base peak chromatogram was generated in full-scan HRMS in positive- and negative-ion modes. Aligned spectra were then further processed using a targeted/untargeted approach.
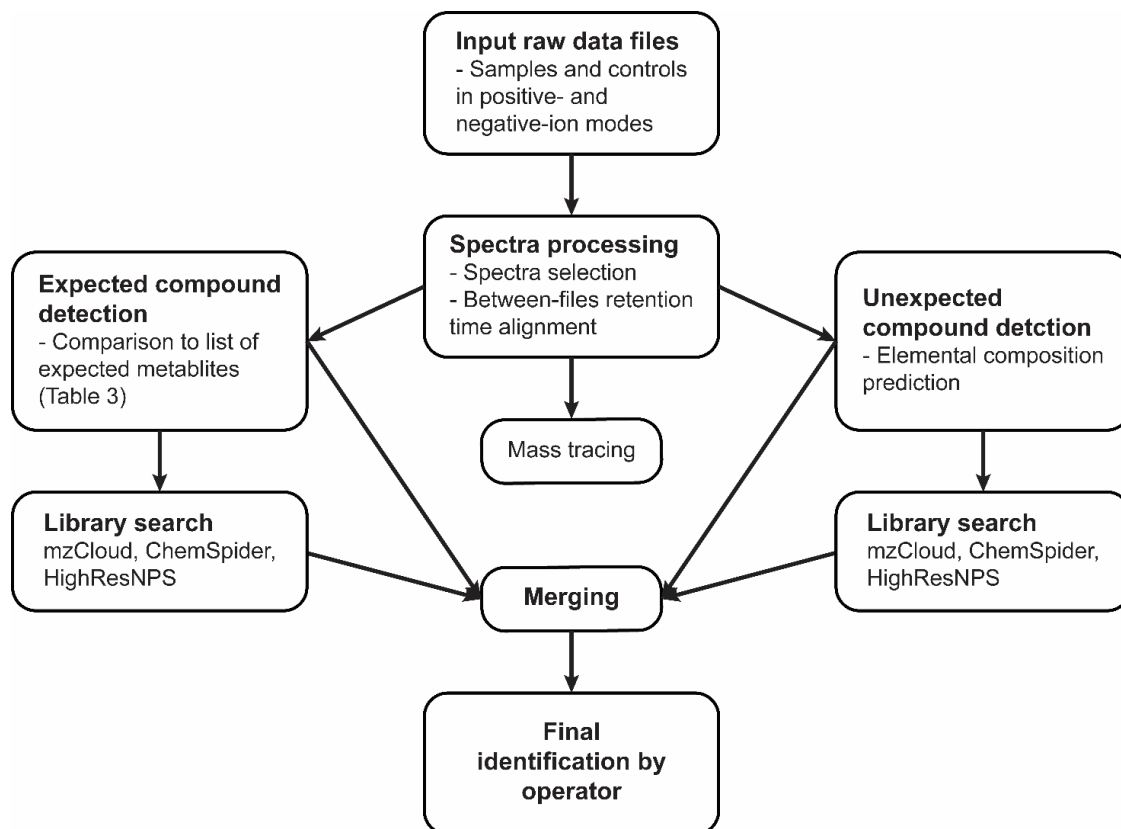
Figura 2 *LC-HRMS/MS raw data processing workflow*

2.1.9.1 Untargeted data mining

Chromatographic peaks with an intensity higher than 10^6, a signal/noise ratio higher than 3, and a 30% intensity tolerance for isotopes were selected; peaks with fewer than 3 scans or larger than 0.5 min were excluded. When applicable, $[M+H]^+$, $[M+Na]^+$, $[M+K]^+$, $[M+NH_4]^+$, $[M+H-H_2O]^+$, $[M-H]^-$, $[M+Cl]^-$, and $[M+HCOOH]^-$ adducts were grouped (5-ppm mass tolerance) and $[M+H]^+$ adduct was used as base ion. Unknown compounds were grouped across the data files with a 5-ppm mass tolerance and a 0.1-min retention time tolerance, and their elemental composition was predicted within a C_7H_6 to $C_{36}H_{50}N_5O_{12}S_2$ range. ddMS^2 spectra and molecular formulas were compared to selected libraries: mzCloud (Drugs of Abuse/Illegal Drugs database), ChemSpider (Cayman Chemical and DrugBank databases), and HighResNPS. mzCloud is a database containing the mass spectra and product-ion spectra at different collision energies of approximately 20,000 compounds in the fields of life sciences, metabolomics, pharmaceutical research, toxicology, forensic investigations,

environmental analysis, food control, and industrial applications (HighChem LLC, 2021). ChemSpider is a database containing various information on more than 100 million chemicals from over 270 data sources (Royal society of chemistry, 2021). HighResNPS is a crowd-sourced HRMS database containing the mass spectra of NPS with over 5200 entries, among which 2100 are unique (Mardal et al., 2019).

2.1.9.2 Targeted data mining

A list of theoretical metabolites was generated by combining probable phase I and phase II metabolic transformations, following the settings displayed in Table 2. Chromatographic peaks with an intensity higher than 5×10^3, a signal/noise ratio higher than 3, and a 30% intensity tolerance for isotopes were compared to the list of expected compounds with a 5-ppm mass tolerance. Compounds were grouped across the data files with a 0.1-min retention time tolerance and compared to mzCloud, ChemSpider, and HighResNPS libraries.

Table 5 Compound Discoverer settings for generating a list of putative phenylfentanyl metabolites

Phase I reactions	Amide hydrolysis (-7C -5H -O → +H or -19C -23H -2N → +H +O)
	Desaturation (-2H →)
	Dihydrodiol formation (→ +2H +2O)
	N-Dealkylation phenethyl (-8C -9H → +H)
	N-Dealkylation phenethylpiperidine (-13C -18H -N → +H or -13C -10H -N -O → +H +O)
	Oxidation (→ +O)
	Oxidative Deamination to alcohol (-2H -N → +H +O)
	Oxidative Deamination to ketone (-3H -N → +O)
	Reduction (→ +2H)
Phase II reactions	Acetylation (-H → +2C +3H +O)
	Glucuronide Conjugation (-H → +6C +9H +6O)
	Glutathione Conjugation (→ +10C +17H +3N +6O +S)
	Methylation (-H → +C +3H)
	Sulfation (-H → +H +3O +S)

Maximum number of dealkylations	3
Maximum number of phase II reactions	2
Maximum number of reactions	5

2.1.9.3 Final identification

The results from untargeted and targeted data mining approaches were merged, and the compounds detected in controls with a similar or higher intensity than those detected in phenylfentanyl incubations were filtered out. The results were finally screened by the operator for final identification and structural elucidation.

2.2 Results and discussion

2.2.1 Analytical strategy

A long 15-cm LC column was chosen for the chromatographic separation to achieve better separation of potential metabolites and matrix components with a good chromatographic resolution. Considering the three phenylfentanyl aromatic groups, a biphenyl stationary phase was employed to achieve good retention, and the gradient was optimized to delay phenylfentanyl retention time, putative metabolites being predominantly more polar than the parent drug and expected to elute earlier (Carlier et al., 2016; X. Diao & Huestis, 2017; Xingxing Diao et al., 2017, 2018). Source settings were then optimized injecting phenylfentanyl reference standard in the LC conditions of the analysis, although the behavior of metabolites is hardly predictable in these particular conditions (Carlier et al., 2021a). Notably, the capillary temperature was maintained at the

lowest recommended value to limit in-source fragmentation of metabolites, which is often observed with glucuronide conjugates (Carlier et al., 2018). NCE was also optimized during the infusion of phenylfentanyl reference standard in MPA:MPB (50:50 v/v) into the HESI source to generate the most relevant fragments for structure elucidation.

Phenylfentanyl fragmentation pattern was consistent with the scientific literature (Figure 3). Ion m/z 188.1433 was produced by the phenethylpiperidine moiety of the molecule and was the fragment with the most intense signal; further fragmentation produced ions m/z 134.0963 and 146.0963, due to the cleavage of the piperidine ring, and ion m/z 105.0698, produced by the phenethyl fragment. Ion m/z 105.0335 was also abundant and was produced by the benzaldehyde group of phenylfentanyl. Interestingly, as opposed to HRMS, classic MS would not allow to discriminate m/z 105.0698 and 105.0335, which are crucial fragments for the structure elucidation of several phenylfentanyl metabolites. Ion m/z 264.1383 was a minor fragment.
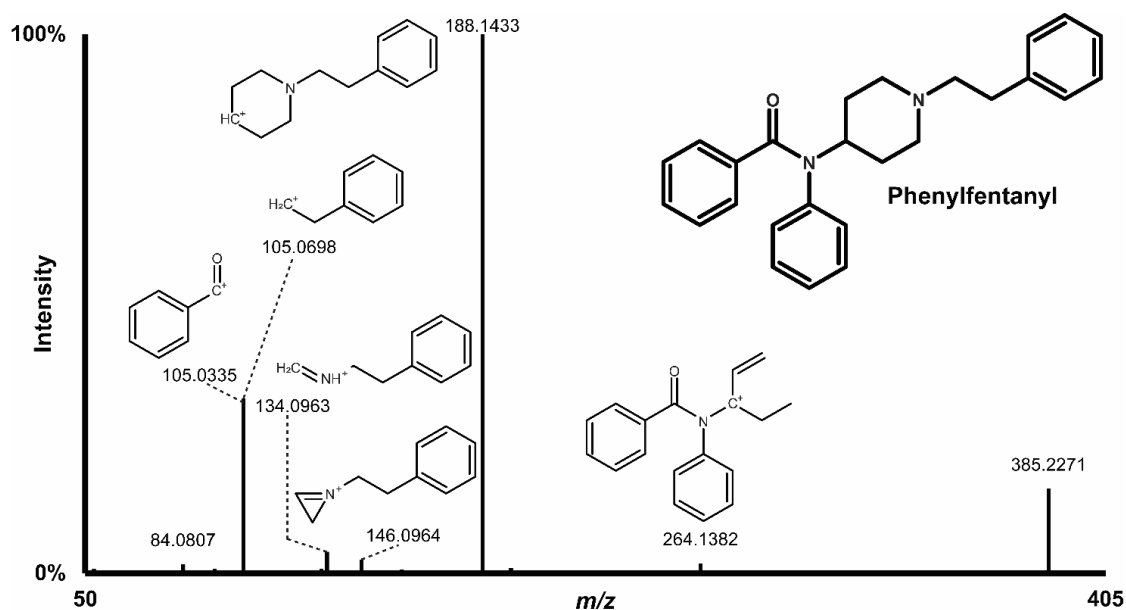
Figure 1 Phenylfentanyl MS/MS spectrum and suggested fragments

Whereas, β'-phenylfentanyl's fragmentation pattern was consistent with the scientific literature (Figure 4). Similarly, Ion m/z 188.1434 was produced by the phenylethylpiperidine moiety of the molecule and was the fragment with the most intense signal; the second most abundant fragment was the ion m/z 105.0699

produced by the two phenethyl portions, proving crucial for the elucidation of several metabolites' structures, together with the ion m/z 281.2011, characteristic of the 4-ANPP. Further fragmentation produced ions m/z 132.0807, 134.0964, 146.0964 and 292.1695, obtained from the cleavage of the piperidine ring.
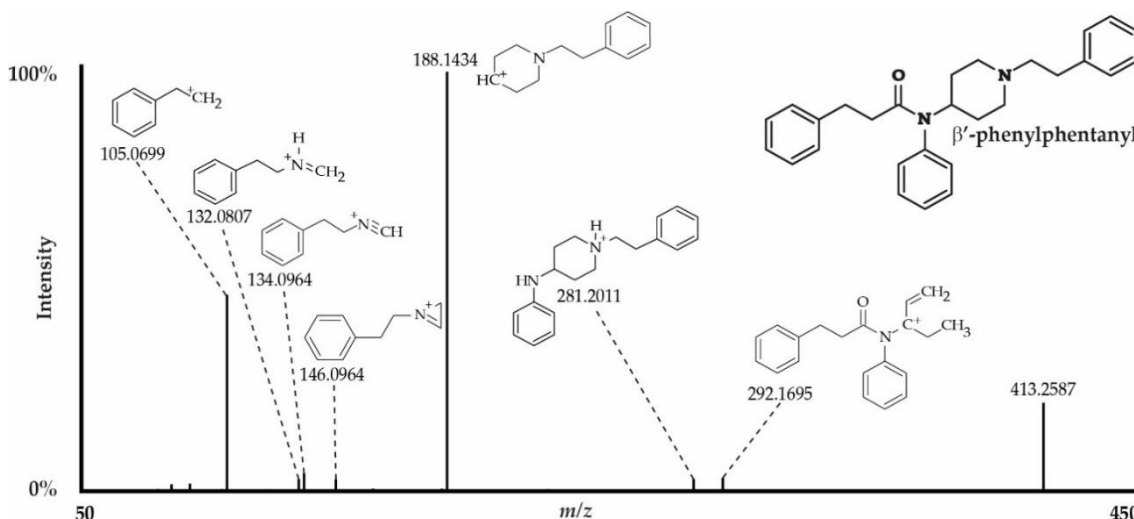
Figure 2 B'-phenylfentanyl MS/MS spectrum and suggested fragments

Although UV detection would more accurately reflect the relative amount of phenylfentanyl metabolites, the sensitivity of HRMS is required to detect the low concentrations in the present experiments.

We designed an original data-mining strategy using Compound Discoverer to quickly and accurately identify the metabolites of a substance. Raw files from incubations and controls were automatically processed within 7 h.

Through the untargeted analysis, 7103 and 3215 compounds were detected in the 3-h incubate with hepatocytes and phenylfentanyl in positive- and negative-ion modes, respectively. Through the targeted analysis, a list of 30,049 theoretical combinations of metabolic transformations was generated, allowing for the detection of 11,683 and 7912 compounds in the 3-h incubate in positive- and negative-ion modes, respectively. A total of 89,469 compounds were detected in all data files after merging results (controls and incubates in positive- and negative-ion modes), including phenylfentanyl metabolites, matrix components, and impurities. Backgrounds compounds were filtered out using controls to rule out interferences and non-enzymatic reactions. The compounds with a chromatographic peak area lower than 0.5% of that of the phenylfentanyl

metabolite with the most intense signal in the 3-h incubate (3.9×10^7) were also filtered out. The list was therefore finally reduced to 115 potential phenylfentanyl metabolites that were manually checked by the operators. The targeted/untargeted strategy employed in this study ensures that any compounds related to phenylfentanyl, even the metabolites produced through unexpected reactions, were identified.

Notably, the β'-phenylfentanyl data analysis resulted in higher number of results to be manually screened, suggesting a more extensive metabolism at the same condition.

Through the untargeted analysis, 22187 compounds were detected in the 3-h incubate with hepatocytes and β'-phenylfentanyl in positive and negative-ion modes, respectively. Through the targeted analysis, a list of 18492 theoretical combinations of metabolic transformations was generated, allowing for the detection of 120834 compounds in the 3-h incubate in positive and negative-ion modes. A total of 46471 compounds were detected in all data files after merging results (controls and incubates in positive- and negative-ion modes), including β'-phenylfentanyl metabolites, matrix components, and impurities. Backgrounds compounds were filtered out using controls to rule out interferences and non-enzymatic reactions. The list was therefore finally reduced to 161 potential β'-phenylfentanyl's metabolites that were manually checked by the operators.

2.2.2 Phenylfentanyl e b'-phenylfentanyl metabolites in human hepatocytes

Phenylfentanyl and β'-phenylfentanyl were not detected in negative-ion mode, but they were automatically identified in positive-ion mode through the targeted and untargeted (mzCloud and HigResNPS libraries) analyses. Phenylfentanyl peak area in the 0-h incubate with hepatocytes was 1.74×10^{10}, consistent with the incubation samples without hepatocytes and approximately 35 times higher than that of the 3-h incubate with hepatocytes. β'-phenylfentanyl's peak area in the 0-h incubate with hepatocytes was 2.08 x 1010, consistent with the incubation samples without hepatocytes and approximately 15 times higher

than that of the 3-h incubate with hepatocytes. Thirteen phenylfentanyl metabolites and 27 β'-phenylfentanyl metabolites were identified and were listed from M1 to M'13 and M'1 to M'23, respectively, by ascending retention time (Fig. 5). The results and spectra were reported to mzCloud and HighResNPS databases to implement their freely available libraries for screening purposes.
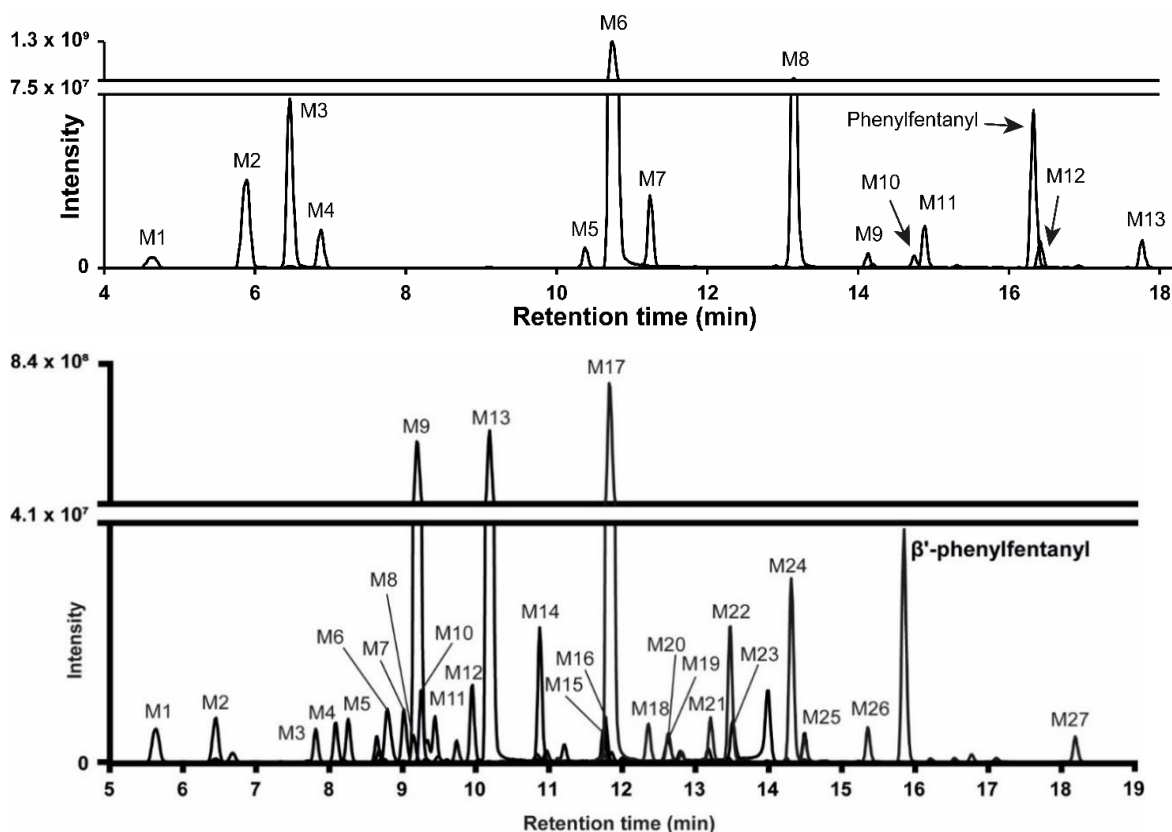
Figure 3 Combined extracted ion chromatogram of phenylfentanyl and metabolites and β'-phenylfentanyl obtained after 3-h incubation with human hepatocytes. Mass tolerance, 5 ppm

The occurred metabolic reactions were similar between the two fentanyl analogues, although some important differences were noticed. The major phase I metabolic transformations included N-dealkylation at the piperidine group (M2, M4, M6, and M9, and M'1-M'5, M'7, M'9, M'11-M'13, M'17, M'19, M'23 and M'25), hydroxylation at the aniline (M1 and M3) and the phenethylpiperidine (M1, M5, M7, M10, M11, and M12) groups, N-oxidation of the piperidine ring (M4, M10, M12, and M13 and M'26); hydroxylation was common in b'-phenylfentanyl metabolism (M'7, M'9, M'11, M'12, M'15, M'18, M'19, M'21 and M'22). The amide

31

hydrolysis was observed only for phenylfentanyl (M1, M3, M5, M7, and M8), while glucuronidation (M'3-M'5, M16 and M20), O-methylation (M'3 and M'10), dihydrodiol formation (M', M'6, M'8 and M'14) and N-oxidation (M'26) were

Lactam formation was a minor phase I reaction in phenylfentanyl metabolic pattern (M9), while ketone/lactame formation produced 6 β'phenylfentanyl metabolites (M'13, M'15, M'21, M'23-M'26 and M'27). Although phase II metabolites were were reported in the metabolism of fentanyl analogues *in vitro* and *in vivo* (Kanamori et al., 2018; Watanabe et al., 2017; Wilde et al., 2019a), phenylfentanyl phase II reactions were infrequent and with an intensity below the intensity threshold established (3.9×10^7, see subsection "3.1. Analytical strategy"). Conversely, phase II metabolites were identified in b'-phenylfentanyl incubates, in particular glucuronic acid conjugates (M'3-M'5, M16 and M20).

M1–M13 metabolic transformation, $[M+H]^+$ accurate mass, elemental composition, retention time, and chromatographic peak areas (extracted ion chromatogram) are reported in Table 6. Thanks to stringent HRMS conditions, phenylfentanyl and metabolites' mass accuracy was always within ±0.75 ppm in positive-ion mode. Phenylfentanyl and β'phenylfentanyl metabolic fate are proposed in figure 6 and 7, respectively and the metabolites' fragmentation pattern is displayed in figures 8-12.

Table 6 *Metabolic transformation, retention time, accurate mass of molecular ion hydrogen adducts in positive-ion mode, elemental composition, chromatographic peak area, and matching in silico predicted metabolites (Table 4) of phenylfentanyl and metabolites after 3-h incubation with human hepatocytes.*

Name	Metabolic transformation	Rt (min)	[M+H]$^+$ (*m/z*)	Elemental composition	Peak Area after 3-h incubation	Matching predicted metabolites
phenylfentanyl						
M1	Amide hydrolysis + Dihydroxylation (phenethylpiperidine & aniline)	4.66	313.1913	$C_{19}H_{24}N_2O_2$	3.97×10^7	-
M2	N-Dealkylation (piperidine)	5.89	206.1541	$C_{13}H_{19}NO$	3.36×10^8	-
M3	Amide hydrolysis + Hydroxylation (aniline)	6.47	297.1962	$C_{19}H_{24}N_2O$	5.40×10^8	-
M4	N-dealkylation (piperidine) + N-Oxidation (piperidine)	6.88	222.1489	$C_{13}H_{19}NO_2$	1.15×10^8	-
M5	Amide hydrolysis + Hydroxylation (phenyl)	10.38	297.1962	$C_{19}H_{24}N_2O$	5.48×10^7	-
M6	N-dealkylation (piperidine)	10.74	281.1646	$C_{18}H_{20}N_2O$	7.85×10^9	PM9
M7	Amide hydrolysis + Hydroxylation (piperidine)	11.24	297.1962	$C_{19}H_{24}N_2O$	1.96×10^8	-
M8	Amide hydrolysis	13.15	281.2012	$C_{19}H_{24}N_2$	9.84×10^8	-

M9	N-dealkylation (piperidine) + Oxidation (piperidine)	14.12	295.1441	$C_{18}H_{18}N_2O_2$	6.34×10^7	PM9.5
M10	Hydroxylation (phenyl) + N-Oxidation (piperidine)	14.74	417.2173	$C_{26}H_{28}N_2O_3$	3.93×10^7	-
M11	Hydroxylation (ethyl)	14.88	401.2224	$C_{26}H_{28}N_2O_2$	1.36×10^8	PM7, PM8
Phenylfentanyl	**Parent**	**16.26**	**385.2272**	**$C_{26}H_{28}N_2O$**	**5.04×10^8**	**NA**
M12	Hydroxylation (phenyl) + N-Oxidation (piperidine)	16.42	417.2173	$C_{26}H_{28}N_2O_3$	7.70×10^7	-
M13	N-Oxidation (piperidine)	17.76	401.2224	$C_{26}H_{28}N_2O_2$	8.59×10^7	PM5
β'phenylfentanyl						
M'1	N-Dealkylation (amide)	5.63	206.1541	$C_{13}H_{19}N_1O_1$	4.49×10^7	-
M'2	N-Dealkylation (phenethyl) + Dihydrodiol formation (left ring)	6.45	343.0180	$C_{20}H_{26}N_2O_3$	5.23×10^7	-
M'3	N-Dealkylation (phenethyl) + Dihydroxilation + Methylation + Glucuronidation	7.81	531.2342	$C_{27}H_{34}N_2O_9$	3.24×10^7	-
M'4	N-Dealkylation (phenethyl) + Hydroxylation (left	8.09	501.2234	$C_{26}H_{32}N_2O_8$	4.03×10^7	-

	ring) + Glucuronidation					
M'5	Hydroxylation (o-piperidine) + Glucuronidation	8.26	501.2233	$C_{26}H_{32}N_2O_8$	4.30×10^7	-
M'6	Polyhydroxylation (left phenylethyl moiety)	8.79	481.2697	$C_{28}H_{36}N_2O_5$	7.45×10^7	-
M'7	N-Dealkylation (phenethyl) + Hydroxylation (left ring)	9.02	325.1911	$C_{20}H_{24}N_1O_7$	4.94×10^7	-
M'8	Dihydrodiol formation (left ring) + Hydroxylation (right ring)	9.14	463.2591	$C_{28}H_{34}N_2O_4$	2.73×10^7	-
M'9	N-Dealkylation (phenethyl) + Hydroxylation (left)	9.14	325.1910	$C_{20}H_{24}N_2O_2$	2.07×10^9	-
M'10	N-Dealkylation (phenethyl) + Dihydroxylation (left ring) + Methylation	9.25	355.2016	$C_{21}H_{26}N_2O_3$	6.23×10^7	-
M'11	N-Dealkylation (phenethyl) + Hydroxylation (ring left)	9.44	325.1911	$C_{20}H_{24}N_2O_2$	4.25×10^7	-
M'12	N-Dealkylation (phenethyl) + Hydroxylation (ring left)	9.95	325.1911	$C_{20}H_{24}N_2O_3$	7.02×10^7	-
M'13	N-Dealkylation (phenethyl) + Oxidation (left)	10.18	323.1754	$C_{20}H_{22}N_2O_2$	2.34×10^9	-

M'14	Di-hydrodiol formation (left)	10.87	447.2644	$C_{28}H_{34}N_2O_3$	1.29×10^8	-
M'15	Dihydroxylation (left ring) + Glucuronidation	11.74	621.2806	$C_{34}H_{40}N_2O_9$	3.49×10^7	-
M'16	Hydroxylation (left) + Glucuronidation	11.76	605.2859	$C_{34}H_{40}N_2O_8$	4.80×10^7	-
M'17	N-Dealkylation (phenethyl)	11.82	309.1960	$C_{20}H_{24}N_2O$	3.91×10^9	P'7
M'18	Hydroxydation (left) + Hydroxylation (Piperidine)	12.35	445.2487	$C_{28}H_{32}N_2O_3$	4.09×10^7	-
M'19	N-Dealkylation (phenethyl) + Hydroxylation (piperidine)	12.62	325.1912	$C_{20}H_{24}N_2O_2$	2.66×10^7	-
M'20	Oxidation (left) + Hydroxylation (right ring)	12.63	443.2331	$C_{28}H_{30}N_2O_3$	3.06×10^7	-
M'21	Oxidation (left) + Hydroxylation (Piperidine)	13.21	443.2331	$C_{28}H_{30}N_2O_4$	4.31×10^7	-
M'22	Hydroxylation (left)	13.47	429.2537	$C_{28}H_{32}N_2O_2$	1.39×10^8	-
M'23	N-Dealkylation (phenethyl) + Oxidation (2-N-piperidine)	13.51	323.1754	$C_{20}H_{22}N_2O_2$	4.65×10^7	-
M'24	Oxidation (left)	14.31	427.2380	$C_{28}H_{30}N_2O_2$	1.99×10^8	-
M'25	N-Dealkylation (phenethyl) +	14.49	323.1755	$C_{20}H_{22}N_2O_2$	2.53×10^7	-

	Oxidation (3-N-piperidine)					
M'26	Oxidation (left) + N (piperidine) Oxidation	15.35	443.2332	$C_{28}H_{30}N_2O_3$	3.42 x 10^7	-
β'-phenylfentanyl	**Parent**	**15.76**	**413.2588**	**$C_{28}H_{32}N_2O$**	**2.44 x 10^8**	**NA**
M'27	Oxidation (left)	18.18	427.2380	$C_{28}H_{30}N_2O_2$	2.66 x 10^7	-
Abbreviations: NA, not applicable.						
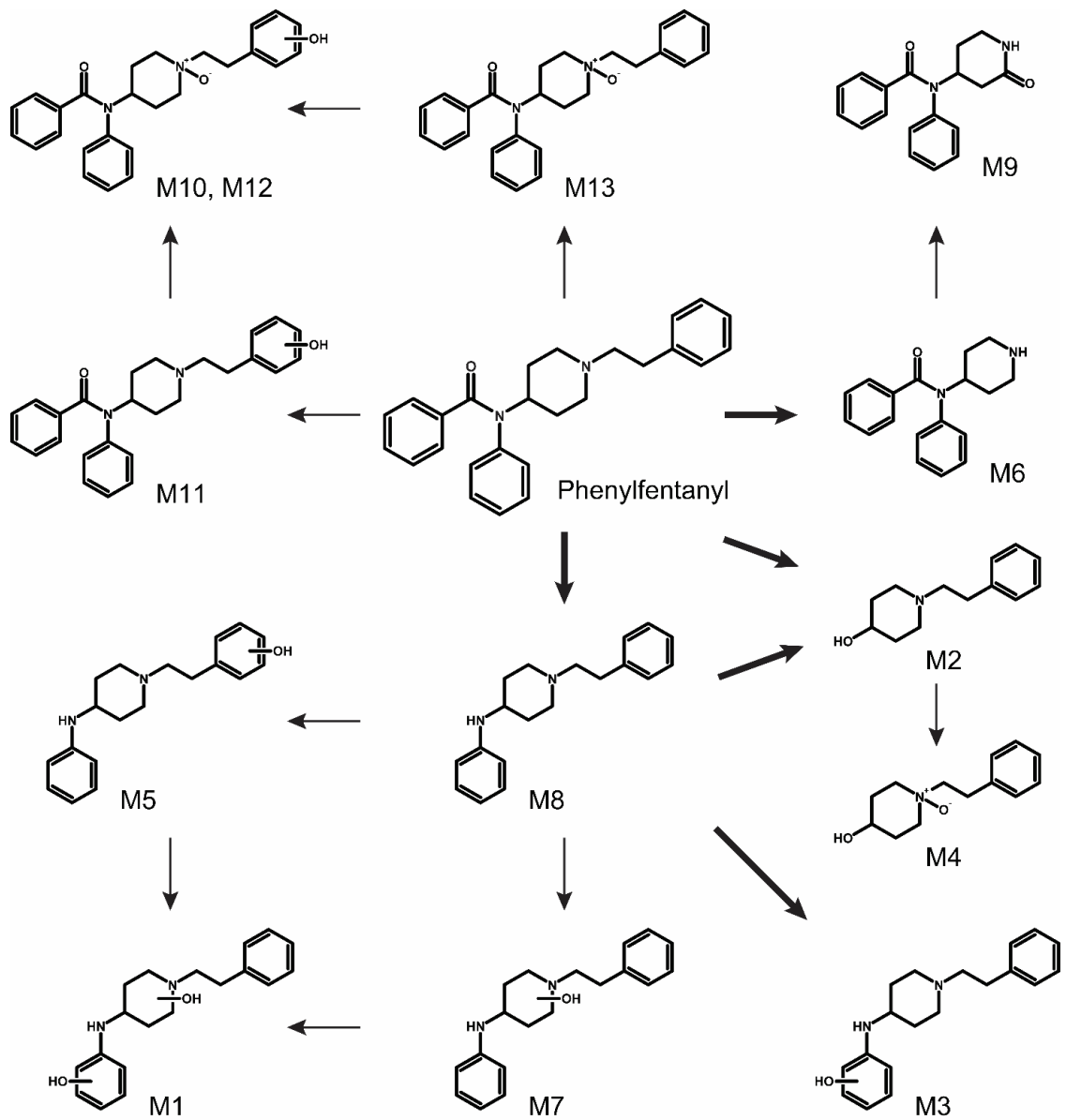
Figure 4 Phenylfentanyl suggested metabolic fate
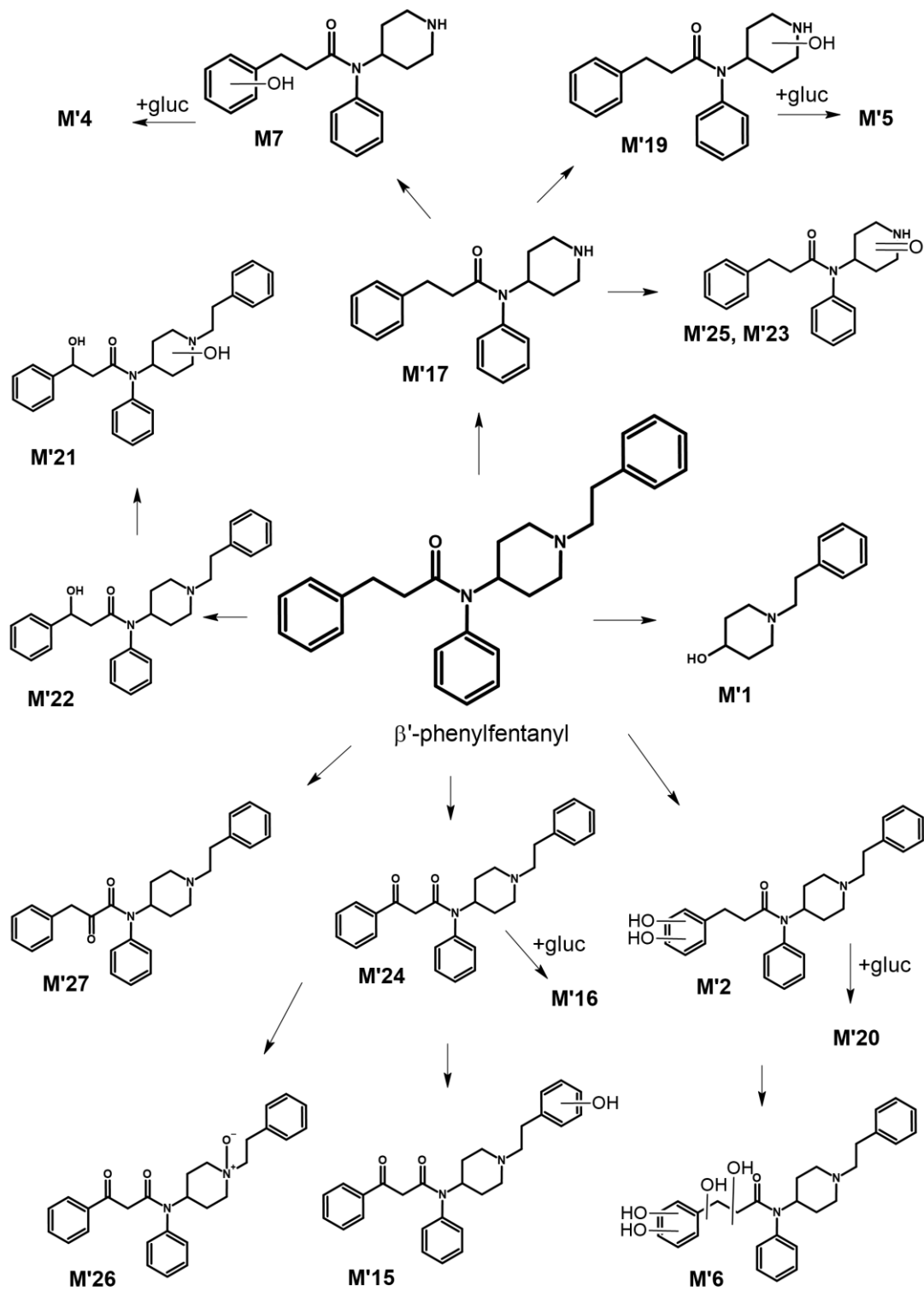
Figure 5 B'-phenylfentanyl suggested metabolic fate

2.2.2.1 Amide hydrolysis

M8 eluted at 13.15 min and was produced through the hydrolysis of phenylfentanyl amide group (−7C −4H −O), as suggested by a −104.0260 Da mass shift from parent. M8 fragmentation pattern contained major phenylfentanyl fragments (*m/z* 188.1432, 105.0698, 134.0963, and 146.0963) with a similar relative intensity, but did not contain *m/z* 105.0335, which is produced by the benzaldehyde group of phenylfentanyl, confirming M8 identity. Moreover, M8 was automatically identified by mzCloud, Chemspider, and HighResNPS libraries, through its accurate mass, elemental composition, and fragmentation pattern. 4-ANPP analytical standard was injected at 1 μg/mL in MPA:MPB, 8:2 v/v, in the same LC-HRMS conditions to confirm metabolite identification: the retention time and fragmentation pattern matched those of M8 (Fig. 8).
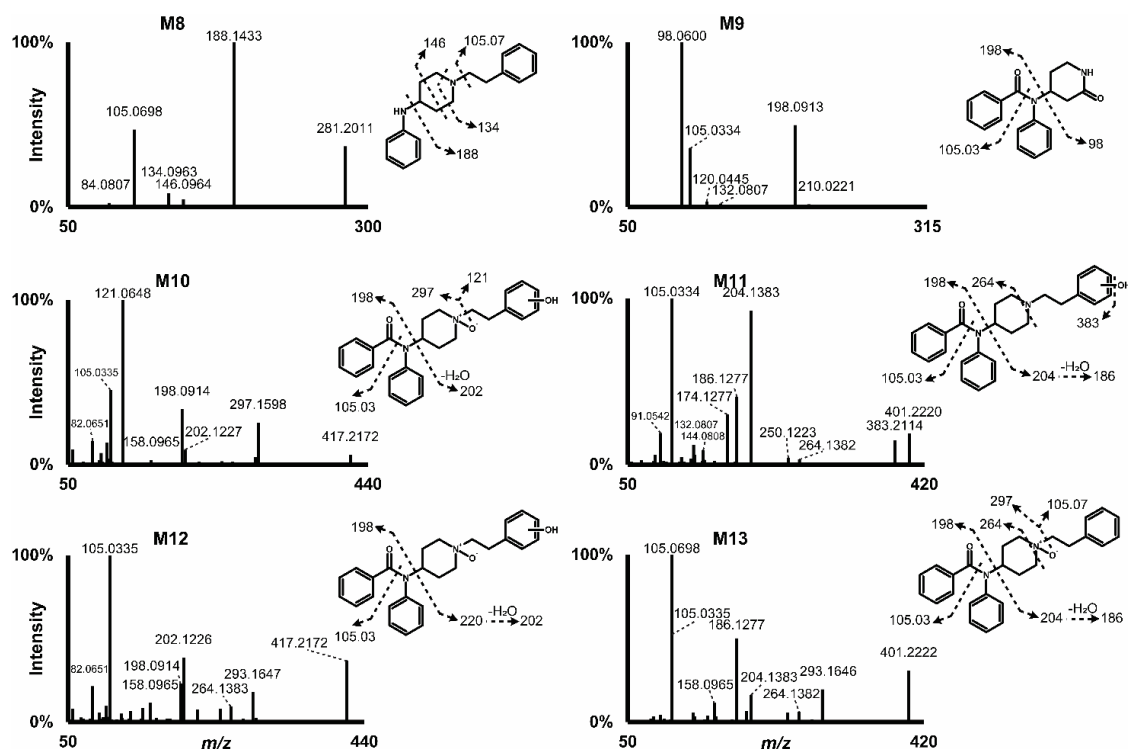
Figure 6 Phenylfentanyl metabolites M8–M13 MS/MS spectra and suggested fragments

Amide hydrolysis is catalyzed by hydrolase enzymes, mainly through amidase, but also through other subclasses such as carboxylesterase and arylacetamide deacetylase enzymes (Bradshaw et al., 2018; Sanghani et al., 2009). This transformation is major in the metabolism of pharmaceuticals such as irinotecan and several fentanyl analogs (Åstrand et al., 2019; Kahns & Bundgaard, 1991). 4-ANPP is indeed a well-known metabolite of several fentanyl analogues (Brunetti et al., 2020; Marchei et al., 2018a; Rodriguez Salas et al., 2021; Salomone et al., 2019; Wilde et al., 2019a). It is also a chemical intermediary of the synthesis of fentanyl and several analogues by Siegfried method (DEA, 2010) and can therefore be present in the drug before use. Sanghani et al. (Sanghani et al., 2009) demonstrated that the steric hindrance generated by the group substituting the carbon of the amide group (length and tridimensional configuration) significantly impacted the substrate selectivity of N-acylethanolamine acid amidase, while the contribution of the groups substituting the nitrogen of the amide group was minor (Ghidini et al., 2021). Recently, Åstrand et al. studied the metabolism of cyclopropyl-, cyclobutyl-, cyclopentyl-, and cyclohexylfentanyl, and demonstrated the composition of the group substituting the carbon of the amide group played a key role in the occurrence of the amide hydrolysis of fentanyl analogues, although no clear pattern was identified (Åstrand et al., 2019). Amide hydrolysis was a major metabolite of cyclobutyl- and cyclohexylfentanyl, but was minor in cyclopentylfentanyl and not detected in cyclopropylfentanyl (Åstrand et al., 2019).

Interestingly, M8 was the phenylfentanyl metabolite with the second highest intensity after 3-h incubation with human hepatocytes, but it was not detected in b'-phenylfentanyl metabolic pattern. Remarkably, 4-ANPP and subsequent metabolites were not predicted by GLORYx as potential phenylfentanyl metabolites, which is a significant drawback of the freeware for this study (Tables 3 and 4). GLORYx is a machine-learning software using the metabolism data freely available in DrugBank and MeXBioDB databases (de Bruyn Kops et al., 2021) but does not directly consider the tridimensional configuration of the substrates or the metabolic enzymes. Amide hydrolysis might be considered as a rare metabolic reaction of the drugs included in the databases

and might therefore be predicted with a low probability. Additionally, the human carboxylesterase 2, which is also involved in amide hydrolysis reactions, was excluded from the list of enzymes for GLORYx predictions (de Bruyn Kops et al., 2021).

2.2.2.2 N-Dealkylation

Eluting at 10.73 min of phenylfentanyl chromatographic run, M6 $[M+H]^+$ presented an accurate mass of m/z 281.1646, consistent with the elemental composition of phenylnorfentanyl, produced by N-dealkylation of phenylfentanyl piperidine ring (–8C –8H) (Fig. 9). M6 α-cleavage at the amide group produced ions m/z 198.0913 and m/z 84.0808, the fragment with the most intense signal, which matches phenethylpiperidine fragment after N-Dealkylation. Fragment m/z 105.0334, also observed in phenylfentanyl fragmentation pattern, was produced by the benzaldehyde group of the metabolite. The lack of fragment m/z 105.0699 further suggested the loss of the phenethyl moiety.
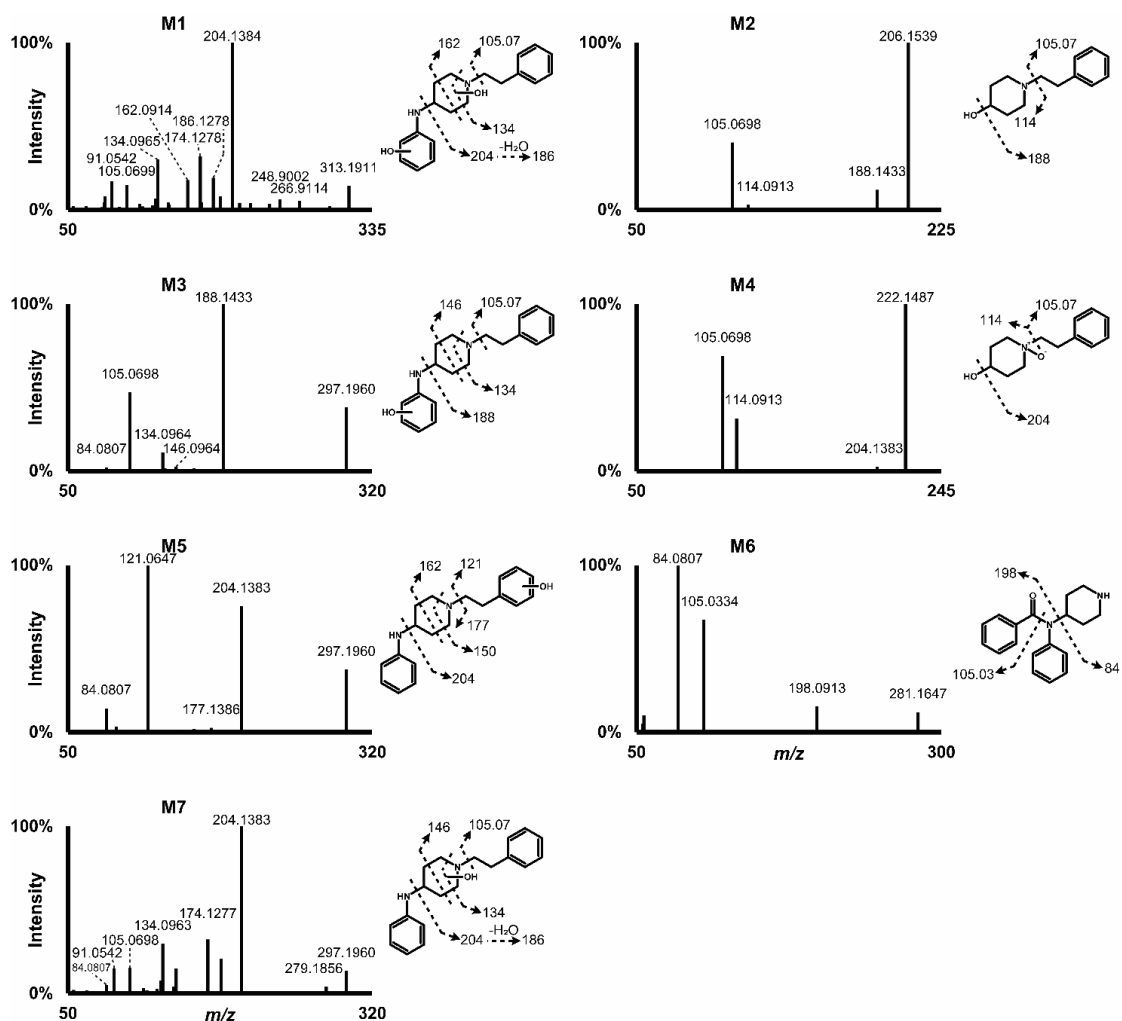
Figure 7 Phenylfentanyl metabolites M1–M7 MS/MS spectra and suggested fragments

M6 was the metabolite with the most intense signal after 3-h incubation with human hepatocytes, with a chromatographic peak area of 7.85 x 10^9. This result was not surprising, considering that this metabolic reaction is major in fentanyl and other analogues (e.g., norfentanyl, norbutyrylfentanyl, furanylnorfentanyl) (Watanabe et al., 2017; Wilde et al., 2019a). In addition, it was predicted with GLORYx (PM7) with a high prediction score (Table 3). This reaction is mediated by CYP3A4 and CYP3A5 in the metabolization of fentanyl and analogues (Saiz-Rodríguez et al., 2019; Wilde et al., 2019a). Despite M6 high intensity, further metabolism was rarely observed in the present experiments (M9, see subsection "3.2.3. Oxidation"). [M+Na]⁺ and [M+K]⁺ adducts, M6 dimer, and major fragments were generated in the ionization source during the analysis,

and were detected after processing the data with Compound Discoverer due to M6 high intensity. However, the cumulated intensity of these ions did not exceed 5% of M6 signal. Interestingly, M6 nominal mass is the same as that of 4-ANPP, which is a common metabolite of fentanyl analogues and is not specific of M6 metabolism: special attention is required to avoid misidentification, and HRMS is particularly suitable for that purpose.

Similarly, the β'-phenylnorfentanyl (M'17) was detected in β'-phenylfentanyl metabolic pattern, eluted at 11.82min. The lack of fragments m/z 188.1434 and 281.2011 further suggested the loss of the phenylethyl moiety, as in case of other N-dealkylated metabolites. Fragment m/z 177.1385, corresponding to N-phenylpiperidin-4-aminuim, was also discriminative for those N-dealkylated metabolites such as M'2-M'4, M'7, M'9-M'13. Another N-dealkylation occurred at the nitrogen of the amidic group generating M'1, which eluted at 5.89 min. M1 accurate mass was of m/z 206.1541 and highest intense fragments were m/z 188.1433 and 105.0698, also detected in parent's fragmentation pattern (fig. 10).
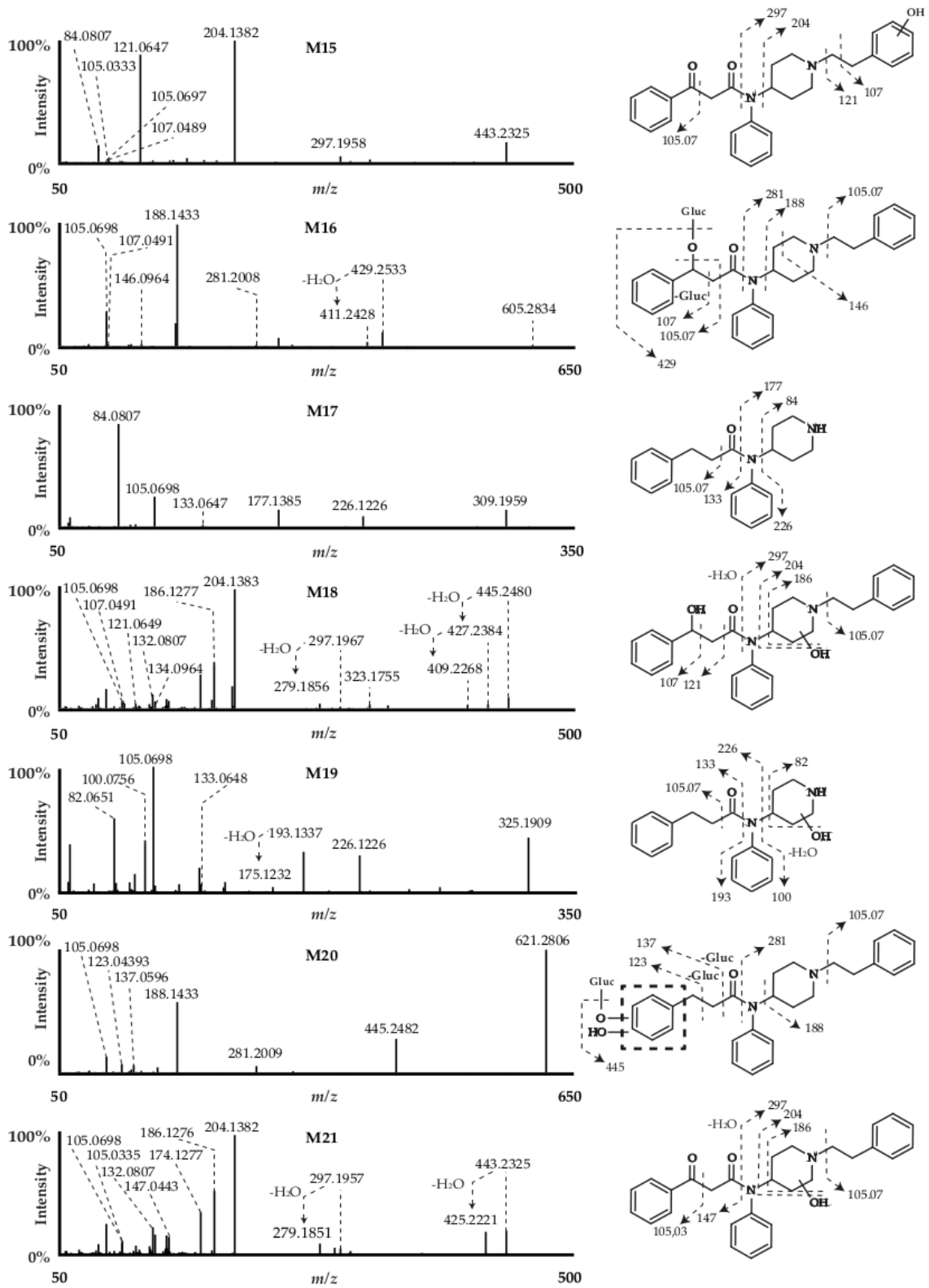
Figure 8 β'-phenylfentanyl metabolites M'15–M'21 MS/MS spectra and suggested fragments

45

In phenyl fentanyl metabolic pattern, another N-dealkylation at the nitrogen of the amide group occurred in M2, which eluted at 5.89 min with an accurate mass of m/z 206.1541. M2 could be produced by N-dealkylation of parent (−13C −9H −N) or M8 (4-ANPP) (−6C −5H −N +O), making it not specific of phenylfentanyl metabolism. M2 fragments with the highest intensity were m/z 188.1433 and 105.0698, also detected in phenylfentanyl fragmentation pattern.

2.2.2.3 Oxidation

Two metabolites were produced by the oxidation of phenylfentanyl (+O), as suggested by the +15.9952 Da mass shift from parent. M11 eluted at 14.19 min and its fragmentation pattern contained ion *m/z* 383.2114, produced by a water loss and indicating a hydroxylated metabolite. Fragment *m/z* 105.0334, also present in parent, suggested that the benzamide part of the molecule was intact, while fragment *m/z* 204.1383, matching phenethylpiperidine fragment after hydroxylation, and the subsequent water loss *m/z* 186.1277 pointed towards a modification of the phenethylpiperidine moiety (Fig. 8). More precisely, the absence of ion *m/z* 105.0699 indicated that the phenethyl group was modified, and the abundant water losses (*m/z* 383.2114 and 186.1277) suggested that M11 was hydroxylated at the ethyl chain. M13 eluted at 17.76 min and its fragmentation pattern also contained ions *m/z* 204.1383, 186.1277, and 105.0335, indicating that the transformation occurred at phenylfentanyl phenethyl group. However, fragment *m/z* 105.0698 was present, suggesting a transformation of the piperidine ring (Fig. 8). M13 late elution, after parent, is specific of an N-oxidation in reversed-phase chromatography and was previously reported in *in vitro* carfentanil and 4-fluoro-isobutyrylfentanyl metabolic pathway (Feasel et al., 2016; Watanabe et al., 2017). Therefore, M13 was likely produced by the N-oxidation of phenylfentanyl piperidine ring.

According to *in silico* predictions, hydroxylated metabolites were highly expected, with a score ranging between 0.43 and 0.30 (Table 3). Hydroxylation was expected to occur mainly at the phenethylpiperidine moiety, preferably at the piperidine ring. Hydroxylation at the ethyl group of the phenethyl chain and in *ortho* and *meta* position of the phenyl ring were also predicted with a similar

score. M11 and M13 could match PM8 and PM5 of *in silico* predictions, respectively.

In respect to b'-phenylfentanyl, the oxidation of the amidic carbonyl's β carbon yields to compounds M'13, M'20, M'21, M'24 and M'26. Their spectra share the signal m/z 105.0335 that, differing from 105.0669 of the parent, is distinctive of this transformation. Fragment 105.0335 was also crucial for discriminating between M'24 and M'27 which display the same exact mass of 427.2380 Da. In fact, the spectrum of M'27 shows only the signal m/z 105.0669 indicating an α instead of a β oxidation. M'23 and M'25 are piperidine-oxidated derivatives of M17 as confirmed by the fragment m/z 98.0600. M'23, in particular, was very challenging to determine due to the presence of fragments m/z 149.0597 and 177.1385 that were apparently incoherent with M'23 fragmentation pattern. These ions are generated from the fragmentation the M'13 enolic tautomer that, eluting at 13.98 min, creates a peak overlapping with that of M'23 at 13.51 min. The correct position the carbonyl at the piperidine ring is not possible to be predicted in present analytical conditions, although the lactam formation is favored (Vickers & Polsky, 2000). M'26 is generated by the M'24 piperidine ring N-oxidation. M'26 shows a similar mass compared to M21 but the N-oxide caused its late elution at 15.35 min (Grafinger et al., 2021).
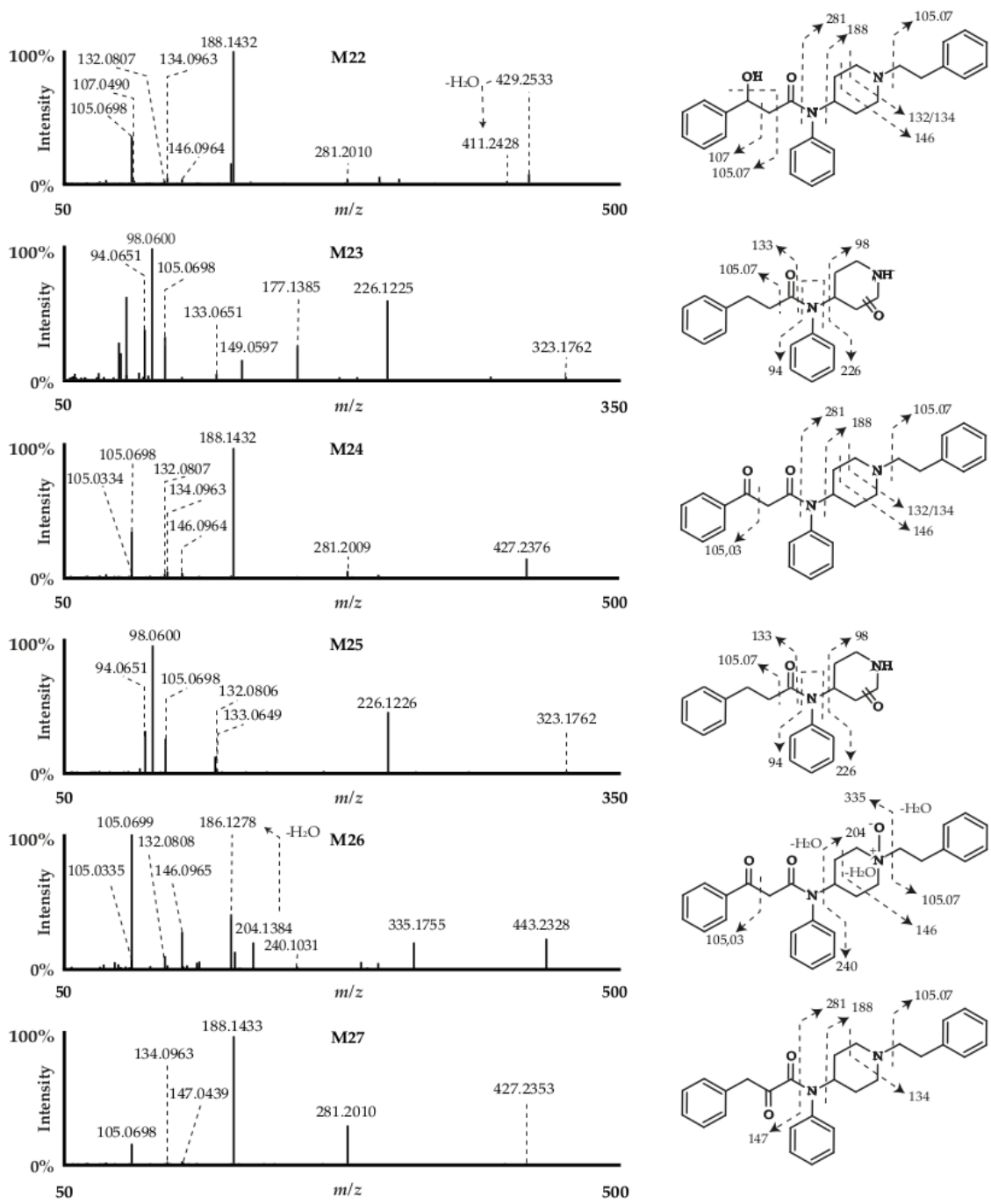
Figure 9 β'phenylfentanyl metabolites M'22–M'27 MS/MS spectra and suggested fragments

Hydroxylation occurred at different position of the β'-phenylfentanyl. With earlier elution of 13.47 min, M'22 is the result of β'-phenylfentanyl hydroxylation (+O) as suggested by the +15.9949-Da mass shift from the parent. The fragments m/z 281.2010, 188.1432 and 107.0490 further indicate that the hydroxylation occurred in the left phenylethyl moiety, and, probably at the β carbon of the amidic

carbonyl as indicated by the loss of water. M'22 underwent to N-dealkylation, generating M9 that displayed the same fragmentation patter of M'22, excluded signals m/z 281.2010 and 188.1432. M'9 shared the same elemental composition and almost the same accurate mass with M'7, M'11 and M'12 (Table 3.). M'7, M'11 and M'12 spectra indicates that hydroxylation occured in ortho, metha and para of the left benzene since water losses were not recorded due to higher stability of phenols (Aczel & Lumpkin, 1960). The order in which these isomers elute is, unfortunately, not possible to determine in present analytical conditions. Also M'18 is probably originated as piperidine-hydroxylate from M'22. With an earlier elution at 12.35 min and a mass shift of 15.995-Da from M'22, M'18 is characterized by a double loss of water. The fragments m/z 204.1383 and 186.1277 further suggest that hydroxylation occured at the piperidine ring. Water loss was also crucial to discriminate the isomers M'20 and M'21 as piperidine and right benzene hydroxylated derivatives.

Benzenedihydrodiols are formed in humans from the oxidation of the benzene via epoxidation followed by epoxide hydration (Snyder & Hedli, 1996). M14 spectrum is characterized by the presence of fragments m/z 105.0689, 281.2010 and 188.1433 which exclude any possible transformation at the 4-ANPP moiety. The loss of water converts the benzenedihydrodiol M'14 in its phenolic derivative as suggested by signals m/z 107.0490 and 121.0647. M14 then undergoes to N-dealkylation (M'2) as suggested by the lack of the right phenylethyl moiety. M8 right phenol is confirmed by the lack of signal m/z 105.0698. Moreover, signals m/z 107.0491 and 121.0648 of M8 are more intense compared to those of M14 due to the contribution of the right phenolic portion. Further transformations of M14 lead to the polyolic metabolite M6 (+4O, +4H), characterized by multiple losses of water. However, as in case of above mentioned benzenedihydrodiols, the correct position of hydroxyl groups is impossible to determine in present analytical conditions. Benzenedihydrodiols are potent carcinogens. It has been proposed that these metabolites are in vivo converted by dihydrodiol dehydrogenase into less reactive cathecols (Bolton & Dunlap, 2017; Smithgall et al., 1986). Furthermore, O-methylation was observed as further reaction of catechols metabolites.
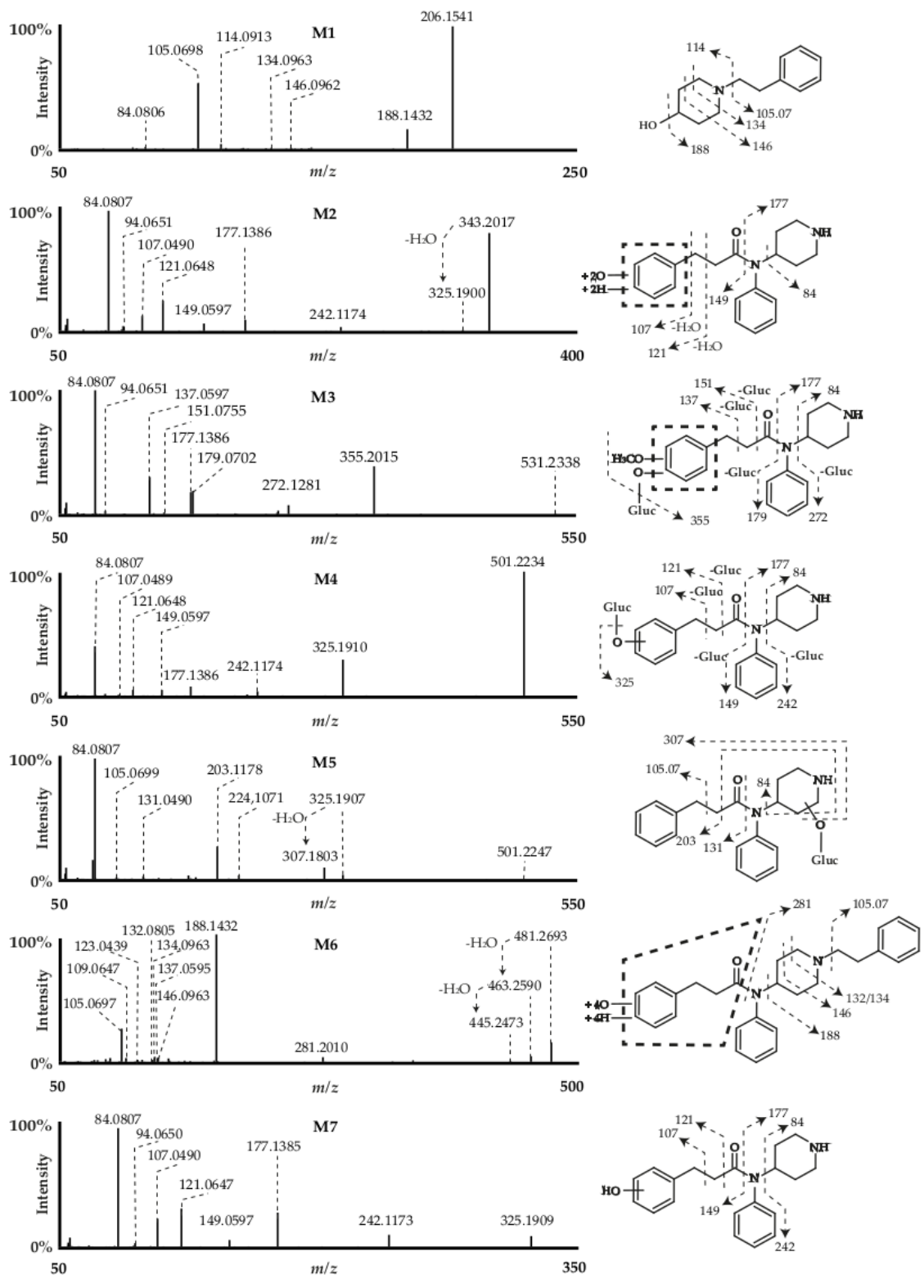
Figure 10 B'-phenylfentanyl metabolites M1–M7 MS/MS spectra and suggested fragments

2.2.2.3.1 Further amide hydrolysis

Three hydroxy-4-ANPP metabolites (M3, M5, and M7), produced by amide hydrolysis (−7C −4H −O) and hydroxylation (+O) of phenylfentanyl, were identified after 3-h incubation with human hepatocytes, as suggested by the 88.0310 Da mass shift from parent. M3, M5, and M7 eluted at 6.46, 10.38, and 11.24 min, respectively. M3 fragmentation was close to that of 4-ANPP (M8) with major fragments m/z 188.1432, 105.0698, 134.0963, and 146.0963 indicating that the phenethyl moiety was not transformed. The absence of water loss further suggests that the hydroxylation occurred at the phenyl ring of the aniline group of the molecule. Although the exact position of the transformation on the phenyl ring could not be determined in present analytical conditions, the para position is the favored site of hydroxylation. Conversely, M5 and M7 fragmentation pattern contained ions m/z 204.1383, matching M11 hydroxy-phenethylpiperidine fragment, although the subsequent water loss was not detected in M5 spectrum. M7 fragmentation pattern contained ion m/z 105.0698 produced by the phenethyl group, while M5 spectrum contained ion m/z 121.0647 matching the phenethyl fragment after hydroxylation; the water loss from m/z 121.0647 also was not detected. Like M11, M5 was hydroxylated at the phenethyl chain, but the absence of water loss rather indicates that the reaction occurred at the phenyl group of the phenethyl chain. Like M3, the para position is the favored site of reaction. M7 however, was likely hydroxylated at the piperidine ring. The exact position of M7 hydroxylation could not be determined, although the formation of a hemiaminal group is favored (Vickers & Polsky, 2000). Amide hydrolysis and hydroxylation was previously reported in incubations of several fentanyl analogues with human hepatocytes (e.g., acetylfentanyl and furanylfentanyl), especially at the alkyl chain of the phenethyl moiety and the phenyl ring of aniline moiety. However, they were not detected in authentic urine samples [11].

Amide hydrolysis (−7C −4H −O) and di-hydroxylation (+2O) occurred in M1, as suggested by the 72.0359 Da mass shift from parent. M1 fragmentation pattern was similar to that of M7, with major fragments m/z 204.1384, 186.1277, 174.1278, and 134.0965, indicating that a hydroxylation occurred at the phenethylpiperidine moiety of the molecule, most likely at the piperidine ring,

while the second hydroxylation occurred at the aniline group. Ion m/z 312.9432, which was detected during the whole time of the chromatographic separation, was fragmented along M1, and generated much interference (e.g., *m/z* 266.9114, 248.9003, 238.9163, 220.9057), limiting the interpretation of the M1 spectrum. M1 was detected with a low intensity in the present experiments, and metabolites with amide hydrolysis and dihydroxylation were not reported in the metabolism of other fentanyl analogues: metabolites are expected to be eliminated before reaching this level of transformation.

2.2.2.3.2 Further N-dealkylation

Although M6 was the phenylfentanyl metabolite with the highest intensity, only one other metabolite was detected with the same transformation. M9 eluted at 14.12 min and was produced by N-dealkylation at the piperidine ring (–7C –4H –O) and oxidation (+O –2H), as indicated by the 90.0831 Da mass shift from parent (Fig. 7). M9 fragmentation pattern contained M6 fragments *m/z* 105.0334 and 198.0913, indicating that the transformation occurred at the piperidine ring of the molecule. Ion *m/z* 98.0600, which matches M6 piperidine fragment after oxidation further confirmed the position of the metabolic reaction. Although present analytical conditions are not sufficient to accurately determine the position of the oxidation at the piperidine ring, oxidation towards the formation of a lactam is predominant in the metabolism of heterocyclic aliphatic amines through CYP reactions (Vickers & Polsky, 2000). Additionally, M9's late elution compared to that of phenylnorfentanyl (M6) supports an oxidation in position 2 of the piperidine (Carlier et al., 2021a; Swortwood, Carlier, et al., 2016). M9 was predicted with a combined score of 0.18 (Table 3, PM9.5).

M4 eluted at 6.88 min was produced by N-dealkylation at the nitrogen atom of the amide group (–13C –9H –N) and oxidation (+O), an indicated by a 163.0783 Da mass shift from parent. The late retention time and fragments *m/z* 105.0698 and 114.0913, also present in M2 fragmentation pattern, indicated an N-oxidation (Fig. 6).

2.2.2.3.3 Further oxidation

M10 and 12 eluted at 14.74 and 16.42 min, respectively, and displayed a similar fragmentation pattern, although the relative abundance of their fragments was somewhat different (Fig. 7). The two metabolites were produced after phenylfentanyl dihydroxylation (+2O), as indicated by their mass shift from parent. Phenylfentanyl fragments m/z 105.0335 and 198.0914 indicated that the reactions occurred at the phenethylpiperidine chain of M10 and 12. Ion m/z 220.1326 and the subsequent water loss 202.1227 match phenylfentanyl phenethylpiperidine fragment after dihydroxylation, further indicating phenethylpiperidine as the site of reactions. Ion m/z 121.0648 without substantial water loss indicated a hydroxylation at the phenyl group of the phenethyl chain, and a hydroxylation at the piperidine ring. Finally, the late retention time indicated that M10 and 12 were N-oxidated metabolites.

2.2.2.3.4 Glucuronidations and O-methylation

Glucuronidation occurred in five metabolites as suggested by the loss of the portion $C_6H_8O_6$ (± 176 Da) from precursors. M5 and M16 come from M19 and M22 respectively, while it is impossible to determine if M4 is the M7, M11 or M12 O-glucuronide. After dehydrogenation to catechol (-2H), M2 underwent to O-methylation (-H, +C, +3H) as suggested by fragments 137.0597 and 151.0753 generating M10 which was in turn converted in its O-glucuronide (M'3) as indicated by the mass shift of 176,0324 Da.

3 In vitro metabolism of 3F-α-pyrrolidinovalerophenone

3.1 Materials and methods

3.1.1 Chemicals and reagents

3F-α-PVP and diclofenac pure standards were obtained from Cayman chemical (Ann Harbor, MI, USA) and Sigma Aldrich (Milan, Italy), respectively. LC-MS grade methanol, acetonitrile, water, and formic acid were purchased from Carlo Erba (Cornaredo, Italy). The standards were solubilized in methanol at 1 mg/mL and were stored at -20°C until analysis.

Williams' medium E (WME), HEPES buffer (2-[4-(2-hydroxyethyl)-1-piperazinyl]ethanesulfonic acid), and l-Glutamine were supplied by Sigma Aldrich. Supplemented Williams' Medium E (SWM) was prepared dissolving HEPES and l-Glutamine at 2 and 20 mmol/L, respectively, in WME. The solution was stored at 4°C until incubation.

Thawing medium, 0.4% trypan blue, and ten-donor-pooled cryopreserved human hepatocytes (HEP) were obtained from Lonza (Basel, Switzerland).

3.1.2 Hepatocyte incubations

3F-α-PVP incubations with HEP were conducted following the same protocol established for the investigated fentanyl analogues, described in the previous chapter (Annagiulia Di Trana et al., 2021).

Briefly, HEP were thawed in 50 mL thawing medium at 37°C. After centrifugation for 5 min, 50-100g, the supernatant was discarded and the pellet was resuspended in 50 mL SWM at 37°C. After centrifugation for 5 min, 50-100g, the supernatant was discarded and the pellet was resuspended in 2 mL SWM at 37°C. SWM volume was adjusted to reach 2 x 10^6 viable cells/mL after assessing cell viability with the Trypan blue exclusion method. In sterile 24-well culture plates, 250 µL HEP suspension was gently mixed with 250 µL 10 µmol/L 3F-α-PVP in SWM. The plates were incubated at 37°C in an ICN35 incubator from ArgoLab (Arezzo, Italy) and the reactions were stopped after 0 or 3 h with 500 µL ice-cold acetonitrile and centrifugation for 10 min, 15,000g. The samples were prepared for injection immediately after the incubation.

Negative controls, i.e., hepatocytes in SWM without 3F-α-PVP and 3F-α-PVP in SWM without HEP, were incubated for 3 h in the same conditions. Diclofenac was also incubated in the same conditions, and 4'-hydroxydiclofenac and diclofenac acyl-glucuronide were monitored to ensure proper metabolic activity. The total number of incubates was eight (HEP alone in SWM for 0 h, HEP alone in SWM for 3 h, HEP and diclofenac in SWM for 0 h, HEP and diclofenac in SWM for 3 h, 3F-α-PVP alone in SWM for 0 h, 3F-α-PVP alone in SWM for 3 h, HEP and 3F-α-PVP in SWM for 0 h, HEP and 3F-α-PVP in SWM for 3 h).

3.1.3 Sample preparation

A volume of 100 µL incubate was mixed with 100 µL acetonitrile and centrifuged for 10 min, 15,000g, at room temperature. The supernatant was dried at 37°C under a nitrogen stream, reconstituted with MPA:MPB (8:2, v/v), and centrifuged for 10 min, 15,000g, at room temperature. The supernatants were transferred into vials with glass inserts and 10 µL was injected onto the chromatographic system.

3.1.4 Instrumental conditions

The analyses were conducted with a DIONEX UltiMate 3000 liquid chromatographer coupled to a Q Exactive quadrupole-Orbitrap hybrid high-resolution mass spectrometer equipped with a heated electrospray ionization (HESI) source from Thermo Scientific (Waltham, MA, USA).

3.1.4.1 Liquid chromatography conditions

The compounds were separated through a Kinetex Biphenyl column (150 x 2.1 mm, 2 µm) from Phenomenex (Torrance, CA, USA), using 0.1% formic acid in water as mobile phase A (MPA) and 0.1% formic acid in acetonitrile as mobile phase B (MPB) at a 0.4-mL/min flow rate.

The gradient was: 2% MPB held for 2 min, increased to 25% MPB within 12 min, increased to 95% within 2 min and held for 4 min; initial conditions were restored within 0.1 min and maintained for 3.9 min. The chromatographic run lasted 24 min. The column oven was set at 37±1°C and the autosampler temperature was 10±1°C.

3.1.4.2 Mass spectrometry conditions

All the samples were analysed in positive- and negative-ion modes with two different injections using the same HESI conditions: spray voltage, ±3.5 kV; sheath gas and auxiliary flow rates, 50 a.u. and 10 a.u., respectively; capillary temperature and auxiliary gas heater temperature, 300°C; S-lens radio frequency level, 50 a.u.; sweep gas flow rate was not used. Mass calibration was performed with certified calibration solutions prior to the analytical session, both in positive and in negative-ion modes. To achieve better accuracy, a lock mass list was compiled in positive- (*m/z* 279.0933, 144.9821, 146.9803) and negative-ion modes (*m/z* 265.1479, 162.9824, 248,9604).

The mass spectrometer acquired from 1 to 20 min of the chromatographic run in full-scan HRMS (FullMS)/data dependent MS/MS (ddMS^2) mode. FullMS settings were: range, *m/z* 100 to 650; resolution at full width at half maximum at *m/z* 200, 70,000; automatic gain control (AGC) target, 1 x 10^6; and maximum injection time (IT), 200 ms. ddMS^2 settings were: ACG target, 2 x 10^5; maximum IT, 64 ms; isolation window, *m/z* 1.2; resolution, 17,500; and stepped normalized collision energy (NCE), 40, 70, and 90 a.u.

A maximum number of five ddMS^2 scans were triggered for each FullMS scan (minimum intensity, 10^4; dynamic exclusion, 2.0 s) depending on an inclusion list of putative metabolites based on *in silico* predictions and postulation (section 2.5) (Table 1). Ions that were not included in the inclusion list also triggered ddMS^2 scans, although they were not priority ("pick others if idle" option). In addition, an exclusion list was compiled based on background noise, as evaluated during the injection of blank control samples (MPA:MPB 80:20 v/v).

Table 7 Inclusion list for the tandem mass spectrometry data-dependent acquisition

Transformation	Molecular formula	[M+H]$^+$ (m/z)	[M-H]$^-$ (m/z)
PARENT (3F-α-PVP)	**C$_{15}$H$_{20}$FNO**	**250.1602**	**248.1456**
+2H	C$_{15}$H$_{22}$FNO	252.1758	250.1613
+O	C$_{15}$H$_{20}$FNO$_2$	266.1551	264.1405

+2O	$C_{15}H_{20}FNO_3$	282.1500	280.1354
-2H +O	$C_{15}H_{18}FNO_2$	264.1394	262.1249
-2H +2O	$C_{15}H_{18}FNO_3$	280.1343	278.1198
-2H	$C_{15}H_{18}FNO$	248.1445	246.1300
+2H +O	$C_{15}H_{22}FNO_2$	268.1707	266.1562
+2H +2O	$C_{15}H_{22}FNO_3$	284.1656	282.1511
+C +2H	$C_{16}H_{22}FNO$	264.1758	262.1613
+6C +10H +6O	$C_{21}H_{30}FNO_7$	428.2079	426.1934
+2H +3O +S	$C_{15}H_{22}FNO_4S$	332.1326	330.1181
+3O	$C_{15}H_{20}FNO_4$	298.1449	296.1304
-2H +3O	$C_{15}H_{18}FNO_4$	296.1293	294.1147
-F +H +O	$C_{15}H_{21}NO_2$	248.1645	246.1499
-F +H	$C_{15}H_{21}NO$	232.1696	230.1550
+2C +3H +N +O	$C_{17}H_{23}FN_2O_2$	307.1816	305.1671
+2C +N +O	$C_{17}H_20FN_2O_2^+$	303.1503	-
+3C +5H +N +O	$C_{18}H_{25}FN_2O_2$	321.1973	319.1827
+3C +2H +N +O	$C_{18}H_{22}FN_2O_2^+$	317.1660	-
+2C +H +N +3O	$C_{17}H_{21}FN_2O_4$	337.1558	335.1413
+3C +3H +N +3O	$C_{18}H_{23}FN_2O_4$	351.1715	349.1569
-8C -15H -N	C_7H_5FO	125.0397	123.0252
-7C -5H -F -O	$C_8H_{15}N$	126.1277	124.1132
-4C -7H -N +O	$C_{11}H_{13}FO_2$	197.0972	195.0827
+6C +8H +7O	$C_{21}H_{28}FNO_8$	442.1872	440.1726
+4O +S	$C_{15}H_{20}FNO_5S$	346.1119	344.0973

+C +2H +O	$C_{16}H_{22}FNO_2$	280.1707	278.1562
-F +H +2O	$C_{15}H_{21}NO_3$	264.1594	262.1449
-4H +2O	$C_{15}H_{16}FNO_3$	278.1187	276.1041
-4C -7H -N +2O	$C_{11}H_{13}FO_3$	213.0921	211.0776
-4C -6H	$C_{11}H_{14}FNO$	196.1132	194.0987
+C +2H +2O	$C_{16}H_{22}FNO_3$	296.1656	294.1511
-F +6C +9H +7O	$C_{21}H_{29}NO_8$	424.1966	422.1820
-F +H +4O +S	$C_{15}H_{21}NO_5S$	328.1213	326.1068
+2H +4O +S	$C_{15}H_{22}FNO_5S$	348.1275	346.1130
+6C +9H +6O	$C_{21}H_{29}FNO_7^+$	426.1923	-
+2H +2O	$C_{15}H_{22}FNO_3$	284.1656	282.1511
+10C +17H +3N +7O +S	$C_{25}H_{37}FN_4O_8S$	573.2389	571.2243
+2C +4H	$C_{17}H_{24}FNO$	278.1915	276.1769
+2C +4H +O	$C_{17}H_{24}FNO_2$	294.1864	292.1718

3.1.5 *In silico* metabolite prediction

3F-α-PVP *in silico* metabolite prediction was conducted using three different online free software, BioTransformer (Djoumbou-Feunang, Fiamoncini, Gil-de-la-Fuente, Greiner, Manach, & Wishart, 2019), GLORYx (BruynKops et al., 2020; Stork et al., 2019), and EAWAG Pathway Prediction System (EAWAG-PPS) (Gao et al., 2009).

BioTransfomer (version 1.0.0) is a software predicting the phase I and phase II metabolism of small molecules in humans using knowledge-based and machine-learning-based approaches (Djoumbou-Feunang, Fiamoncini, Gil-de-la-Fuente, Greiner, Manach, & Wishart, 2019). "Metabolism Prediction" and "Metabolic Identification" options allow the prediction of the metabolism of a target compound or the identification of its putative metabolites, respectively. The set of metabolic transformations is selected depending on the type of metabolism

assessed (e.g., "Phase I (CYP450) Transformation" to only predict CYP450 metabolism, "Human Gut Microbial Transformation" to only predict compound metabolism by gut microbial enzymes, "AllHuman" to predict compound metabolism in the human superorganism) and the SMILES string of the target compound is imported to initiate the prediction. Only first-generation metabolites, i.e., metabolites with a single metabolic transformation, are predicted, but these metabolites can be reprocessed to predict second-generation metabolites, i.e., metabolites with two metabolic transformations. 3F-α-PVP metabolism was predicted using "AllHuman" and "Metabolism Prediction" options after importing the SMILES string generated by ChemSketch (freeware version 2.1) (Djoumbou-Feunang, Fiamoncini, Gil-de-la-Fuente, Greiner, Manach, & Wishart, 2019). The software also describes the type of enzymes involved for each transformation.

GLORYx is a New E-resource for Drug Discovery (NERDD) tool predicting the sites of metabolism (FAME) and phase I and phase II metabolites (GLORYx) of molecules in humans, and freely available at https://nerdd.zbh.uni-hamburg.de/ (de BruynKops et al., 2020; Stork et al., 2019). The freeware integrates machine learning-based site of metabolism prediction, assigning a score to the metabolites based on their likelihood to occur. The target molecule can be input either as a SMILES string or using the drawing plugin provided by the website. "Phase I metabolism" and/or "Phase II metabolism" transformation options are available. 3F-α-PVP metabolites were predicted using the ChemSketch-generated SMILES string and "Phase I and phase II metabolism" options. All the metabolites with a score higher than 0.30 were reprocessed to predict second-generation metabolites; only first-generation metabolites and second-generation metabolites with a combined score higher than 0.25 were considered (de BruynKops et al., 2020; Stork et al., 2019).

EAWAG-PPS is a free tool available at https://eawag-bbd.ethz.ch/index.html, allowing the prediction of plausible microbial degradation of a chemical compound. Although the software is intended to predict the microbial degradation of molecules in the environment in standard conditions, the panel of metabolic reactions includes also common metabolic transformations. Moreover, the software provided consistent results with BioTransformer in a previous study,

despite the different conceptualization (Djoumbou-Feunang, Fiamoncini, Gil-de-la-Fuente, Greiner, Manach, & Wishart, 2019). EAWAG-PPS identifies the possible sites of metabolism according to an atom-to-atom mapping, recognizing the functional groups of the target molecule. Thence, it lists the possible transformation following the rules reported in the EAWAG Biocatalysis/Biodegradation database (EAWAG-BBD) (Gao et al., 2009). A score is assigned to each putative metabolite, i.e., "very likely", "likely", or "neutral", depending on their likelihood to occur in aerobic or all conditions. The SMILES string of a molecule can be directly input or generated through its structure as drawn through the plugins Chemaxon's MarvinSketch Java applets. First- to third-level 3F-α-PVP metabolites in aerobic conditions were predicted with 20 putative metabolites per generation; only metabolites with at least three carbons were considered (Gao et al., 2009). The results are provided with a rule-code corresponding to the predicted biotransformation, reported in EAWAG-BBD.

3.1.6 Data mining

LC-HRMS/MS data mining was performed with Compound Discover (Thermo Scientific, version 3.2.0.421), applying a mixed targeted/untargeted workflow as previously described (Section), with minor modifications (Annagiulia Di Trana et al., 2021). Briefly, after spectrum selection and retention time alignment between raw data files, the ions were compared to a list of theoretical metabolites generated according to the settings displayed in Table 2 (intensity threshold, 5 x 10^3; HRMS mass tolerance, 5 ppm). The potential metabolites were then compared to mzCloud, ChemSpider and HighResNPS libraries (HRMS mass tolerance, 5 ppm; HRMS/MS mass tolerance, 10 ppm) (targeted data mining). Besides, the HRMS/MS spectra and theoretical elemental composition of all ions with an intensity higher than 1 x 10^5 were compared to the same databases (untargeted data mining). Finally, the results were merged to exclude redundant data and independently screened by two operators to identify 3F-α-PVP metabolites with minimal human error (the two operators obtained the same results).

Table 8 Compound Discoverer settings for generating a list of putative 3F-α-PVP metabolites.

Phase I	Dehydration (-H2 +O →)
transformation	Desaturation (-H2 →)
	Dihydrodiol formation (→ +H2 +O2)
	Hydration (→ +H2 +O)
	Oxidation (→ +O)
	Oxidative defluorination (-F → +H +O)
	Reduction (→ -2H)
	Reductive defluorination (-F → +H)
Phase II	Acetylation (-H → +C2 +H3 +O)
transformation	Glucuronide Conjugation (-H → +C6 +H9 +O6)
	Glycine Conjugation (-H -O → +C2 +H4 +N +O2)
	Glutathione conjugation on fluorine (-F → +C10 +H16 +N3 +O6 +S)
	Glutathione conjugation (→ +C10 +H17 +N3 +O6 +S)
	Methylation (-H → +C +H3)
	Sulfation (-H → +H +O3 +S)
Max # dealkylation	3
Max # phase II	2
Max # all step	5
Ions	$[M+H]^+$, $[M-H]^-$

3.2 Result and discussion

3.2.1 *In silico* prediction software

Recently, *in silico* predictions raised particular attention for drug metabolism assessment, as a cost- and time-saving complement to *in vitro* experiments (Kazmi et al., 2019; Kirchmair et al., 2015). The research on *in silico* metabolism prediction is on the rise, as it may help characterize more comprehensively the metabolic pattern of chemical substances (Kirchmair et al., 2015). The comprehensive prediction of the metabolism is crucial not only to compile an effective HRMS inclusion list, but also to help identify the metabolites structure during the analysis. To date, a large variety of computational tools based on different approaches were developed for drug metabolism prediction, either as freeware or licensed software (Xingxing Diao & Huestis, 2019; Fever, 2019; Kirchmair et al., 2015; Peach et al., 2012). Although freeware specifically designed for the metabolic profile prediction of NPSs were not yet developed, some licensed software have been applied to characterize the metabolic pathway of different SCs, with varying degrees of success (Ellefsen et al., 2016; Swortwood, Ellefsen, et al., 2016a). GLORYx, Biotransformer, and EAWAG-PPS were identified as potential free software for clearly, rapidly, and exhaustively predicting 3F-α-PVP metabolic profile, as they were applied in other metabolite identification studies or the prediction of NPS biodegradation/biotransformation (Campos et al., 2021; Annagiulia Di Trana et al., 2021; Djoumbou-Feunang, Fiamoncini, Gil-de-la-Fuente, Greiner, Manach, Wishart, et al., 2019; Espinosa-Barrera et al., 2021; *Predicting Metabolism | Cambridge MedChem Consulting*, n.d.; Zheng et al., 2021). Moreover, BioTransformer provided consistent results with EAWAG-PPS in the prediction of the environmental biodegradation of drugs in wastewater (Campos et al., 2021).

A total of 51 phase I and phase II metabolites were predicted (Table 9). For the first generation of metabolites EAWAG-PPS, GLORYx, and BioTransformer predicted 3, 7, and 15 metabolites, respectively. Four and 24 additional second-generation metabolites were predicted by EAWAG-PPS and GLORYx, respectively. GLORYx predicted 9 phase II metabolites that were not predicted
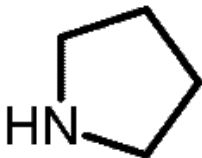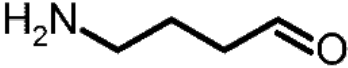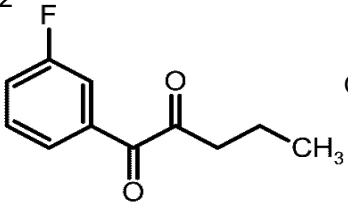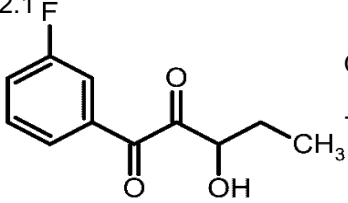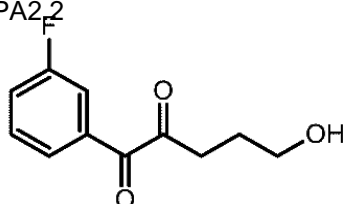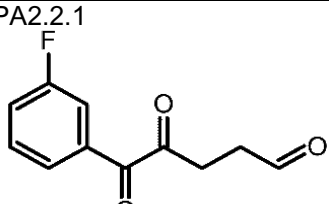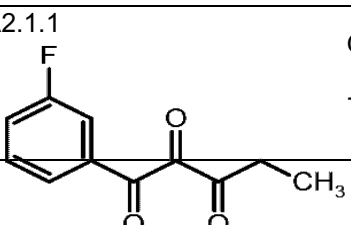
by the other software. Due to the different conceptualization, reference databases, and scope of the three software, their results only partially matched. In fact, none of the metabolites were predicted by all three software, whereas most were predicted by at least two software. In particular, the major transformations described by at least two software were *N*-dealkylation (EWAG-PPS, BioTransformer), hydroxylation at the pyrrolydine moiety, hydroxylation at the β- or ω- position of the alkyl chain (GLORYx, BioTransformer), β-ketoreduction (GLORYx, BioTransformer), and hydroxylation at the *para* or *meta* position of the aromatic ring (GLORYx, BioTransformer). The major transformations predicted by EAWAG-PPS only were oxidative *N*-dealkylation, hydroxylation, oxidation, *O*-sulfation, and β-ketoreduction. Only GLORYx predicted *O*-glucuronidation and *O*-sulfation as possible metabolic transformations. BioTransformer predicted other hydroxylation, epoxidation, and desaturation reactions. Noteworthy, the metabolites with an accurate mass beyond the range of HRMS acquisition (Section 2.4.2.) were not considered in the inclusion list due to their lack of specificity.
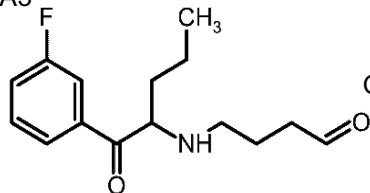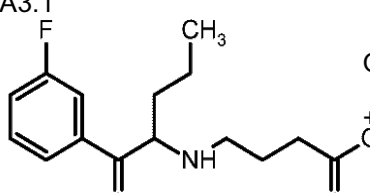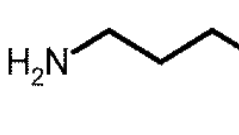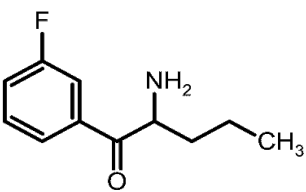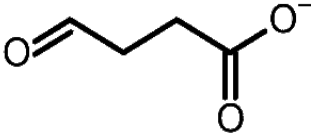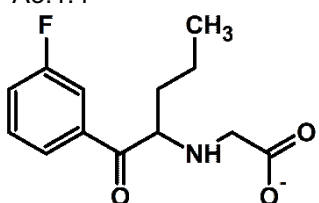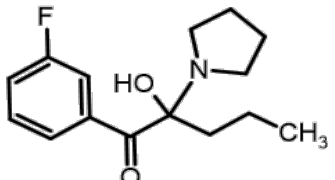
EAWAG-PPS and BioTransformer showed partially inconsistent results despite their similar conceptualization. Unexpectedly, 66% of the first-generation metabolites were predicted both by EAWAG-PPS and BioTransformer, and BioTransformer predicted 12 more metabolites than EAWAG-PPS (Djoumbou-Feunang, Fiamoncini, Gil-de-la-Fuente, Greiner, Manach, Wishart, et al., 2019). GLORYx was the computational tool with the highest number of predicted metabolites. None of the metabolites predicted by GLORYx were predicted also by EAWAG-PPS. Out of 31 metabolites predicted by GLORYx, only 6 were predicted also by BioTransformer.
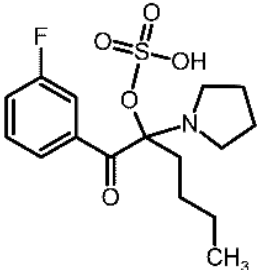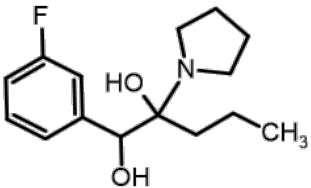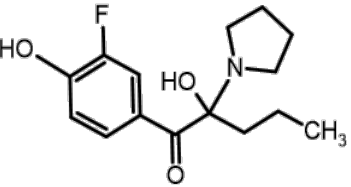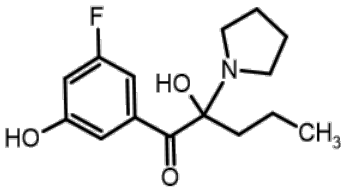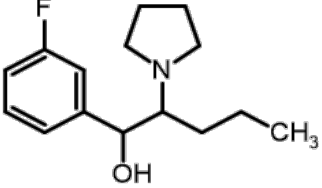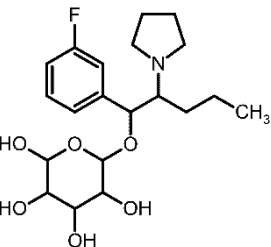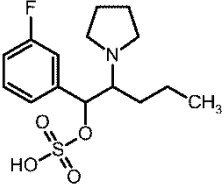
In previous *in vitro* studies on pyrrolidinophenones, hydroxylation, β-ketoreduction, oxidation, and *N*-dealkylation were the most common reactions (Carlier et al., 2021b; Ellefsen et al., 2016; Swortwood, Ellefsen, et al., 2016b). However, 7 metabolites identified in our hepatocyte incubations (M3-8, and M10) of 10 were predicted by one of the software, suggesting that a multiple approach may be satisfactory (M1 and M2 could not be predicted as they were the consequence of more than two metabolic transformations, see Subsection 3.5).

Noteworthy, the metabolites with the most intense signal were predicted by EAWAG-PPS (M7), GLORYx (M8), and BioTransformer (M8). A literature search was conducted to complete the inclusion list based on *in silico* results (Table 1 and 3, respectively). Glycine and alanine conjugation, dehalogenation, oxidative dehalogenation, dihydrodiol formation, and glutathione conjugation were also considered (Carlier et al., 2021a; Manier et al., 2020; Swortwood, Carlier, et al., 2016).
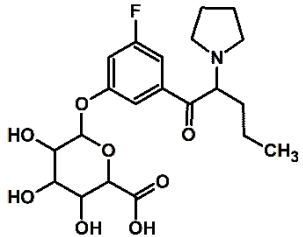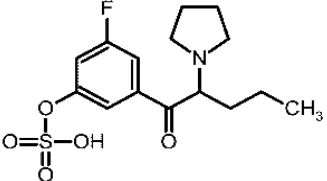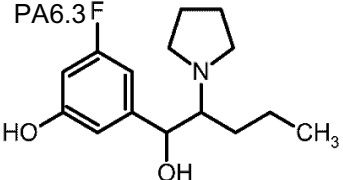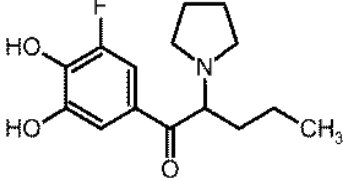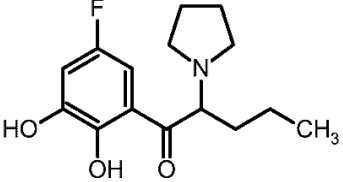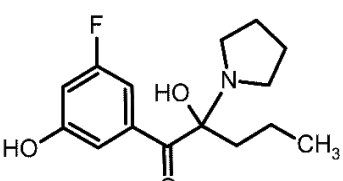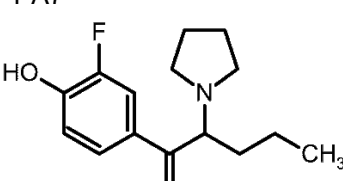
Table 9 Molecular structure, transformation, prediction software, and relative score of in silico prediction of 3F-α-PVP metabolites.

Molecular Structure	Transformation	Prediction Software	Score
PA1*	N-Dealkylation	EAWAG-PPS	*Likely*
		GLORYx	*N.P.*
		BioTransformer	*Predicted*
PA1.2*	N-Dealkylation + Oxidative N-dealkylation	EAWAG-PPS	*Likely*
		GLORYx	*N.P.*
		BioTransformer	*N.P.*
PA2	Oxidative N-dealkylation	EAWAG-PPS	*Likely*
		GLORYx	*N.P.*
		BioTransformer	*Predicted*
PA2.1	Oxidative N-dealkylation + Hydroxylation	EAWAG-PPS	*Neutral*
		GLORYx	*N.P.*
		BioTransformer	*N.P.*
PA2.2	Oxidative N-dealkylation + Hydroxylation	EAWAG-PPS	*Neutral*
		GLORYx	*N.P.*
		BioTransformer	*N.P.*
PA2.2.1	Oxidative N-dealkylation + Oxidation	EAWAG-PPS	*Likely*
		GLORYx	*N.P.*
		BioTransformer	*N.P.*
PA2.1.1	Oxidative N-dealkylation + Oxidation	EAWAG-PPS	*Neutral*
		GLORYx	*N.P.*
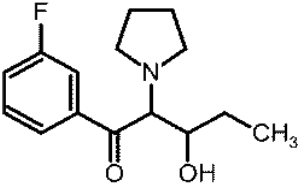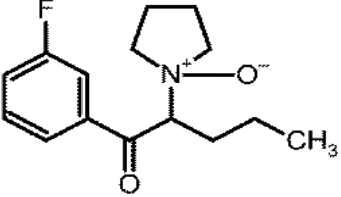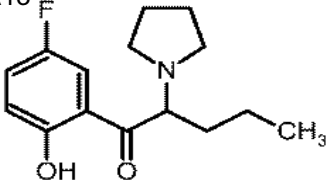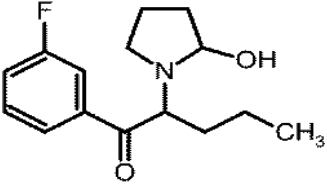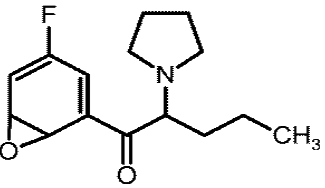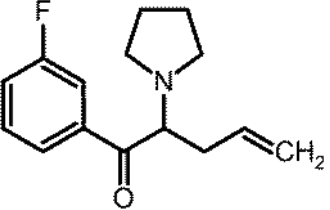
		BioTransformer	*N.P.*
PA3	Oxidative *N*-dealkylation	EAWAG-PPS	*Likely*
		GLORYx	*N.P.*
		BioTransformer	*N.P.*
PA3.1	Oxidative *N*-dealkylation + Hydroxylation	EAWAG-PPS	*Likely*
		GLORYx	*N.P.*
		BioTransformer	*N.P.*
PA3.1.1*	Oxidative *N*-dealkylation + Hydroxylation + *N*-Dealkylation	EAWAG-PPS	*Likely*
		GLORYx	*N.P.*
		BioTransformer	*N.P.*
PA3.1.2	Oxidative *N*-dealkylation + Hydroxylation + *N*-dealkylation	EAWAG-PPS	*Likely*
		GLORYx	*N.P.*
		BioTransformer	*N.P.*
PA3.1.3*	Oxidative *N*-dealkylation + Hydroxylation + Oxidative *N*-dealkylation	EAWAG-PPS	*Likely*
		GLORYx	*N.P.*
		BioTransformer	*N.P.*
PA3.1.4	Oxidative *N*-dealkylation + Hydroxylation + Oxidative dealkylation	EAWAG-PPS	*Likely*
		GLORYx	*N.P.*
		BioTransformer	*N.P.*
PA4	Hydroxylation	EAWAG-PPS	*N.P.*
		GLORYx	*0.58*
		BioTransformer	*Predicted*

PA4.1	Hydroxylation + *O*-Sulfation	EAWAG-PPS	*N.P.*
		GLORYx	*0.27*
		BioTransformer	*N.P.*

PA4.2	Hydroxylation + β-Ketoreduction	EAWAG-PPS	*N.P.*
		GLORYx	*0.26*
		BioTransformer	*N.P.*

PA4.3	Hydroxylation + Hydroxylation	EAWAG-PPS	*N.P.*
		GLORYx	*0.26*
		BioTransformer	*N.P.*

PA4.4	Hydroxylation + Hydroxylation	EAWAG-PPS	*N.P.*
		GLORYx	*0.26*
		BioTransformer	*N.P.*

PA5	β-Ketoreduction	EAWAG-PPS	*N.P.*
		GLORYx	*0.58*
		BioTransformer	*Predicted*

PA5.1	β-Ketoreduction + *O*-Glucuronidation	EAWAG-PPS	*N.P.*
		GLORYx	*0.43*
		BioTransformer	*N.P.*

PA5.2	β-Ketoreduction + *O*-Sulfation	EAWAG-PPS	*N.P.*
		GLORYx	*0.34*
		BioTransformer	*N.P.*

PA5.2	β-Ketoreduction + Oxidative *N*-dealkylation	EAWAG-PPS	*N.P.*
		GLORYx	*0.22*
		BioTransformer	*N.P.*
PA5.3	β-Ketoreduction + *N*-Oxidation	EAWAG-PPS	*N.P.*
		GLORYx	*0.22*
		BioTransformer	*N.P.*
PA5.5	β-Ketoreduction + Hydroxylation	EAWAG-PPS	*N.P.*
		GLORYx	*0.22*
		BioTransformer	*N.P.*
PA5.6	β-Ketoreduction + Oxidation	EAWAG-PPS	*N.P.*
		GLORYx	*0.22*
		BioTransformer	*N.P.*
PA5.7	β-Ketoreduction + Hydroxylation	EAWAG-PPS	*N.P.*
		GLORYx	*0.22*
		BioTransformer	*N.P.*
PA5.8	β-Ketoreduction + Hydroxylation	EAWAG-PPS	*N.P.*
		GLORYx	*0.21*
		BioTransformer	*N.P.*
PA5.9	β-Ketoreduction + Hydroxylation	EAWAG-PPS	*N.P.*
		GLORYx	*0.21*
		BioTransformer	*N.P.*
PA6	Hydroxylation	EAWAG-PPS	*N.P.*
		GLORYx	*0.58*

			BioTransformer	*Predicted*
PA6.1	Hydroxylation + O-Glucuronidation		EAWAG-PPS	*N.P.*
			GLORYx	*0.53*
			BioTransformer	*N.P.*
PA6.2	Hydroxylation + O-Sulfation		EAWAG-PPS	*N.P.*
			GLORYx	*0.52*
			BioTransformer	*N.P.*
PA6.3	Hydroxylation + β-Ketoreduction		EAWAG-PPS	*N.P.*
			GLORYx	*0.27*
			BioTransformer	*N.P.*
PA6.4	Hydroxylation + Hydroxylation		EAWAG-PPS	*N.P.*
			GLORYx	*0.27*
			BioTransformer	*N.P.*
PA6.5	Hydroxylation + Hydroxylation		EAWAG-PPS	*N.P.*
			GLORYx	*0.27*
			BioTransformer	*N.P.*
PA6.6	Hydroxylation + Hydroxylation		EAWAG-PPS	*N.P.*
			GLORYx	*0.27*
			BioTransformer	*N.P.*
PA7	Hydroxylation		EAWAG-PPS	*N.P.*
			GLORYx	*0.58*
			BioTransformer	*Predicted*

PA7.1 Hydroxylation + O-Glucuronidation	EAWAG-PPS	*N.P.*
	GLORYx	*0.56*
	BioTransformer	*N.P.*

PA8 Hydroxylation	EAWAG-PPS	*N.P.*
	GLORYx	*0.30*
	BioTransformer	*Predicted*

PA8.1 Hydroxylation + O-Glucuronidation	EAWAG-PPS	*N.P.*
	GLORYx	*0.26*
	BioTransformer	*N.P.*

PA8.2 Hydroxylation + O-Sulfation	EAWAG-PPS	*N.P.*
	GLORYx	*0.29*
	BioTransformer	*N.P.*

PA9 Hydroxylation	EAWAG-PPS	*N.P.*
	GLORYx	*0.30*
	BioTransformer	*Predicted*

PA9.1 Hydroxylation + O-Sulfation	EAWAG-PPS	*N.P.*
	GLORYx	*0.29*
	BioTransformer	*N.P.*

PA9.2 Hydroxylation + O-Glucuronidation	EAWAG-PPS	*N.P.*
	GLORYx	*0.29*
	BioTransformer	*N.P.*

PA10 Carboxylation	EAWAG-PPS	*N.P.*

		GLORYx	*0.30*
		BioTransformer	*N.P.*
PA11	Hydroxylation	EAWAG-PPS	*N.P.*
		GLORYx	*N.P.*
		BioTransformer	*Predicted*
PA12	*N*-Oxidation	EAWAG-PPS	*N.P.*
		GLORYx	*N.P.*
		BioTransformer	*Predicted*
PA13	Hydroxylation	EAWAG-PPS	*N.P.*
		GLORYx	*N.P.*
		BioTransformer	*Predicted*
PA14	Hydroxylation	EAWAG-PPS	*N.P.*
		GLORYx	*N.P.*
		BioTransformer	*Predicted*
PA15	Epoxidation	EAWAG-PPS	*N.P.*
		GLORYx	*N.P.*
		BioTransformer	*Predicted*
PA16	Desaturation	EAWAG-PPS	*N.P.*
		GLORYx	*N.P.*
		BioTransformer	*Predicted*
	Desaturation	EAWAG-PPS	*N.P.*
		GLORYx	*N.P.*

| PA17 | BioTransformer | *Predicted* |

3.2.2 3F-α-PVP metabolite identification

Prior to the analysis, a 1 µg/ml solution of 3F-α-PVP pure standard in MPA:MPB (95:5, v/v) was injected in the same LC-HRMS/MS conditions as described above to set the LC gradient and optimize the HESI conditions and collision energy in positive-ion mode (3F-α-PVP was not detected in negative-ion mode). 3F-α-PVP base peak ([M+H]$^+$, m/z 250.1601) was detected at 11.94 min, with a fragmentation pattern consistent with that of 4F-α-PVP [6]: 3F-α-PVP MS/MS spectrum contained ions m/z 109.0448 and 84.0808, corresponding to the fluorotropylium and pyridinium ions, respectively, m/z 126.1277 and 123.0241, produced through C-C cleavage at the α carbons of the carbonyl and pyrrolidinyl groups, and m/z 179.0867, produced by pyrrolidine loss (Fig. 13).

.
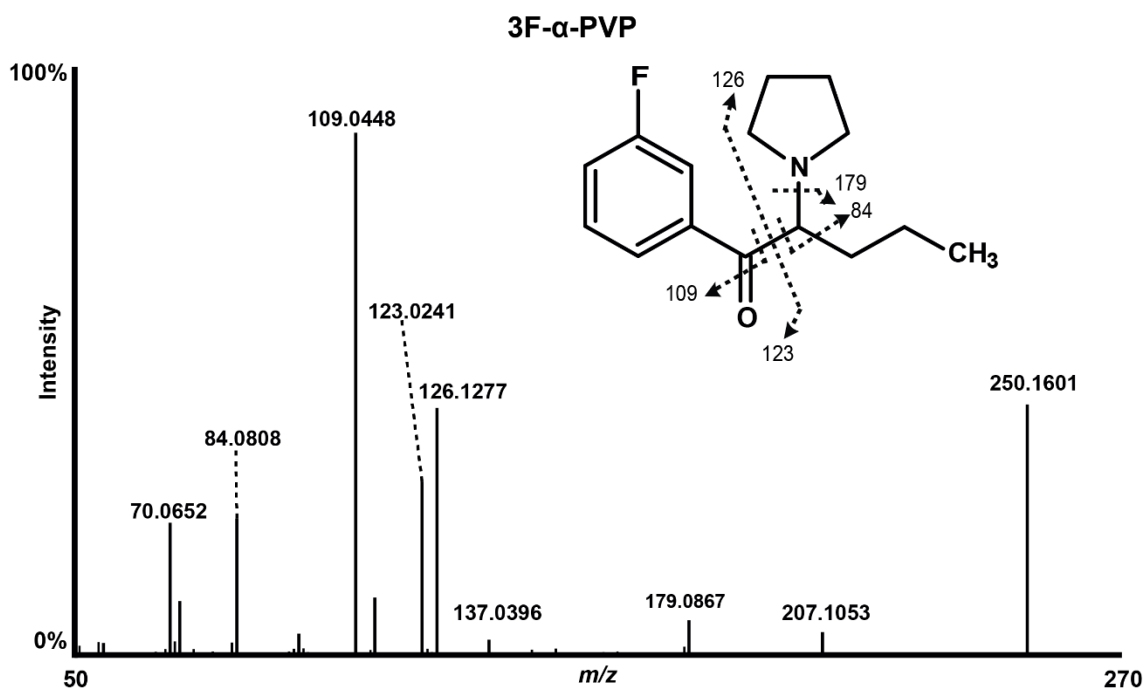
Figure 11 3F-α-PVP MS/MS spectrum and proposed fragments.

3F-α-PVP LC-HRMS peak area was 5 times lower after 3 h incubation with hepatocytes. Through Compound Discoverer untargeted analysis, 21,205 compounds were detected in the 3-h incubate with hepatocytes and 3F-α-PVP in positive- and negative-ion modes. Through the targeted analysis, a list of 22,025 theoretical combinations of metabolic transformations was generated, allowing for the detection of 132,202 compounds in the 3-h incubate in positive- and negative-ion modes. A total of 86,061 compounds were detected in all data files after merging the results. After filtering out background compounds, matrix components, and interferences using the control samples, and the compounds with a signal intensity lower than 0.5% of that of the 3F-α-PVP metabolite with the most intense signal (signal intensity threshold: 1.4×10^7), 93 potential metabolites were individuated and their mass deviation from theoretical elemental composition, isotopic pattern, and fragmentation pattern were scrutinized by two operators. A total of 10 3F-α-PVP metabolites were identified and listed from M1 to M10 by ascending retention time (figure 14, Table 10).
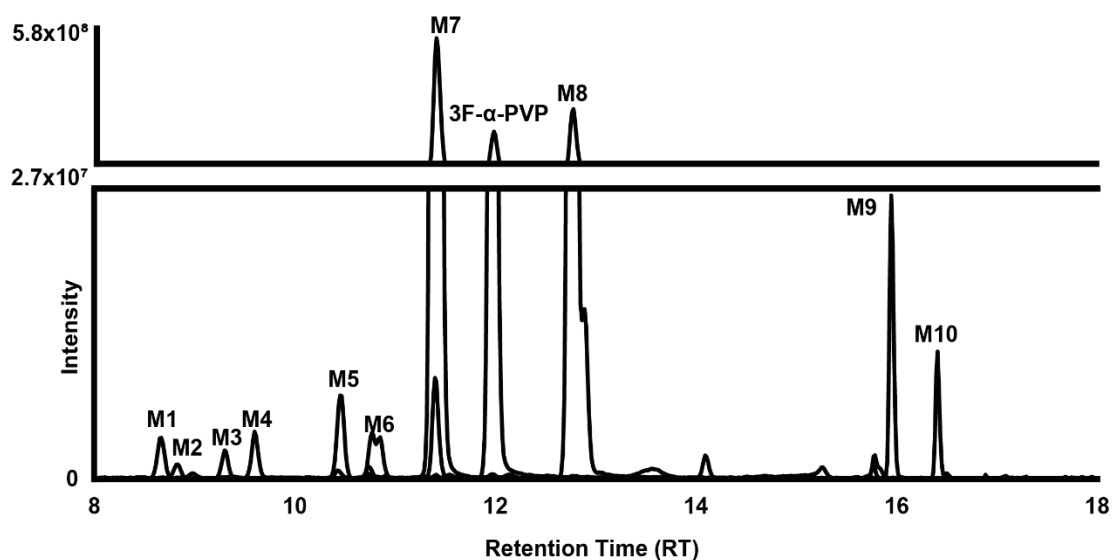
Figure 12 Combined extracted ion chromatogram of 3F-α-PVP and metabolites obtained after 3h human hepatocytes.

Major transformations were *N*-dealkylation at the pyrrolidine ring (Ma1, Ma2, Ma3, Ma5, and Ma7), β-ketoreduction of the carbonyl group (Ma1, Ma2, Ma8, and Ma10), hydroxylation/oxidation at the pyrrolidine ring (Ma5, Ma6, Ma7, Ma9, and Ma10) and hydroxylation at the fluorophenyl ring (Ma4). Although reported in the literature in the metabolic pattern of structural analogues and predicted *in silico*, phase II metabolites were not identified (Manier et al., 2018, 2020). 3F-α-PVP metabolic fate in humans is suggested in Figure 15. The fragmentation pattern of 3F-α-PVP metabolites is displayed in Figures 16 and 17.

Table 10 Matching predicted metabolite, metabolic transformation, retention time, accurate mass of molecular ion hydrogen adduct in positive-ion mode, elemental composition, deviation from theoretical mass, and chromatographic peak area of 3F-α-PVP metabolites after 3h incubation

Name	Metabolic transformation	Retention time (min)	$[M+H]^+$ (m/z)	Elemental composition	Peak Area after 3h incubation	Matching predicted metabolites
Ma1	β-Ketoreduction + *N*-Dealkylation	8.66	198.1289	$C_{11}H_{16}FNO$	2.3×10^7	-
Ma2	β-Ketoreduction + *N*-Dealkylation	8.83	198.1289	$C_{11}H_{16}FNO$	8.0×10^7	-
Ma3	*N*-Dealkylation	9.30	196.1132	$C_{11}H_{14}FNO$	1.4×10^7	EAWAG-PPS (P3.1.2)
Ma4	Hydroxylation (fluoro-phenyl)	9.60	266.1551	$C_{15}H_{20}FNO_2$	2.3×10^7	GLORYx, BioTransformer (P6, P7)
Ma5	Pyrrolidine opening + Oxidative dealkylation to *N*-ethanolic acid	10.46	254.1180	$C_{13}H_{16}FNO_3$	4.6×10^7	EAWAG-PPS (P3.1.4)

Ma6	Hydroxylation (pyrrolidine)	10.80	266.1550	$C_{15}H_{20}FNO_2$	3.5x10^7	BioTransformer (P14)
Ma7	Pyrrolidine opening to *N*-butanoic acid	11.40	282.1498	$C_{15}H_{20}FNO_3$	3.0x10^9	EAWAG-PPS (P3.1)
3F-α-PVP	N.A.	11.93	250.1601	$C_{15}H_{20}FNO$	8.9x10^8	N.A.
Ma8	β-Ketoreduction	12.76	252.1760	$C_{15}H_{22}FNO$	1.5x10^9	GLORYx, BioTransformer (P5)
Ma9	β-Ketoreduction + Oxidation (pyrrolidine)	15.94	266.1552	$C_{15}H_{20}FNO_2$	8.9x10^7	-
Ma10	Oxidation (pyrrolidine)	16.41	264.1396	$C_{15}H_{18}FNO_2$	4.0x10^7	GLORYx (P5.6)

N.A: Not applicable
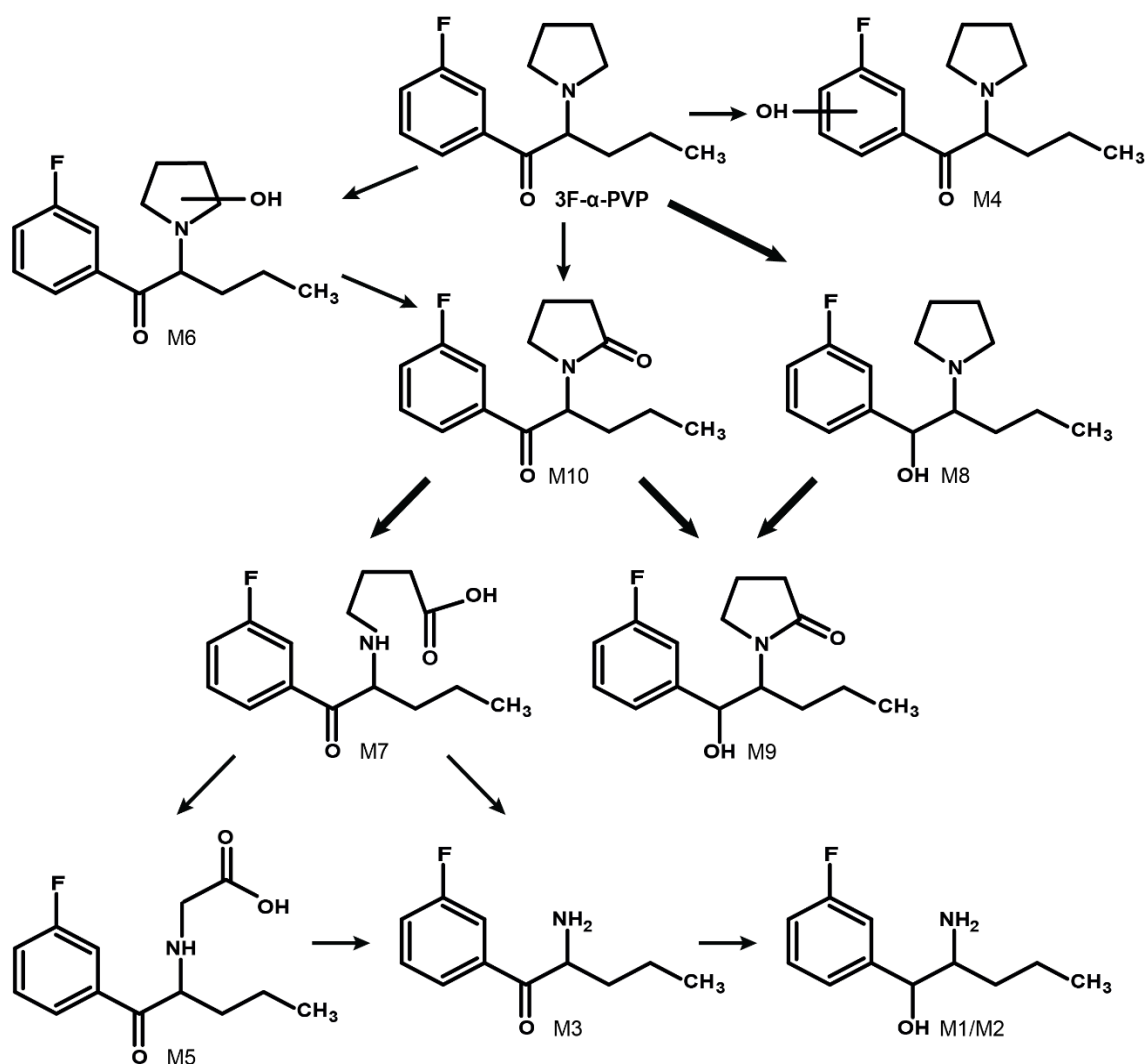
Figure 13 Proposed metabolic pattern of the 3F-α-PVP

3.2.3   3F-α-PVP β-ketoreduction

Similar to other pyrovalerone cathinones, 3F-α-PVP β−ketoreducted metabolite (Ma8, figure 17) was preponderant (Carlier et al., 2021a; Manier et al., 2018, 2020; Swortwood, Carlier, et al., 2016; Swortwood, Ellefsen, et al., 2016b). M8 eluted shortly after the parent drug at 12.76 min, similar to other cathinones with a β-ketoreduction in reversed-phase LC (Carlier et al., 2021a; Swortwood, Ellefsen, et al., 2016b), and M8 base peak was *m/z* 252.1760, corresponding to a +2.0159-Da mass shift from parent (+2H). Water loss (*m/z* 234.1651) was substantial in M8 fragmentation pattern and was also formed in the ionization source, further pointing towards the reduction of 3F-α-PVP carbonyl. M8 fragment

m/z 181.1024 (parent fragment *m/z* 179.0866 +2H) confirmed the transformation. Although 3F-α-PVP diagnostic ions *m/z* 123.0604 and 126.1277 were not detected, a metabolic reaction at the *N*-alkylpyrrolidine or fluorophenyl moieties were excluded due to the presence of ions *m/z* 71.0491 and 109.0448. Interestingly, M8 LC-HRMS peak presented a shoulder, most likely indicating the formation of two coeluted diastereoisomers, the reduction of the ketone group implying the formation of a chiral center. M8 was predicted through GLORYx (major metabolite) and BioTransformer (Pa5, Table 3).

BioTransformer suggests that the NADPH-dependent carbonyl reductase may be involved in this metabolic reaction. Negreira et al. demonstrated that the cytochrome P (CYP) 2D6 was involved in the β-ketoreduction of α-PVP, the 3F-α-PVP non-fluorinated analogue, using recombinant CYP, but the authors did not assess the role of the carbonyl reductase. They did not identify the enzyme involved in the β-ketoreduction of MDPV and methedrone, two other structural analogues (Negreira et al., 2015).
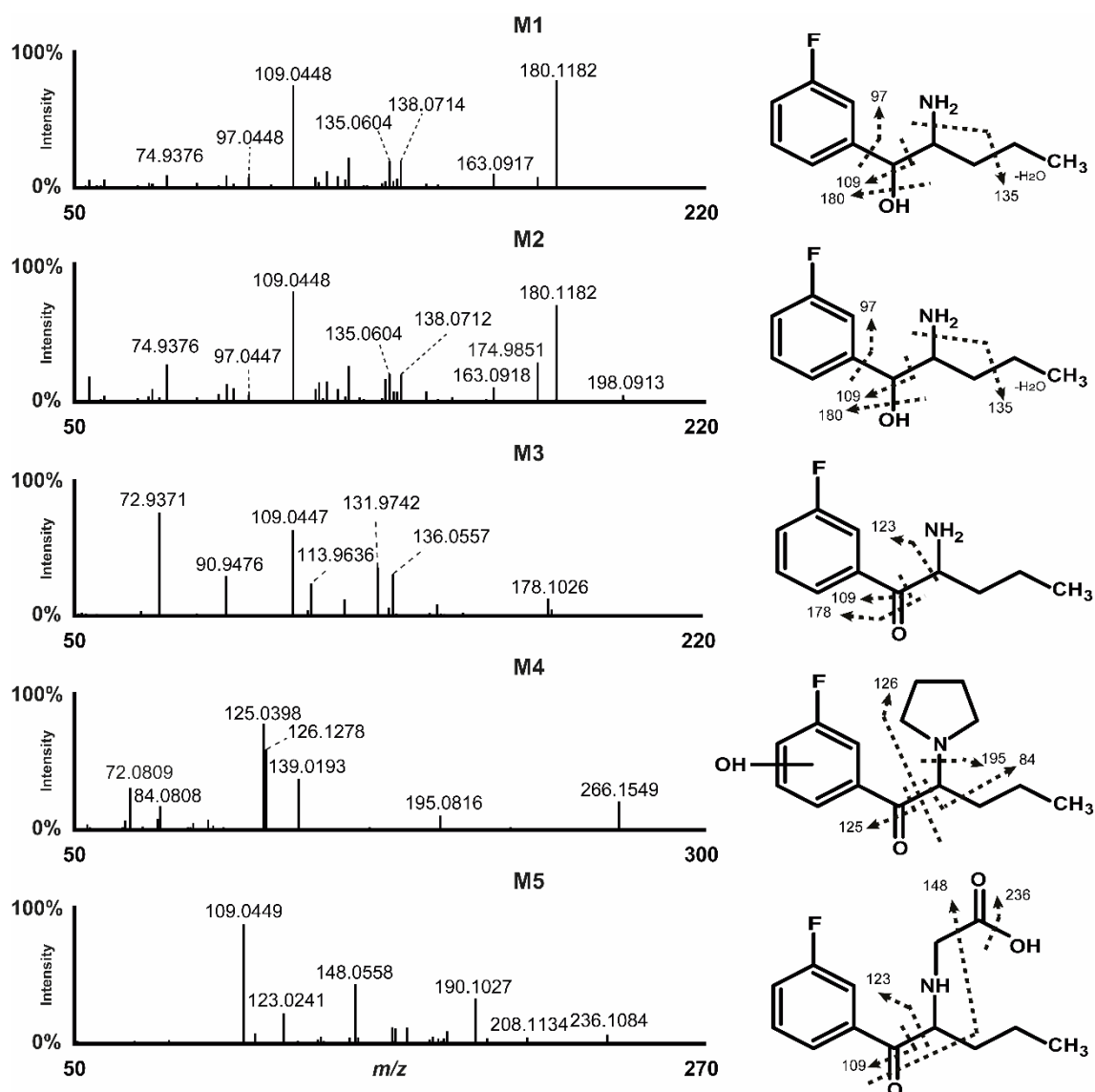
Figure 14 3F-α-PVP metabolites M1-M5 MS/MS spectrum and proposed fragments.

3.2.4 3F-α-PVP hydroxylation or oxidation

Hydroxylation is a common phase I transformation, and several hydroxylated metabolites were identified in the metabolism of pyrovalerone SCs, mainly at the pyrrolidine ring or the alkyl chain. In the present experiments, two isobaric compounds, Ma4 and Ma6, eluted at 9.60 and 10.80 min, respectively, with a base peak at m/z 266.1551, corresponding to a +15.9950-Da mass shift from parent (+O). Ma4 an Ma6 fragmentation patterns substantially differed (Fig. 4 and 5). Ma4 MS/MS spectrum contained 3F-α-PVP fragments m/z 84.0808 and 126.1278, indicating that the reaction did not occur at the pyrrolidine ring or the

alkyl chain of the molecule. However, fragments *m/z* 125.0398 and 139.0193 were detected instead of 3F-α-PVP fluorotropylium ion (*m/z* 109.0448) and fragment *m/z* 123.0241, respectively, further indicating that Ma4 was hydroxylated at the fluorophenyl ring. No water loss was detected, as the hydroxyl group was stabilized by the phenyl ring. Although the aromatic hydroxylation was not previously reported in the metabolic pattern of structural analogues, two possible sites of hydroxylation, in *meta* and *para* of the carbonyl group, were predicted by GLORYx and BioTransformer (Pa6 and Pa7, respectively, Table 9). The combined inductive effect of the carbonyl group and the fluorine atom suggests that the transformation likely occurred at position 5 of the fluorophenyl in Ma4, although the exact position cannot be confirmed in the present experiments. Interestingly, the corresponding metabolite was not detected in the metabolism of the positional isomer 4F-α-PVP, maybe due to the tridimensional configuration of the molecule or the absence of inductive effect. As such, Ma4 may be a specific biomarker of 3F-α-PVP to discriminate the two isomers in real cases. M6 MS/MS spectrum contained a water loss (*m/z* 248.1443) and 3F-α-PVP fragments *m/z* 109.0449, 123.0241, and 179.0866, suggesting that the metabolite was hydroxylated at the pyrrolidine ring. Fragment *m/z* 142.1226, corresponding to the hydroxy-*N*-alkylpyrrolidine moiety, further confirmed the position of the transformation. M6 LC-HRMS signal was a double peak, which may indicate the coelution of two position isomers or diastereoisomers. One hydroxy-pyrrolidinyl metabolite was predicted through BioTransformer (Pa14, Table 9), in position 2 of the pyrrolidine. Following the *in vitro* experiments of Manier et al. (Manier et al., 2018) and Negreira et al. (Negreira et al., 2015), several CYPs are involved in the hydroxylation of the pyrrolidine ring of other SCs, although the degree of involvement of specific CYPs is variable from an analogue to another. BioTransformer suggests CYP1A2 as the main metabolic enzyme responsible for M6 formation, and CYP1A2 and 2A6 for Ma4 formation.

Ma10 eluted at 16.41 min with a base peak at *m/z* 264.1396, corresponding to a +13.9795-Da mass shift from parent (+O -2H). M10 MS/MS total ion current had a low intensity and the background noise was substantial (Figure 17). M10 MS/MS spectrum contained 3F-α-PVP fragments *m/z* 109.0448, 123.0240, and

179.0866, suggesting that only the pyrrolidine ring was transformed, consistent with an oxidation. M10 late elution supported an oxidation at the position 2 of the pyrrolidine ring (γ-lactam), which acts as a hindrance for hydrogen bonding [29] . Although M10 was not predicted, it is a common metabolite of pyrrolidine SCs (Ellefsen et al., 2016; Swortwood, Carlier, et al., 2016). This reaction is mediated by various CYPs, as demonstrated with structural analogues (Manier et al., 2018).
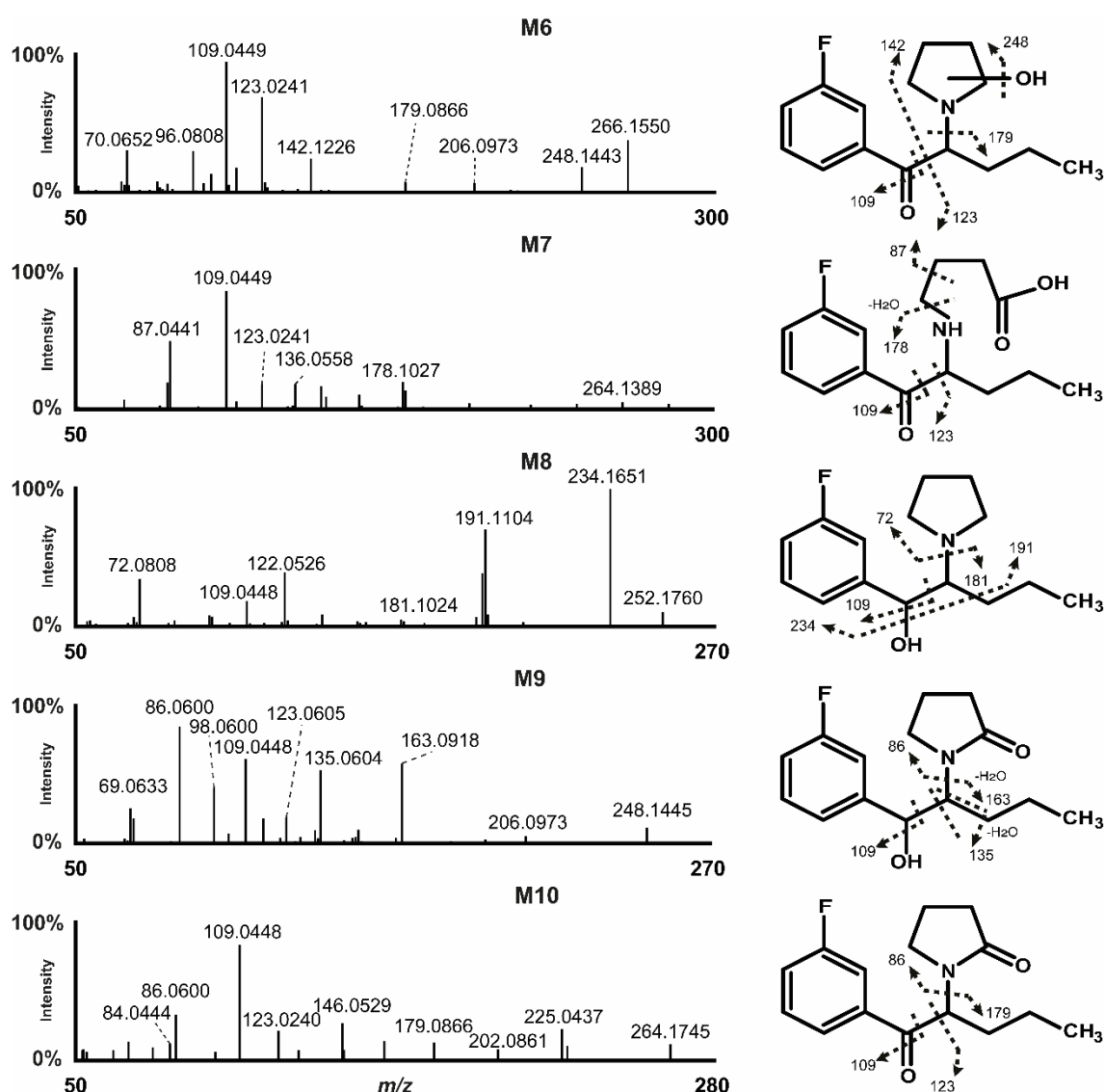
Figure 15 3F-α-PVP metabolites Ma6-Ma10 MS/MS spectrum and proposed fragments.

3.2.5 3F-α-PVP oxidation and β-ketoreduction

Ma9 eluted at 15.94 min with a base peak at m/z 266.1552, corresponding to a +15.9951-Da mass shift from parent (+O). Ma9 fragments m/z 86.0600 and 98.0600, also detected in Ma10 MS/MS spectrum indicated an oxidation at the pyrrolidine ring (+O -2H), while Ma8 fragments m/z 163.0918, produced by ketopyrrolidine and water losses, and sequential fragment m/z 135.0604, indicated a β-ketoreduction (+2H) (Fig. 5). Similar to Ma10, Ma9 late elution suggested an oxidation at the position 2 of the pyrrolidine ring (γ-lactam). Ma9 was predicted by EAWAG-PPS (P3, Table 3). *N*-Dealkylation to the corresponding *N*-butanal metabolite was considered as it matches Ma9 accurate mass. However, The *N*-butanal chain would be quickly transformed to the corresponding *N*-butanol or *N*-butanoic acid, which hardly fits with M9 signal intensity. Additionally, Ma9 fragments m/z 86.0600 and 98.0600 more likely point towards a β-ketoreduction and a pyrrolidine oxidation.

3.2.6 3F-α-PVP *N*-dealkylation

Ma7 was the 3F-α-PVP metabolite with the most intense signal (Fig. 2). The compound eluted at 11.40 min with a base peak at m/z 282.1498 in positive-ion mode, corresponding to a +31.9897-Da mass shift from parent (+2O). M7 MS/MS spectrum contained 3F-α-PVP fragments m/z 109.0449, 123.0241, and 179.0867, suggesting that the transformation occurred at the pyrrolidine ring (Fig. 5). Fragment m/z 87.0441, corresponding to the formation of butanoic acid, was intense, indicating that *N*-dealkylation to the corresponding *N*-butanoic acid occurred in M7, most likely following γ-lactam formation (Section 3.4.). Ma7 also produced a signal in negative-ion mode (m/z 280.1351), consistent with the presence of an acidic group, and the detection of acetic acid in Ma7 fragmentation pattern in negative-ion mode (m/z 59.0138) confirmed the formation of a carboxylic acid group. This transformation is major in the metabolic pathway of pyrrolidine SCs and was highly expected. It was also predicted through EAWAG-PPS (P3.1, Table 3), but not through BioTransformer nor GLORYx, although these two freeware were designed for metabolic studies in humans. The corresponding metabolite was identified in the metabolic pathway of α-PVT, 4-

methoxy-α-PVP, α-PHP, and 4F-α-PVP, but was identified as a dihydroxy-pyrrolidine instead of an *N*-butanoic acid, due to the two losses of water detected after fragmentation (Carlier et al., 2021a; Ellefsen et al., 2016; Swortwood, Ellefsen, et al., 2016a). However, the absence of screening in negative-ion mode, which may have helped structure elucidation, is a drawback of these studies. γ-Lactam hydrolysis can occur spontaneously in basic and acidic conditions, although it is not clear what metabolic enzyme is involved in the transformation.

Ma7 was further transformed to the corresponding *N*-ethanoic acid M5. M5 eluted at 10.46 min with a base peak at *m/z* 254.1180 in positive-ion mode, corresponding to a +3.9579-Da mass shift from parent (+2O-2C-4H). 3F-α-PVP fragment *m/z* 109.049 and 123.0241 in M5 MS/MS spectrum indicated that the fluorophenyl ring was not transformed (Fig. 4). Similar to Ma7, Ma5 produced a signal in negative-ion mode (*m/z* 252.1040), and the signal of the acetic acid (*m/z* 59.0138) was intense, confirming the formation of a carboxylic acid group. Although this transformation was predicted through EAWAG-PPS (P3.1.4, Table 3), it was not compiled in the LC-HRMS/MS inclusion list, as it was not identified in the metabolic pathway of other pyrrolidine SCs. However, the metabolite was detected through Compound Discoverer untargeted data mining, highlighting the importance of an exhaustive screening of LC-HRMS/MS raw data in metabolite identification studies. This reaction is typical of fatty acid metabolism.

Further Ma5 and Ma7 *N*-dealkylation produced Ma3, which eluted at 9.30 min with a base peak at *m/z* 196.1132, corresponding to a -54.0469-Da mass shift from parent (-4C-6H). Ma3 MS/MS spectrum contained 3F-α-PVP fragments *m/z* 109.0447 and 123.0241, indicating that the transformation did not occur at the fluorophenyl ring. However, 3F-α-PVP pyridinium ion was not detected, and fragment *m/z* 72.0808 was detected instead of fragment *m/z* 123.0241, indicating that Ma3 was *N*-dealkylated. Fragment *m/z* 72.9371 had the most intense signal in Ma3 HRMS/MS spectrum, but was produced by ion m/z 196.0168, which was an interference present during the whole chromatographic separation and was fragmented along with M3. M3 was predicted by EAWAG-PPS (P3.1.2, Table 9).

3.5.1. 3F-α-PVP N-dealkylation and β-ketoreduction

Following the same reasoning, we found that Ma1 and Ma2 (*m/z* 198.1289, eluting at 8.66 and 8.83 min, respectively) were formed by *N*-dealkylation, as observed in M3 (Section 3.5), and β-ketoreduction, as observed in M8 (Section 3.3). M1 and M2 are diastereoisomers, resulting from the formation of a chiral center after β-ketoreduction. These two metabolites were not predicted, as they are the consequence of several successive metabolic transformations (Fig. 16). For the same reason, their detection *in vivo* is unlikely.

3.2.7 3F-α-PVP phase II metabolites

Although different phase II metabolites were observed both *in vitro* and *in vivo* in the metabolic pathway of other pyrovalerone SCs as minor metabolites, conjugated metabolites were not detected in the present experiments (Manier et al., 2018, 2020). A particular attention was paid for the detection of conjugated metabolites with glycine and alanine (with and without rearrangement), which were recently reported for the first time as metabolites of pyrrolidine SCs α-PBP and α-PEP after incubation with human hepatocytes (Manier et al., 2020). However, these metabolites could not be detected. Glucuronidation, sulfation, and glutathione conjugation did not occur either, although glucuronides and sulphates were predicted (Table 9), suggesting that 3F-α-PVP phase II metabolic transformations are not frequent.

3.2.8 Comparison to 4F-α-PVP metabolism

4F-α-PVP metabolism, assessed in similar conditions, was previously described (Carlier et al., 2021a). The following metabolites were described: 4F-α-PVP 2'-hydroxypyrrolidinyl (F1), 4F-α-PVP dihydroxy-pyrrolidinyl (F2), 4F-α-PVP pentanol (F3), 4F-α-PVP 2'-ketopyrrolidinyl-pentanol (F4), and 4F-α-PVP 2'-ketopyrrolidinyl (F5). The same metabolic reactions occurred in 3F-α-PVP, with similar relative intensities: F1 matched Ma6, F2 matched Ma7 (as F2 likely was misidentified, see Subsection 3.5), F3 matched Ma8, F4 matched Ma9, and F5 matched Ma10. Additional metabolites were observed in 3F-α-PVP metabolic pattern. Ma1–Ma5 were minor in the present experiments and the corresponding

metabolites were not detected in 4F-α-PVP experiments, probably due to an intensity below the reporting threshold. Fluorophenyl hydroxylation, however, was not detected in 4F-α-PVP experiments. 3F-α-PVP and 4F-α-PVP major metabolites are similar and may be hardly distinguishable with regular LC-MS/MS screening. However, the detection of 3F-α-PVP hydroxy-fluorophenyl (Ma4), although a minor metabolite in the present experiments, might be necessary.

4 . Conclusions

Nowadays, the NPS phenomenon affects more than 100 countries all over the World, causing an increasing number of deaths. Among the 1,100 substances characterised to date, SCs and fentanyl analogues are the most representative and the most deadly class of NPS on the black market. A big challenge for forensic toxicologists is to be updated with new trends of NPS that continuously appear in the black market, especially the dark web. In this respect, the in vitro metabolism studies are a crucial first step in the elucidation of toxicokinetic profiles of the new NPS.

The applied experimental protocol allowed us to efficiently study the in vitro metabolic fate of three substances. The developed protocols demonstrated to be suitable for different structural class of substances (fentanyl analogues and cathinone). Furthermore, interesting aspects of metabolism of similar molecules were observed, confirming the role of certain moieties in the enzymatic interactions.

4.1 Phenylfentanyl and β'-phenylfentanyl in vitro metabolism

Although common metabolic reactions can be identified within the NPS subclass of fentanyl analogues, the metabolic fate of these substances is hardly predictable. *In silico* predictions with GLORYx freeware were unsuitable for the prediction of phenylfentanyl metabolites, as the hydrolysis of the amide group was not considered. Therefore, investigating the *in vitro* metabolism of fentanyl analogues is a fundamental first step towards the characterization of their *in vivo* metabolism.

We hereby provide the first metabolite profiling of phenylfentanyl and β'-phenylfentanyl, proposing an original workflow including 1) *in silico* predictions to assist metabolite identification, 2) *in vitro* human hepatocyte incubations to generate a comprehensive metabolic profile of the substance, 3) data-dependent LC-HRMS/MS analysis, 4) software-assisted data mining with comprehensive targeted/untargeted strategy, and 5) report of results to mzCloud and HighResNPS databases for screening purposes. The overall workflow is suitable for NPS metabolite identification studies, considering the rapid and continuous emergence of new substances onto the drug market.

We identified 13 phenylfentanyl and 27 β'-phenylfentanyl metabolites, mostly produced by N-dealkylation, amide hydrolysis, oxidation, and combinations thereof. We suggest phenylnorfentanyl (M6) and β'-phenylnorfentanyl as the main biological marker of these fentanyl analogues use, and we proposed the inclusion of the fragmentation pattern in online libraries mzCloud and HighResNPS. Surprisingly, 4-ANPP was observed only for phenylfentanyl (M8), as well as 1-(2-phenylethyl)-4-piperidinol (M2), and further metabolites. A role of the N-amide substituent steric bulk is suggested for this metabolic reaction, since it was reported also for other fentanyl analogues during synthesis and/or metabolism. However, the detection of these metabolites in authentic samples should prompt the toxicologist to search for the presence of specific markers of phenylfentanyl use. Phase II transformations were detected only for β'phenylfentanyl as minor metabolites, therefore the hydrolysis of the biological samples would not increase the detection capability of non-conjugated metabolites. These few key metabolites will guide manufacturers in their synthetic efforts, to enable the quantification of phenylfentanyl metabolites with a properly validated method and the conduction of further pharmacokinetic studies.

4.2 3F-α-PVP *in vitro* metabolism

We characterized 3F-α-PVP *in vitro* metabolism in human hepatocyte incubations with multiple *in silico* metabolite predictions, LC-HRMS/MS analysis, and software-assisted targeted/untargeted data mining. Ten metabolites were identified after 3 h incubation, including hydrogenated,

hydroxylated, oxidated, and *N*-dealkylated metabolites; phase II transformations were not detected. We suggest 3F-α-PVP *N*-butanoic acid (Ma7), 3F-α-PVP pentanol (Ma8), and 3F-α-PVP 2-ketopyrrolidinyl-pentanol (Ma9) as specific biomarkers of 3F-α-PVP intake; 3F-α-PVP itself might be marker of exposure, but it is not assessed in the present experiments. 3F-α-PVP metabolism was consistent with the *in vitro* and *in vivo* metabolism of other pyrrolidine SCs. To the best of our knowledge, this is the first time that an *N*-ethanoic acid (Ma5) was detected in the metabolic pathway of a pyrrolidine SC and was unexpected, demonstrating the importance of a dual targeted/untargeted data mining strategy. The detection of 3F-α-PVP hydroxy-fluorophenyl (Ma4), although a minor metabolite in the present experiments, might be necessary to discriminate 3F-α-PVP and 4F-α-PVP use. *In vivo* experiments with authentic human specimens is necessary to confirm the results. However, we could not obtain such specimens. The identification of *in vitro* metabolites will help toxicologists identify 3F-α-PVP-positive specimens.

The metabolite prediction software were not able to accurately predict 3F-α-PVP metabolism, highlighting the importance of *in vitro* models of human metabolism. However, the combination of the three software generated an exhaustive list of putative metabolites that supported the present experiments for compiling the LC-HRMS/MS inclusion list and the list of potential metabolic transformations in Compound Discoverer and help manual metabolite identification after software-assisted data mining. The multiple *in silico* approach allowed the prediction of 7 out of 10 detected metabolites, all major metabolites being predicted.

5 References

Aczel, T., & Lumpkin, H. E. (1960). Correlation of mass spectra with structure in aromatic oxygenated compounds.Aromatic alcohols and phenols. *Analytical Chemistry*, *32*(13), 1818–1822.

Åstrand, A., Töreskog, A., Watanabe, S., Kronstrand, R., Gréen, H., & Vikingsson, S. (2019). Correlations between metabolism and structural elements of the alicyclic fentanyl analogs cyclopropyl fentanyl, cyclobutyl fentanyl, cyclopentyl fentanyl, cyclohexyl fentanyl and 2,2,3,3-tetramethylcyclopropyl fentanyl studied by human hepatocytes and LC-QTOF-MS. *Archives of Toxicology*, *93*(1), 95–106. https://doi.org/10.1007/s00204-018-2330-9

Bolton, J. L., & Dunlap, T. (2017). Formation and biological targets of quinones: Cytotoxic versus cytoprotective effects. *Chemical Research in Toxicology*, *30*(1), 13–37. https://doi.org/10.1021/acs.chemrestox.6b00256

Bradshaw, P. R., Wilson, I. D., Gill, R. U., Butler, P. J., Dilworth, C., & Athersuch, T. J. (2018). Metabolic Hydrolysis of Aromatic Amides in Selected Rat, Minipig, and Human in Vitro Systems. *Scientific Reports*, *8*(1), 2405. https://doi.org/10.1038/S41598-018-20464-4

Brunetti, P., Pirani, F., Carlier, J., Giorgetti, R., Busardò, F. P., & Lo Faro, A. F. (2020). A 2017–2019 Update on Acute Intoxications and Fatalities from Illicit Fentanyl and Analogs. *Journal of Analytical Toxicology*, 1–18. https://doi.org/10.1093/jat/bkaa115

BruynKops, C. de, Šícho, M., Mazzolari, A., & Kirchmair, J. (2020). GLORYx: Prediction of the Metabolites Resulting from Phase 1 and Phase 2 Biotransformations of Xenobiotics. *Chemical Research in Toxicology*, *34*(2), 286–299. https://doi.org/10.1021/ACS.CHEMRESTOX.0C00224

Campos, E., De Martinis, E., & De Martinis, B. (2021). Forensic Analysis of Illicit Drugs and Novel Psychoactive Substances in Wastewater: A review of Toxicological, Chemical and Microbiological Aspects. *Brazilian Journal of Analytical Chemistry*, *February*, 1–20. https://doi.org/10.30744/brjac.2179-3425.rv-19-2021

Carlier, J., Diao, X., Giorgetti, R., Busardò, F. P., & Huestis, M. A. (2021a). Pyrrolidinyl synthetic cathinones α-php and 4f-α-pvp metabolite profiling using human hepatocyte incubations. *International Journal of Molecular Sciences*, *22*(1), 1–17. https://doi.org/10.3390/ijms22010230

Carlier, J., Diao, X., Giorgetti, R., Busardò, F. P., & Huestis, M. A. (2021b). Pyrrolidinyl Synthetic Cathinones α-PHP and 4F-α-PVP Metabolite Profiling Using Human Hepatocyte Incubations. *International Journal of Molecular Sciences*, *22*(1), 1–17. https://doi.org/10.3390/IJMS22010230

Carlier, J., Diao, X., & Huestis, M. A. (2018). Synthetic cannabinoid BB-22 (QUCHIC): Human hepatocytes metabolism with liquid chromatography-high resolution mass spectrometry detection. *Journal of Pharmaceutical and Biomedical Analysis*, *157*, 27–35. https://doi.org/10.1016/j.jpba.2018.05.007

Carlier, J., Diao, X., Scheidweiler, K. B., & Huestis, M. A. (2017). Distinguishing intake of new synthetic cannabinoids ADB-PINACA and 5F-ADB-PINACA with human hepatocyte metabolites and high-resolution mass spectrometry. *Clinical Chemistry*, *63*(5), 1008–1021. https://doi.org/10.1373/clinchem.2016.267575

Carlier, J., Diao, X., Wohlfarth, A., Scheidweiler, K., & Huestis, M. A. (2017). In Vitro Metabolite Profiling of ADB-FUBINACA, A New Synthetic Cannabinoid. *Current Neuropharmacology*, *15*(5), 682–691. https://doi.org/10.2174/1570159x15666161108123419

Carlier, J., Scheidweiler, K. B., Wohlfarth, A., Salmeron, B. D., Baumann, M. H., & Huestis, M. A. (2016). Quantification of [1-(5-fluoropentyl)-1H-indol-3-yl](naphthalene-1-yl)methanone (AM-2201) and 13 metabolites in human and rat plasma by liquid chromatography-tandem mass spectrometry. *Journal of Chromatography A*, *1451*, 97–106. https://doi.org/10.1016/j.chroma.2016.05.020

de Bruyn Kops, C., Šícho, M., Mazzolari, A., & Kirchmair, J. (2021). GLORYx: Prediction of the Metabolites Resulting from Phase 1 and Phase 2 Biotransformations of Xenobiotics. *Chemical Research in Toxicology*, *34*(2), 286–299. https://doi.org/10.1021/acs.chemrestox.0c00224

DEA. (2010). Federal Register : Control of Immediate Precursor Used in the Illicit Manufacture of Fentanyl as a Schedule II Controlled Substance. *Federal Register*, *75*(124), 37295–37299. https://www.federalregister.gov/documents/2010/06/29/2010-15520/control-of-immediate-precursor-used-in-the-illicit-manufacture-of-fentanyl-as-a-schedule-ii

Di Trana, A., & Del Rio, A. (2020). Fentanyl analogues potency: What should be known. *Clinica Terapeutica*, *171*(5), e412–e413. https://doi.org/10.7417/CT.2020.2250

Di Trana, A., & La Maida, N. (2021). New Psychoactive Substances consumption and their monitoring during COVID-19 pandemic. *Clinica Terapeutica*, *172*(4), 271–272. https://doi.org/10.7417/CT.2021.2330

Di Trana, Annagiulia, Brunetti, P., Giorgetti, R., Marinelli, E., Zaami, S., Busardò, F. P., & Carlier, J. (2021). In silico prediction, LC-HRMS/MS analysis, and targeted/untargeted data-mining workflow for the profiling of phenylfentanyl in vitro metabolites. *Talanta*, *235*(July). https://doi.org/10.1016/j.talanta.2021.122740

Di Trana, Annagiulia, Carlier, J., Berretta, P., Zaami, S., & Ricci, G. (2020). Consequences of COVID-19 Lockdown on the Misuse and Marketing of Addictive Substances and New Psychoactive Substances. *Frontiers in Psychiatry*, *11*, 584462. https://doi.org/10.3389/fpsyt.2020.584462

Diao, X., & Huestis, M. A. (2017). Approaches, Challenges, and Advances in Metabolism of New Synthetic Cannabinoids and Identification of Optimal Urinary Marker Metabolites. In *Clinical Pharmacology and Therapeutics* (Vol. 101, Issue 2, pp. 239–253). Nature Publishing Group. https://doi.org/10.1002/cpt.534

Diao, Xingxing, Carlier, J., Zhu, M., & Huestis, M. A. (2017). Human hepatocyte metabolism of novel synthetic cannabinoids MN-18 and its 5-fluoro analog 5F-MN-18. *Clinical Chemistry*, *63*(11), 1753–1763. https://doi.org/10.1373/clinchem.2017.277152

Diao, Xingxing, Carlier, J., Zhu, M., & Huestis, M. A. (2018). Metabolism of the new synthetic cannabinoid EG-018 in human hepatocytes by high-

resolution mass spectrometry. *Forensic Toxicology*, *36*(2), 304–312. https://doi.org/10.1007/s11419-018-0404-2

Diao, Xingxing, & Huestis, M. A. (2019). New Synthetic Cannabinoids Metabolism and Strategies to Best Identify Optimal Marker Metabolites. *Frontiers in Chemistry*, *7*(MAR), 109. https://doi.org/10.3389/fchem.2019.00109

Djoumbou-Feunang, Y., Fiamoncini, J., Gil-de-la-Fuente, A., Greiner, R., Manach, C., & Wishart, D. S. (2019). BioTransformer: A comprehensive computational tool for small molecule metabolism prediction and metabolite identification. *Journal of Cheminformatics*, *11*(1), 2. https://doi.org/10.1186/s13321-018-0324-5

Djoumbou-Feunang, Y., Fiamoncini, J., Gil-de-la-Fuente, A., Greiner, R., Manach, C., Wishart, D. S., Yousefnejad, D., Johnson, E., Djoumbou-Feunang, Y., Fiamoncini, J., Gil-de-la-Fuente, A., Greiner, R., Manach, C., & Wishart, D. S. (2019). BioTransformer: A comprehensive computational tool for small molecule metabolism prediction and metabolite identification. *Journal of Cheminformatics*, *11*(1), 2. https://doi.org/10.1186/s13321-018-0324-5

Ellefsen, K. N., Wohlfarth, A., Swortwood, M. J., Diao, X., Concheiro, M., & Huestis, M. A. (2016). 4-Methoxy-α-PVP: in silico prediction, metabolic stability, and metabolite identification by human hepatocyte incubation and high-resolution mass spectrometry. *Forensic Toxicology*, *34*(1), 61–75. https://doi.org/10.1007/s11419-015-0287-4

EMCDDA. (2020). *European Drug Report 2020: Trends and Developments*. https://doi.org/10.2810/123451

Espinosa-Barrera, P. A., Delgado-Vargas, C. A., Martínez-Pachón, D., & Moncayo-Lasso, A. (2021). Using computer tools for the evaluation of biodegradability, toxicity, and activity on the AT1 receptor of degradation products identified in the removal of valsartan by using photo-electro-Fenton process. *Environmental Science and Pollution Research*, *28*(19), 23984–23994. https://doi.org/10.1007/s11356-020-11949-9

European Monitoring Centre for Drugs and Drug Addiction. (2021). *European*

Drug Report 2021: Trends and Developments. Publications Office of the European Union. https://doi.org/10.2810/18539

Feasel, M. G., Wohlfarth, A., Nilles, J. M., Pang, S., Kristovich, R. L., & Huestis, M. A. (2016). Metabolism of Carfentanil, an Ultra-Potent Opioid, in Human Liver Microsomes and Human Hepatocytes by High-Resolution Mass Spectrometry. *AAPS Journal*, *18*(6), 1489–1499. https://doi.org/10.1208/s12248-016-9963-5

Fever, D. (2019). DrugFacts: Fentanyl | National Institute on Drug Abuse (NIDA). *February 2019*, *Febr. 2019*, 1–6.

Gao, J., Ellis, L. B. M., & Wackett, L. P. (2009). The University of Minnesota Biocatalysis/Biodegradation Database: Improving public access. *Nucleic Acids Research*, *38*(SUPPL.1), D488–D491. https://doi.org/10.1093/nar/gkp771

Ghidini, A., Scalvini, L., Palese, F., Lodola, A., Mor, M., & Piomelli, D. (2021). Different roles for the acyl chain and the amine leaving group in the substrate selectivity of N-Acylethanolamine acid amidase. *Https://Doi.Org/10.1080/14756366.2021.1912035*, *36*(1), 1411–1423. https://doi.org/10.1080/14756366.2021.1912035

Grafinger, K. E., Wilde, M., Otte, L., & Auwärter, V. (2021). Pharmacological and metabolic characterization of the novel synthetic opioid brorphine and its detection in routine casework. *Forensic Science International*, *327*, 110989. https://doi.org/10.1016/j.forsciint.2021.110989

HighChem LLC. (2021). *mzCloud – Advanced Mass Spectral Database*. https://www.mzcloud.org/

Kahns, A. H., & Bundgaard, H. (1991). N-Acyl derivatives as prodrug forms for amides: Chemical stability and enzymatic hydrolysis of various N-acyl and N-alkoxycarbonyl amide derivatives. *International Journal of Pharmaceutics*, *71*(1–2), 31–43. https://doi.org/10.1016/0378-5173(91)90065-V

Kanamori, T., Iwata, Y. T., Segawa, H., Yamamuro, T., Kuwayama, K., Tsujikawa, K., & Inoue, H. (2018). Metabolism of Fentanyl and Acetylfentanyl in Human-Induced Pluripotent Stem Cell-Derived

Hepatocytes. *Biol. Pharm. Bull*, *41*(1), 106–114.
https://doi.org/10.1126/science.291.5512.2398

Kazmi, S. R., Jun, R., Yu, M. S., Jung, C., & Na, D. (2019). In silico approaches
and tools for the prediction of drug metabolism and fate: A review.
Computers in Biology and Medicine, *106*(September 2018), 54–64.
https://doi.org/10.1016/j.compbiomed.2019.01.008

Keller, B. O., Sui, J., Young, A. B., & Whittal, R. M. (2008). Interferences and
contaminants encountered in modern mass spectrometry. In *Analytica
Chimica Acta* (Vol. 627, Issue 1, pp. 71–81).
https://doi.org/10.1016/j.aca.2008.04.043

Kirchmair, J., Göller, A. H., Lang, D., Kunze, J., Testa, B., Wilson, I. D., Glen, R.
C., & Schneider, G. (2015). Predicting drug metabolism: Experiment and/or
computation? *Nature Reviews Drug Discovery*, *14*(6), 387–404.
https://doi.org/10.1038/nrd4581

La Maida, N., Di Trana, A., Giorgetti, R., Tagliabracci, A., Busardò, F. P., &
Huestis, M. A. (2021). A Review of Synthetic Cathinone-Related Fatalities
From 2017 to 2020. *Therapeutic Drug Monitoring*, *43*(1), 52–68.
https://doi.org/10.1097/FTD.0000000000000808

Labroo, R. B., Paine, M. F., Thummel, K. E., & Kharasch, E. D. (1997). Fentanyl
metabolism by human hepatic and intestinal cytochrome P450 3A4:
Implications for interindividual variability in disposition, efficacy, and drug
interactions. *Drug Metabolism and Disposition*, *25*(9), 1072–1080.

Lo Faro, A. F., Di Trana, A., La Maida, N., Tagliabracci, A., Giorgetti, R., &
Busardò, F. P. (2019). Biomedical analysis of New Psychoactive
Substances (NPS) of natural origin. *Journal of Pharmaceutical and
Biomedical Analysis*, 112945. https://doi.org/10.1016/j.jpba.2019.112945

Manier, S. K., Richter, L. H. J., Schäper, J., Maurer, H. H., & Meyer, M. R.
(2018). Different in vitro and in vivo tools for elucidating the human
metabolism of alpha-cathinone-derived drugs of abuse. *Drug Testing and
Analysis*, *10*(7), 1119–1130. https://doi.org/10.1002/DTA.2355

Manier, S. K., Wagmann, L., Flockerzi, V., & Meyer, M. R. (2020).
Toxicometabolomics of the new psychoactive substances α-PBP and α-

PEP studied in HepaRG cell incubates by means of untargeted metabolomics revealed unexpected amino acid adducts. *Archives of Toxicology 2020 94:6*, *94*(6), 2047–2059. https://doi.org/10.1007/S00204-020-02742-1

Marchei, E., Pacifici, R., Mannocchi, G., Marinelli, E., Busardò, F. P., & Pichini, S. (2018a). New synthetic opioids in biological and non-biological matrices: A review of current analytical methods. *Trends in Analytical Chemistry*, *102*, 1–15. https://doi.org/10.1016/j.trac.2018.01.007

Marchei, E., Pacifici, R., Mannocchi, G., Marinelli, E., Busardò, F. P., & Pichini, S. (2018b). New synthetic opioids in biological and non-biological matrices: A review of current analytical methods. *TrAC - Trends in Analytical Chemistry*, *102*, 1–15. https://doi.org/10.1016/j.trac.2018.01.007

Mardal, M., Andreasen, M. F., Mollerup, C. B., Stockham, P., Telving, R., Thomaidis, N. S., Diamanti, K. S., Linnet, K., & Dalsgaard, P. W. (2019). HighResNPS.com: An Online Crowd-Sourced HR-MS Database for Suspect and Non-targeted Screening of New Psychoactive Substances. *Journal of Analytical Toxicology*, *43*(7), 520–527. https://doi.org/10.1093/jat/bkz030

Maurer, H. H., & Brandt, S. D. (2017). New psychoactive substances. In *Essentials of Autopsy Practice: Reviews, Updates, and Advances*. https://doi.org/10.1007/978-3-319-46997-3_4

Negreira, N., Erratico, C., Kosjek, T., van Nuijs, A. L. N., Heat, E., Neels, H., & Covaci, A. (2015). In vitro Phase I and Phase II metabolism of a-pyrrolidinovalerophenone (a-PVP), methylenedioxypyrovalerone (MDPV) and methedrone by human liver microsomes and human liver cytosol. *Analytical and Bioanalytical Chemistry*, *407*, 5803–5816. https://doi.org/10.1007/s00216-015-8763-6

Pantano, F., Graziano, S., Pacifici, R., Busardò, F. P., & Pichini, S. (2019). New Psychoactive Substances: A Matter of Time. *Current Neuropharmacology*, *17*(9), 818–822. https://doi.org/10.2174/1570159x1709190729101751

Peach, M. L., Zakharov, A. V., Liu, R., Pugliese, A., Tawa, G., Wallqvist, A., & Nicklaus, M. C. (2012). Computational tools and resources for metabolism-

related property predictions. 1. Overview of publicly available (free and commercial) databases and software. *Future Medicinal Chemistry*, *4*(15), 1907–1932. https://doi.org/10.4155/fmc.12.150

Pichini, S., Solimini, R., Berretta, P., Pacifici, R., & Busardò, F. P. (2018). Acute Intoxications And Fatalities From Illicit Fentanyl And Analogues. *Therapeutic Drug Monitoring*, *40*(1), 38–51. https://doi.org/10.1097/FTD.0000000000000465

Pieprzyca, E., Skowronek, R., Nižnanský, Ľ., & Czekaj, P. (2020). Synthetic cathinones – From natural plant stimulant to new drug of abuse. *European Journal of Pharmacology*, *875*(September 2019). https://doi.org/10.1016/j.ejphar.2020.173012

Predicting Metabolism | Cambridge MedChem Consulting. (n.d.).

Prekupec, M. P., Mansky, P. A., & Baumann, M. H. (2017). Misuse of Novel Synthetic Opioids: A Deadly New Trend. *Journal of Addiction Medicine*, *11*(4), 256–265. https://doi.org/10.1097/ADM.0000000000000324

Rodriguez Salas, J., Krotulski, A. J., Newman, R., Thogmartin, J. R., Mohr, A. L. A., & Logan, B. K. (2021). Concentrations of para -Fluorofuranylfentanyl in Paired Central and Peripheral Blood Collected during Postmortem Death Investigations . *Journal of Analytical Toxicology*. https://doi.org/10.1093/jat/bkab025

Royal society of chemistry. (2021). *ChemSpider | Search and share chemistry*. http://www.chemspider.com/

Saiz-Rodríguez, M., Ochoa, D., Herrador, C., Belmonte, C., Román, M., Alday, E., Koller, D., Zubiaur, P., Mejía, G., Hernández-Martínez, M., & Abad-Santos, F. (2019). Polymorphisms associated with fentanyl pharmacokinetics, pharmacodynamics and adverse effects. *Basic and Clinical Pharmacology and Toxicology*, *124*(3), 321–329. https://doi.org/10.1111/bcpt.13141

Salomone, A., Palamar, J. J., Bigiarini, R., Gerace, E., Corcia, D. Di, & Vincenti, M. (2019). Detection of fentanyl analogs and synthetic opioids in real hair samples. *Journal of Analytical Toxicology*, *43*(4), 259–265. https://doi.org/10.1093/jat/bky093

Sanghani, S. P., Sanghani, P. C., Schiel, M. A., & Bosron, W. F. (2009). Human Carboxylesterases: An Update on CES1, CES2 and CES3. *Protein & Peptide Letters*, *16*(10), 1207–1214. https://doi.org/10.2174/092986609789071324

Scholl, L., Seth, P., Kariisa, M., Wilson, N., & Baldwin, G. (2018). Drug and opioid-involved overdose deaths - United States, 2013-2017. *MMWR. Morbidity and Mortality Weekly Report*, *67*(5152), 1419–1427. https://doi.org/10.15585/mmwr.mm675152e1

Smithgall, T. E., Harvey, R. G., & Penning, T. M. (1986). Regio- and stereospecificity of homogeneous 3α-hydroxysteroid-dihydrodiol dehydrogenase for trans-dihydrodiol metabolites of polycyclic aromatic hydrocarbons. *Journal of Biological Chemistry*, *261*(14), 6184–6191. https://doi.org/10.1016/s0021-9258(19)84546-5

Snyder, R., & Hedli, C. C. (1996). An overview of benzene metabolism. *Environmental Health Perspectives*, *104 Suppl.*(Suppl. 6), 1165–1171. https://doi.org/10.1289/ehp.96104s61165

Solimini, R., Pichini, S., Pacifici, R., Busardò, F. P., & Giorgetti, R. (2018). Pharmacotoxicology of non-fentanyl derived new synthetic opioids. *Frontiers in Pharmacology*, *9*(JUN), 1–8. https://doi.org/10.3389/fphar.2018.00654

Stork, C., Embruch, G., Šícho, M., de Bruyn Kops, C., Chen, Y., Svozil, D., & Kirchmair, J. (2019). NERDD: a web portal providing access to in silico tools for drug discovery. *Bioinformatics*, *36*(4), 1291–1292. https://doi.org/10.1093/bioinformatics/btz695

Swortwood, M. J., Carlier, J., Ellefsen, K. N., Wohlfarth, A., Diao, X., Concheiro-Guisan, M., Kronstrand, R., & Huestis, M. A. (2016). In vitro, in vivo and in silico metabolic profiling of α-pyrrolidinopentiothiophenone, a novel thiophene stimulant. *Bioanalysis*, *8*(1), 65–82. https://doi.org/10.4155/bio.15.237

Swortwood, M. J., Ellefsen, K. N., Wohlfarth, A., Diao, X., Concheiro-Guisan, M., Kronstrand, R., & Huestis, M. A. (2016a). First metabolic profile of PV8, a novel synthetic cathinone, in human hepatocytes and urine by high-

resolution mass spectrometry. *Analytical and Bioanalytical Chemistry*, *408*(18), 4845–4856. https://doi.org/10.1007/s00216-016-9599-4

Swortwood, M. J., Ellefsen, K. N., Wohlfarth, A., Diao, X., Concheiro-Guisan, M., Kronstrand, R., & Huestis, M. A. (2016b). First metabolic profile of PV8, a novel synthetic cathinone, in human hepatocytes and urine by high-resolution mass spectrometry. *Analytical and Bioanalytical Chemistry*, *408*(18), 4845–4856. https://doi.org/10.1007/s00216-016-9599-4

United Nations Office On Drugs & Crime(UNODC). (2021). *World Drug Report 2021- Drug demand drug supply*. https://doi.org/10.21428/cb6ab371.e39c4e60

UNODC. (2013). The challenge of new psychoactive substances. In *United Nations Publication*.

UNODC Early Warning Advisory on New Psychoactive Substances. (n.d.). *What are NPS?* Retrieved July 7, 2019, from https://www.unodc.org/LSS/Page/NPS

Vandeputte, M. M., Krotulski, A. J., Hulpia, F., Van Calenbergh, S., & Stove, C. P. (2021). Phenethyl-4-ANPP: A Marginally Active Byproduct Suggesting a Switch in Illicit Fentanyl Synthesis Routes. *Journal of Analytical Toxicology*. https://doi.org/10.1093/jat/bkab032

Vickers, S., & Polsky, S. (2000). The Biotransformation of Nitrogen Containing Xenobiotics to Lactams. *Current Drug Metabolism*, *1*(4), 357–389. https://doi.org/10.2174/1389200003338929

Watanabe, S., Vikingsson, S., Roman, M., Green, H., Kronstrand, R., & Wohlfarth, A. (2017). In Vitro and In Vivo Metabolite Identification Studies for the New Synthetic Opioids Acetylfentanyl, Acrylfentanyl, Furanylfentanyl, and 4-Fluoro-Isobutyrylfentanyl. *The AAPS Journal*, *19*(4), 1102–1122. https://doi.org/10.1208/s12248-017-0070-z

Wilde, M., Pichini, S., Pacifici, R., Tagliabracci, A., Busardò, F. P., Auwärter, V., & Solimini, R. (2019a). Metabolic pathways and potencies of new fentanyl analogs. *Frontiers in Pharmacology*, *10*(APR), 1–16. https://doi.org/10.3389/fphar.2019.00238

Wilde, M., Pichini, S., Pacifici, R., Tagliabracci, A., Busardò, F. P., Auwärter, V.,

& Solimini, R. (2019b). Metabolic pathways and potencies of new fentanyl analogs. In *Frontiers in Pharmacology* (Vol. 10, Issue 238, pp. 1–16). Frontiers Media S.A. https://doi.org/10.3389/fphar.2019.00238

Zheng, Z., Arp, H. P. H., Peters, G., & Andersson, P. L. (2021). Combining in Silico Tools with Multicriteria Analysis for Alternatives Assessment of Hazardous Chemicals: Accounting for the Transformation Products of decaBDE and Its Alternatives. *Environmental Science and Technology*, *55*(2), 1088–1098. https://doi.org/10.1021/acs.est.0c02593

6 Acknowledgments

Although it is not consistent to the rest of the manuscript, I think it is more appropriate to report this section in my native language to better express my gratefulness to all the people who had a role in this 3 year-experiment, called Ph.D. program.

La collaborazione più preziosa e necessaria al completamento di questo lavoro, in tutte le sue fasi, è stata sicuramente quella della mia famiglia. Ancora una volta, voglio ringraziare loro per primi per l'ennesima prova di pazienza che hanno superato. È grazie al supporto, ai consigli e alla presenza di mia madre, di mio padre, di mio fratello Giuseppe e dell'architetto Irene, grazie alla stima e alla fiducia che mi hanno sempre dimostrato, grazie alla loro disponibilità che non ho mai perso di vista i miei obiettivi e ho imparato a crescere giorno per giorno, anche quando non è stato facile. Anche da lontano.

Questo progetto non sarebbe neanche nato senza la presenza e l'aiuto del mio tutor, il professor Francesco Paolo Busardò, che chiamo professore forse per la prima volta in queste pagine. In questi lunghi 3 anni (e mezzo), mi ha dato la possibilità di crescere come ricercatore, come professionista, ma anche come persona, ponendomi sempre nuove sfide. Il suo supporto scientifico e umano è stato prezioso per il raggiungimento di questo traguardo. E anche se può suonare come una melensa sviolinata, gli sarò sempre grata per avermi reso parte di questa squadra. Perché so che non gli ho reso sempre il gioco facile, ma ha sempre avuto fiducia in me. Spero di non averla delusa.

La continuazione è quasi ovvia. La dottoressa Simona Pichini. Grazie per tutti i messaggi e le telefonate dalle 7 alle 23, dal lunedì alla domenica, festivi inclusi. Grazie per la tua rumorosa presenza, per aver battuto un ritmo sempre più incalzante. Grazie per il sovraccarico di energia che mi hai sempre trasmesso, per essere sempre stata trainante. Grazie per le critiche, i rimproveri, i cazziatoni, l'ansia, i momenti no, i momenti si, i momenti forse. Grazie per aver visto la mia passione e averla alimentata sempre. Grazie per i consigli, per il tuo supporto, per il tuo sostegno. Grazie per tutto quello che mi hai insegnato, ma soprattutto per tutto quello che mi hai trasmesso. Grazie per tutto questo e anche per molto altro.

Una menzione speciale va alla mia compagna di avventura, la dottoressa Nunzia La Maida, che ha iniziato e finirà il dottorato con me. E' sempre stata un esempio di tenacia e caparbietà per me, a cui ho cercato di ispirarmi. Al di là della stima personale, nutro per lei una profonda stima professionale e parte di tutto quello che ho raggiunto è merito sicuramente del costante confronto costruttivo che ho avuto con lei. Non avrei potuto scegliere compagna migliore di lei per affrontare questi anni, sotto tutti i punti di vista. Grazie Nunzia, spero che questo sia solo il primo capitolo di una lunga serie di capitoli che scriveremo insieme.

E quindi, ora, il ringraziamento ad un altro elemento fondamentale al raggiungimento di questo traguardo. Il prof Botré, Francesco. Ero immersa in un'altra vita quando mi ha chiamata per dirmi di provarci ancora, di non arrendermi. Di continuare a credere nei miei sogni. Lui lo sapeva, lo ha sempre saputo. Lui mi ha scientificamente cresciuta, non si sbagliava quando ha visto

quel bagliore. Ma ringraziarlo per aver insistito sarebbe solo riduttivo. Se qualche anno fa lo ringraziavo per avermi insegnato chi volessi essere da grande, oggi voglio ringraziarlo per avermi dato i mezzi per costruirmi la strada verso il diventare grande. E per la sua preziosa stima che è sempre il principale motivo di orgoglio.

Grazie ai miei primi colleghi, Giulio, Roberta e Flaminia. Grazie per non esservi fermati alle spine, ma aver visto molto oltre. Grazie per la pazienza con cui mi avete mostrato ed insegnato i fondamenti, ma grazie soprattutto per avermi arricchito con la vostra esperienza. Grazie a Sara e Anastasio, che hanno fatto parte della mia lenta e traumatica transizione da Roma ad Ancona. Conservo gelosamente il ricordo di tanti bei momenti passati insieme, fuori e dentro il laboratorio. Grazie per essere stati leggeri quando io non ci sono riuscita, per le vostre risate e per le vostre canzoni.

Vorrei poi ringraziare Jeremy per il suo supporto tecnico-scientifico, per avermi insegnato molto. Il confronto scientifico con lui è stato sempre stimolante e mi ha dato sempre un sacco di idee. Vorrei ringraziarlo soprattutto per i suoi consigli imparziali ed i suoi commenti parziali.

Grazie anche a Fabrizio. Un grazie, questo, più sentito di quello che si immagini. Nonostante il nostro rapporto abbia oscillato tra il teso ed il pessimo a variabile frequenza, lo ritengo comunque il confronto più duro e prezioso che abbia avuto in questi anni. Perché mi ha spinto a mettermi in gioco ogni volta di più, dovendo mettere sempre in discussione me stessa e il mio punto di vista per convivere con un punto di vista diametralmente opposto al mio, in molte

cose. E' stata una dura palestra, ma che ha portato molti buoni frutti. Per cui grazie, davvero. Però facciamo che la prossima volta anche meno.

Grazie a Pietro, Eva, Giulia, Alessandro, Diletta e a tutte le persone con cui ho lavorato a diverso titolo in questi anni, perché ciascuno di voi mi ha insegnato qualcosa di diverso.

Grazie ai miei amici di sempre, ma soprattutto a Nicola e Piero che da più di 15 anni (quasi 20 a dirla tutta) assistono alle strane vicende della mia vita, ormai quasi con rassegnazione, ma sempre con lo stesso affetto e la stessa infinita disponibilità. Grazie per avermi accolta ed ascoltata sempre, ancora. E grazie anche ai miei nuovi amici Ambra, Simone, Diego, Roberta, Alessandra e Nicola, perché sono stati un po' la mia famiglia in questo luogo lontano dal mio mondo e dalla mia vera famiglia. Grazie per aver alleggerito le mie giornate e per essere diventati importanti in poco tempo.

Dulcis in fundo, grazie a Marco. Compagno allegro, polemico, presente, complicato, dolce, disponibile. Giudice implacabile, compagno assiduo, compagno prezioso. Compagno quotidiano, compagno indispensabile e necessario. Grazie perché senza di te forse ce l'avrei fatta, ma con te ce l'ho fatta indubbiamente meglio. Grazie per sopportarmi. Grazie per avermi resa più sopportabile da parte dei miei colleghi, sappi che loro te ne sono molto grati. Grazie per avermi dato serenità quando ne avevo bisogno. Grazie per tutto quello che abbiamo fatto e per quello che ancora abbiamo da fare.

E ancora una volta grazie a tutti coloro che non hanno mai dubitato e a coloro che non hanno mai smesso di farlo.